FOCUS

MECHANICAL ENGINEERING AND SOLID MECHANICS SERIES

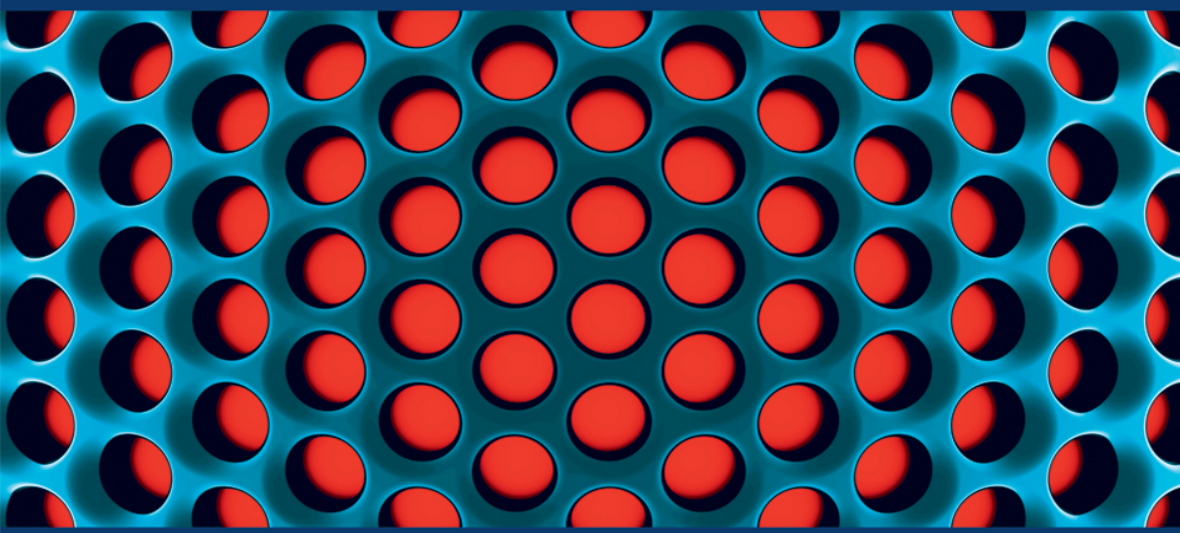

Experimental Mechanics of Solids and Structures

Jérôme Molimard

ISTE

WILEY

Experimental Mechanics of Solids and Structures

FOCUS SERIES

Series Editor Bruno Salgues

Experimental Mechanics of Solids and Structures

Jérôme Molimard

ISTE

WILEY

First published 2016 in Great Britain and the United States by ISTE Ltd and John Wiley & Sons, Inc.

ISTE Ltd
27-37 St George's Road
London SW19 4EU
UK

www.iste.co.uk

John Wiley & Sons, Inc.
111 River Street
Hoboken, NJ 07030
USA

www.wiley.com

Library of Congress Control Number: 2016933399

British Library Cataloguing-in-Publication Data
A CIP record for this book is available from the British Library
ISSN 2051-2481 (Print)
ISSN 2051-249X (Online)
ISBN 978-1-84821-996-0

Contents

Foreword

Mechanics is an ancient discipline that has been through major changes in recent decades with the advent of the finite element method. The possibility of calculating the spatial distribution of variables such as displacements, strains, and stresses, using adapted models for geometries and complex loading conditions, had initially led to the purely experimental aspects related to characterization of the mechanical behavior of materials and structures to be pushed into the background. Even though the final validation tests have always remained necessary to validate geometries or choice of materials, the number of preliminary tests carried out on the structural elements has naturally decreased the calculations which enable us at least to significantly "refine" the designing of systems and structures, if not to propose near-optimal solutions. Material characterization tests, though still indispensable for providing the calculation codes with finer laws, have for a long time remained somewhat rigid in well-established procedures, along with the measurement methods which have also changed very little over a long period of time – since the release of "classic" sensors such as point displacement sensors or strain gauges.

In recent years, however, there has been an increased interest in experimental mechanics. The emergence and rapid dissemination of new investigative methods, such as kinematic measurement systems, have enabled access to spatially continuous information, at least on the surface of tested specimens. Several heterogeneities were thus brought to light in the fields of displacements and deformations which were only partially seen using classical instrumentation based on point measurements. However, with the numeric sizing calculations improving over time, it has become necessary to provide experimental information also in line with the improved

calculation results. Though the above-mentioned full field measurement methods are effective, the proliferation of conventional sensors distributed over large structures requires optimal management of the information collected. Finally, the increasing overlap between numerical models and elaborately instrumented test results has led to the emergence of identification strategies for material and structural properties in contrast with conventional procedures which are well-established, but unsuitable for mining of data available in large volumes.

It is in this context that this book written by Jérôme Molimard is presented to us. Its content covers many of the issues mentioned above in a language particularly adapted for technicians or engineers. First, the author briefly reviews the principles of "classic" standardized tests. He then addresses the performance of the usual force, displacement, and deformation sensors, with particular attention drawn to the metrological performance that users can expect. The author then continues with the main techniques, whether purely geometric or interferometric, for measuring kinematic fields; and finally, discusses the consideration of uncertainties related to measurement procedures. The book includes the description of experimental designs to provide the reader with a rigorous framework to address the optimal management of a large volume of data and unknowns.

In terms of the form, the author shares his knowledge from extensive experience in mechanical testing through many short exercises that appear throughout the book, and a final chapter dedicated entirely to case studies.

In conclusion, the work of Jérôme Molimard is well-timed to respond, in a clear and concise manner, to the queries raised by traditional tools and methods of experimental mechanics, but also related to recent changes within this discipline. Amply illustrated, the book will certainly help the reader to find examples of application close to their own interests, complemented with insightful background information on the experimental mechanical techniques and methodologies found in the book.

Michel GREDIAC
Professor at Blaise Pascal University
Clermont-Ferrand
February 2016

Introduction

I.1. Experiments for solid and structural mechanics

The modern mechanics of solids and structures relies heavily on the numerical solution of a mechanical problem. Since the early 1970s, the Finite Element Method was widely used for very complex cases. In the present day, a Computer-Aided Design software which generally integrates a small calculation module predicts the behavior of complete mechanical systems, something impossible as few as twenty years ago. The training of a mechanical technician or engineer today largely incorporates this tool, sometimes abandoning the practical work altogether. However, the numerical calculation only responds, in a more or less accurate manner, to an inevitably idealised mathematical problem. It is therefore necessary to *validate the simplifying assumptions* introduced in the modeling. Furthermore, the *values used* in the calculation should be *well-known* (structural damping, binding strength, or boundary conditions). This all requires experimental work which is sometimes difficult, even in the case of a relatively simple behavior that can be easily modelled. Firstly, numerical codes have to be fed with *experimental data*. For example, the current development of elaborate composite parts requires characterization of the anisotropic stiffness tensor (9 parameters), whereas the contemporary practice reflects only the properties of the plate (4 to 6 parameters) where one dimension is negligible in the face of others. Furthermore, the boundary conditions, either restraint or contact, are often subject to strong assumptions that an experimental approach can improve, by defining a recessed stiffness, for example.

But mechanical design is based on various functioning patterns of the proposed device. There is of course normal functioning, very often under static loading, but also a dynamic functioning linked to possible shocks, abrupt load changes (e.g. emergency stop), or a challenging external environment with variations in temperature or humidity. Moreover, any mechanical device must guarantee a certain lifetime. In a conventional design approach, it is possible to size the apparatus by numerical method for some cases and then *experimentally test the prototype* with the objective of validation, whereas other cases will only be studied experimentally.

Finally, even though Mechanics is an ancient discipline, the formalism is sometimes lacking. It is then necessary to return to the basic approach of experimental science and conduct *experiments for understanding*. These situations beyond the mathematical formalism are very common in everyday life: in the study of interaction between two solids in contact – tribology – friction and wear are beyond the scope of intrinsic material properties and modeling of infinitesimal elements, as is usually done in mechanical modeling. More recently, mechanicians were interested in the mechanics of powders, where the material studied is neither a liquid nor a solid. The recent interest in biomechanics also raises the question of the nature of the medium studied; the skin, for example, could be considered as a linear elastic material, or hyper-elastic, anisotropic, viscoelastic, poro-elastic… Therefore, presently, a well-conducted experimental study is the only reasonable approach to this category of problems.

These different types of experiments rely on common concepts such as data processing, choice of sensors, or experimental modelling. However, the strategies are quite different, depending on whether we can or cannot rely on a reliable formalism. The three following examples will illustrate the experimental approaches for different purposes, directly related to the degree of knowledge of a system.

I.1.1. *Study of a bicycle wheel; an example of a complete structural validation*

This work was conducted as part of a technology transfer from a university lab to an SME, in the form of a doctoral thesis [MOU 98]. The objective was to provide the company with a software to assist the designing

of bicycle wheels. In particular, the software should be able, via a Finite Element analysis, to recognize and analyze the natural modes of a wheel.

The program was written in MATLAB© using a graphical interface and numerical analysis facilities. This solution enables the SME not to invest human and financial resources in a generic finite element software; the developed application can be used by the technicians of the research department without any special knowledge of the calculation method.

From the mechanical point of view, the numerical modelling is as follows:

– the spoke beams are highly slender structures with negligible flexural rigidity and compression. Their behavior has a geometric nonlinearity. So we have:

$$\in_{xx} = \frac{\partial u}{\partial x} + \frac{1}{2}\left[\left(\frac{\partial u}{\partial x}\right)^2 + \left(\frac{\partial v}{\partial x}\right)^2 + \left(\frac{\partial w}{\partial x}\right)^2\right] \qquad [I.1]$$

– given the number of spokes and considering the thickness of the rim relative to its diameter, it is approximated as a simple beam element (not a curve). The section of the rim is complex, such that the beam element is a strong approximation required to maintain a reasonable calculation time;

– the hub is considered infinitely rigid;

– the connections are assumed to be perfect; the point of application of stress of the spokes is shifted with respect to the torsion center of the rim.

The main elements of the research method of eigenvalues and eigenvectors are:

– a search for solutions to the dynamic equation in a pseudo-modal base which enables a reduced calculation time;

– numerical method of resolution of the nonlinear behavior of the wheel is the incremental Newton–Raphson method. The change of state is divided into n steps, for which the stiffness matrix is updated at each step; the total change is the sum of individual changes.

The software developed is used to find the static behavior, frequency response, and the time response of a bicycle wheel with defined assembly.

This software has been validated by an experimental approach, particularly for the frequency response. The assembly is reproduced in Figure I.1.

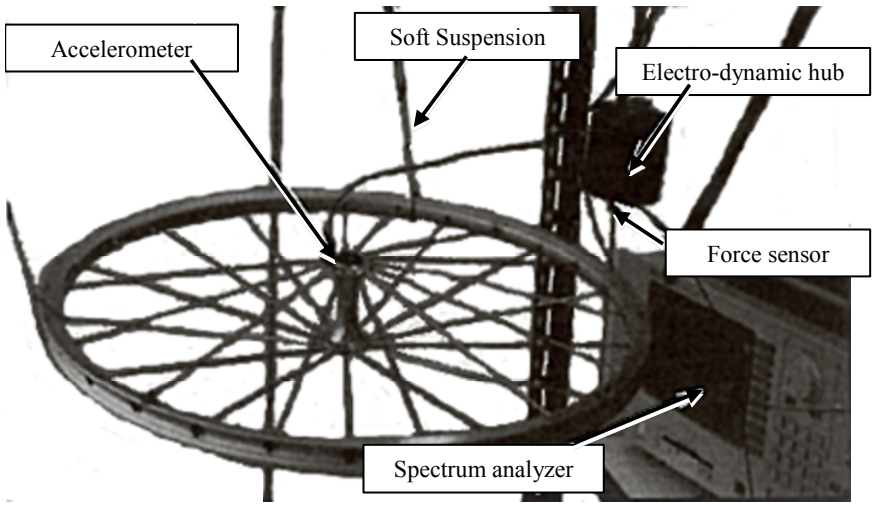

Figure I.1. *Assembly for frequency analysis of a bicycle wheel (according to [MOU 98])*

The wheel is mounted on flexible supports simulating free-free boundary conditions. An accelerometer is placed on the upper side of the hub. The excitation takes place on one side of the rim. This excitation requires movement off the periodic plan.

Just as the digital model is questionable due to various assumptions and required approximations, a test like this is only an approximation of the real situation. This is an *experimental model*, simplifying the structure, the boundary conditions and the load. The experimental model also offers only a few measuring points, based on *a priori* judgment of the designers of this model, which gives a limited view of the examined physical reality. Finally, the modifications of the experimental model in relation to the physical reality it explores leads to distortion of the obtained solution.

In this specific case, an accelerometer weight sensor is generally likely to alter the natural modes of the wheel. Likewise, the positioning of

the accelerometer may also affect the observation of certain occurrences. Therefore, an accelerometer placed at the node of a mode does not allow its identification.

It may be noted, according to these rules, that the choice of positioning is especially important: in an infinitely rigid zone, the accelerometer does not change the stiffness matrix. With regard to assumed or calculated modes, it can be predicted that the accelerometer will be sensitive to different degrees. For example, Figure I.2 shows the "2Φ–plan" mode which is barely visible and the "umbrella" mode that should be easily identifiable.

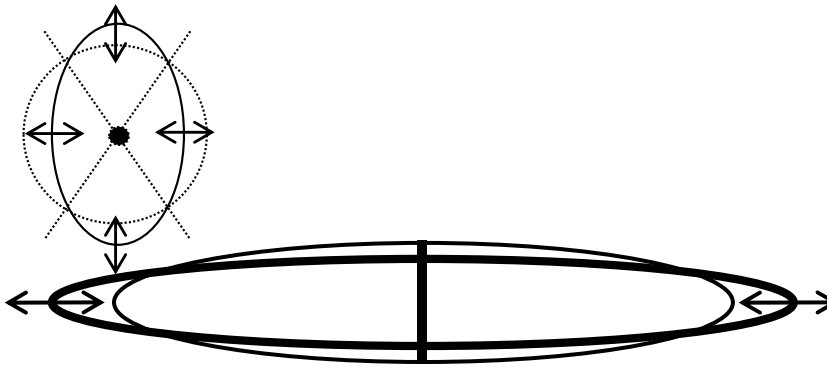

2Φ–plan mode

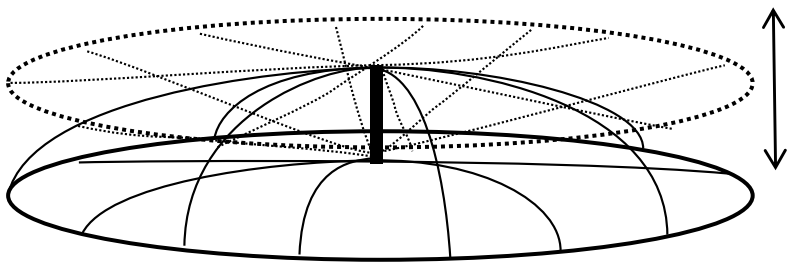

Umbrella Mode

Figure I.2. *Examples of vibration modes of a bicycle wheel (according to [MOU 98])*

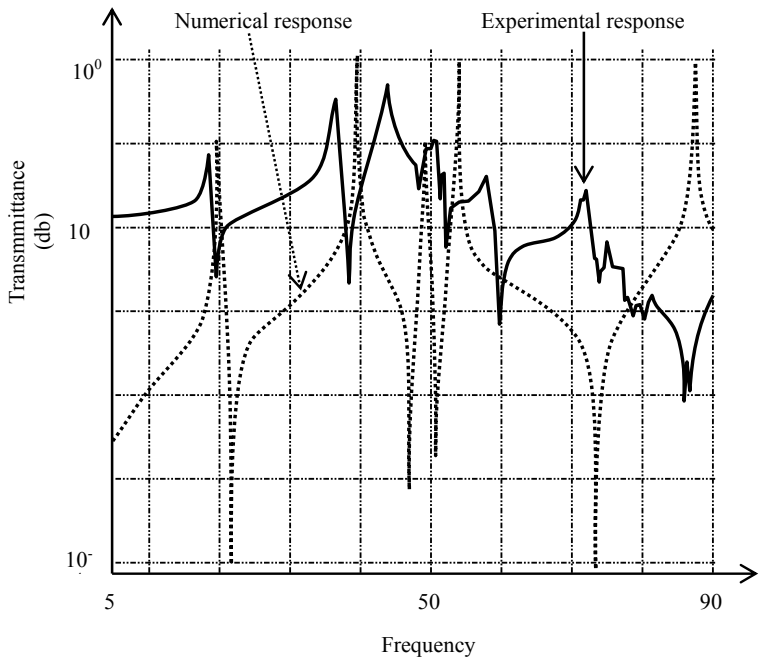

Figure I.3. *Numerical and experimental response of a bicycle wheel (according to [MOU 98])*

Comparison of numerical and experimental approaches gives the results shown in Figure I.3. The first resonance, which corresponds to the "2Φ off-plan" mode shows a very good theory/experiment correlation. In contrast, the frequencies corresponding to other modes differ more and more, until the error reaches 15%. Even if the prediction model works well, this variance is a representative of many modal analyses: the approximations are manifested especially when the frequency is high.

On the other hand, the theoretical and experimental values of the transmittances are somewhat similar. But these values, which are directly related to damping (structural damping, spoke connections), show the acuteness of the natural frequency to be taken into account: with zero damping, the structure will break; with a critical damping $(c = 2\sqrt{km})$, the natural frequency will be in noise.

This example shows that a mechanical analysis cannot be conducted without the three traditional pillars of science: a well-established mechanical model, a predictive tool using numerical analysis, and experimental tool for validation. From this point of view, the numerical model and the experimental model are both based on a set of assumptions that are generally not the same. A discussion between the numerical and experimental approach of both these sets of assumptions is required to ensure proper understanding of what is being studied.

I.1.2. *Mechanical effect of lumbar belts: an example of phenomenological analysis*

Biomechanics presents many examples illustrating another use of the experimental approach in the design process or product optimization. Biomechanics is concerned with subjects that are lesser-known and difficult to describe. Soft tissues (muscles, liver, skin, etc.) are nonlinear elastic, viscous, porous, anisotropic, and are subject to pre-tension. In some cases, their properties also vary spatially. Simplifications in their behavior allow modelling, but corroboration with experiments is essential. However, the context presents even more specifics: the work on model geometries allowing simplifications is usually impossible and load types are often limited because the studies involve live subjects. This requires unconventional experimental methods often based on imaging. Furthermore, there is great variability in geometry and mechanical properties within subjects, with significant temporal variations (circadian cycles, external factors such as stress, pollution) and between subjects. The development of medical devices must, therefore, rely largely on an experimental approach in a high variability context. Tests on patients or healthy individuals are also limited by ethical and medical considerations. The probability of an occurrence of a medical complication increases with the number of cases but if this number is too low, the power of the tests will not always be sufficient to achieve a significant result[1].

For illustration, a recent study was conducted on lumbar belts, frequently used in the treatment of lumbago [BON 15]. Though the feedback from doctors and patients is very positive and clinically proven, there are very few

1 The power of a statistical test measures its ability to separate two groups of results. Refer to section 5.4.

scientific studies objectifying the mechanical effect of these belts. A belt, by applying external compression around the abdomen, is assumed to cause a change in the posture and thus exert pressure on the intervertebral discs which are the site of pain in the lower back. However, this mechanism is little-documented in the scientific literature. The adopted method consists of a pairing of both numerical and experimental approaches.

The pressure and the deformation of the belt is measured. Thus, a clear link between the level of stress on the belts and transmission to the torso can be established. As distributions of pressure and deformation are not a priori known, and as the peak pressure values can be of major interest in the analysis of the comfort of the belts, a full field measurement is the chosen method. Finally, a measurement of the shape of the torso, with and without belt, allows monitoring of the changes in posture, which is then compared using a subjective pain rating scale from 0 to 10.

Then, as in any mechanical design, the nature of representative load must be addressed. This issue should be dealt with in the context of the possible interpretation of the results and prior knowledge level. So, the choice was made to compare, in static, a situation where the brace has no apparent mechanical effect (in place, but not tight) and a situation where the effect was felt (close brace). To avoid the temporary effects related to the fitting of the belt, each patient is asked to make a few movements, in a particular order at pre-set amplitude.

Finally, the elements that were more likely to change the posture were selected using a very simplified numerical model: the torso is assumed to be linear elastic; the geometry is reduced to sets of ellipses; the role of the belt is stated as pressure output given by Laplace's law. This law describes in first approximation the pressure P generated by a taut band with a force T on an object with radius of curvature R:

$$P = \frac{T}{R} \qquad [I.2]$$

The parameters of the belt (height and rigidity), the shape of the patient's torso (radius of curvature, size) and the applied tension (deformation and rigidity of the belt) are selected. In practice, three belt models (hence, three rigidities) are available for two different heights. Fifteen subjects were called; their sizes were measured. Six subjects were measured to be of

normal build, six were overweight, two were moderately obese and one was severely obese. The tension is set according to the manufacturer's recommendations, which prescribes a belt deformation of 20%. It is not possible for each subject to test six belts, owing to the length of time of each experiment and due respect to the patient. Therefore, to obtain the maximum information, each patient is to test two belts as per the experimental design in incomplete blocks.

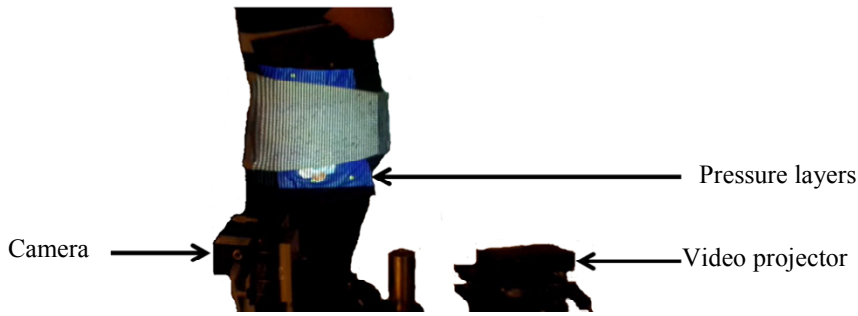

Figure I.4. *Study of mechanical effects of a lumbar belt (according to [BON 15])*

This study involves a very large amount of data with 67 field measurements generated for each patient. Statistical tools had to be used to discriminate the descriptive parameters of the mechanical brace (Principal Component Analysis): the pressure on the torso and the circumferential strain of the belt are sufficient discriminating factors to explain the different belts tested. The transverse and shear deformations, therefore, are not measured. Given the variability of the results, a difference related to a parameter (e.g. sex of the patient) is analyzed using a hypothesis testing approach to determine its significance. For example, in all cases, the load on each of the iliac crests is significantly different, showing an unbalanced mode of action between the right and left sides.

The study indicated that the lumbar support belts reduce pain and seem to change the posture. The belts are identical in their mode of action for even tightening. However, they differ in terms of pain relief, their tolerance by the subject and different possibilities of their tightening. Moreover, Laplace's law (Equation [I.2]) is valid on an average but does not apply locally: additional efforts to fully understand the transmission of mechanical effect to the torso are still required.

This type of study is common in biomechanics, but also in many other fields of application where mechanics or modelling is not sufficiently effective: tribology and powder mechanics, for example. The experimental approach must rely on tools from the statistics (experimental designs, hypothesis testing in particular). A numerical approach can be used to support the experimental approach, either before selecting the priority study parameters or after building or validating a mechanism. The result of the experimental study is primarily a set of trends to determine optimum functioning. This result is sufficient for many applications in engineering, but in the context of research and development, further understanding of what is being studied is also necessary. It often requires further study where the learning process becomes iterative.

I.1.3. *Coefficient of rolling friction: identification of parameters*

Rolling is a method widely used for manufacturing semi-finished flat products (steel or aluminium sheets) or rods as well as finished products (rail tracks). This method involves thinning out a metal by way of friction between two rollers. The diagram in Figure I.5 shows the two-dimensional structural analysis of the rolling process. This means that any possible enlargement is considered negligible.

The objective of rolling is to reduce the thickness e_1 of a metal sheet to a value e_2 under the action of a compressive force F and a driving torque C. The reduction rate $(1\text{-}e_2/e_1)$ is an essential element in the process, as an increased rate means a shorter and less expensive dimensioning range. As the material flow rate is constant, the reduction in the thickness of the sheet means that its speed increases during the rolling.

The area where the reduction of thickness takes place is called the roll-gap. It can be broken down into different parts (from left to right as in Figure I.5): first, the strip and the rolls deform elastically. Then the plastic deformation of the strip occurs before elastic recovery and the contact output. The speed of the rolls is constant while the speed of the strip increases from V_1 at the input of the contact to V_2 at the output according to the deformation, and thus from the position in the roll-gap. This means an area exists where the strip is slower than the cylinders (at the input of the roll-gap) and an area where it is faster (at the exit of the roll-gap). In

between these two areas, a particular point can be defined as the only pure rolling contact point: it is called the neutral point.

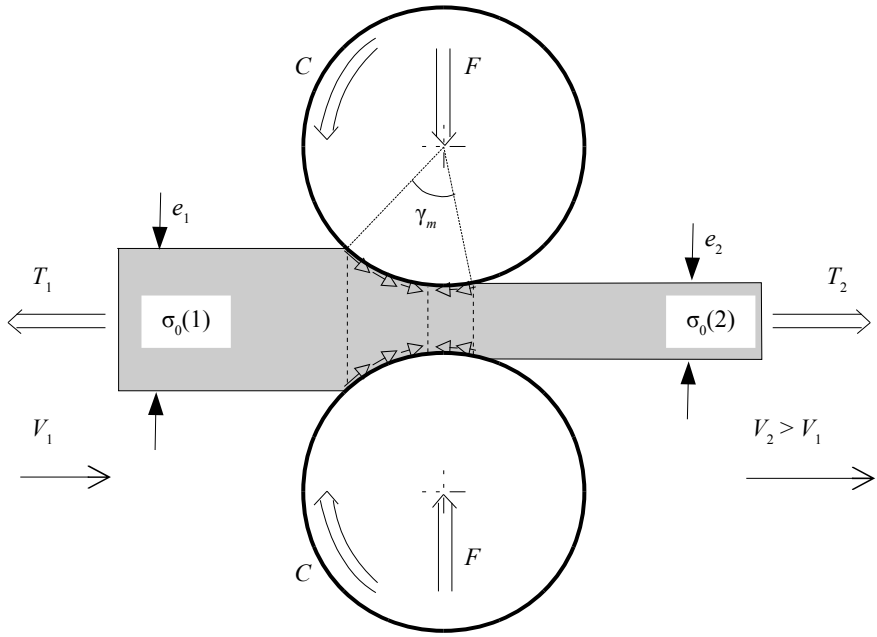

Figure I.5. *Mechanical description of rolling (according to [MOL 99])*

From the perspective of forces, the friction opposes the local movement. The friction before the neutral point is a propelling friction for the strip, whereas the friction occurring after the neutral point opposes the advancement of the strip. The position of the neutral point is an essential element for the rolling operation. It is controlled by traction T_2 and counter-traction T_1. We can observe that *this is the friction which drives the strip between the rolls and causes the rolling process*. The friction appears as a fundamental component of the process. Finally, during the rolling process, the metallurgical structure of the strip changes; it hardens and its flow limit varies between $\sigma_0(1)$ and $\sigma_0(2)$.

The example discussed here involves the evaluation of friction. All rolling calculation codes assume the friction coefficient. When cold, the friction

model used is the Coulomb's model. If N is the normal force to the surface and T is the tangential force, the friction μ is given by:

$$\mu = \left| \frac{T}{N} \right| \qquad [I.3]$$

The oldest method for determining the coefficient is to position the system in a particular configuration of rolling, when the neutral point is at the exit of the contact. Friction is then exerted in one direction and it can be calculated using the following equation:

$$\mu = \left| \frac{R_c F}{C} - \frac{Y_m}{2} \right| \qquad [I.4]$$

The situation used for the evaluation of friction is undesirable in an industrial rolling configuration owing to slip limits. But for several years, tribologists have known that the friction coefficient is highly dependent on the operating conditions: it is thus necessary to verify the relevance of the values obtained, by decoupling the various parameters of rolling: load, speed, temperature, and shear rate; these conditions are given in Table I.1.

Normal pressure	≤ 1 GPa
Increase in temperature	≈ 20 to 200 °C
Slip rate	≈ 0 to 15 %
Rolling speed	≈ 5 to 30 m/s
Roughness σ_{Ra} of the band	≈ 0.1 to 5 µm
Transit time of the lubricant in the roll-gap	≈ 0.2 to 3 ms
Reduction rate of the strip	≈ 1 to 40 %

Table I.1. *Contact conditions for rolling*

Additionally, in order to predict the thermal effects occurring locally (heat waves) a local description of the gap, geometric (see Figure I.6) as well as tribological, must be available.

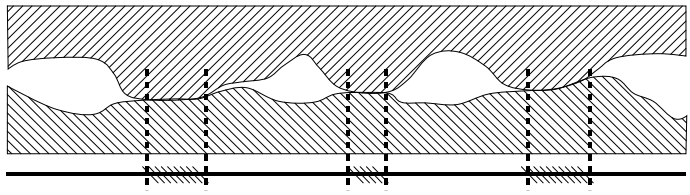

Figure I.6. *Representation of joint contact; the hatched areas correspond to direct metal–metal contacts (in [MOL 99])*

A series of tests on the same materials were developed using:

– a roller machine: allows the measurement of an overall friction coefficient by adapting each of the operating conditions present during the rolling process;

– a UHV tribometer, which is one of the very few tools to provide a local measurement on the scale of a few μm²;

– a pilot rolling mill: this is the conventional method described above. This test is the accepted reference in the field.

Figures I.7, I.8 and I.9 compare the results obtained by various methods: the coefficients of friction are expressed with respect to different quantities, indicating that an understanding of the physical processes is essential for the interpretation of results. In addition, the friction coefficient values are very different: physically, comparable values could be 6%, 3.8%, and 60% respectively.

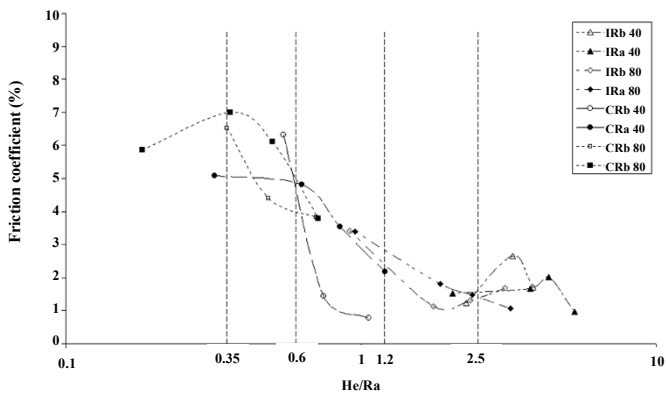

Figure I.7. *Synthetic result of the "rolling machine" test; Coulomb friction coefficient (in %) with respect to the ratio of average oil height and average height of roughness (in [MOL 99])*

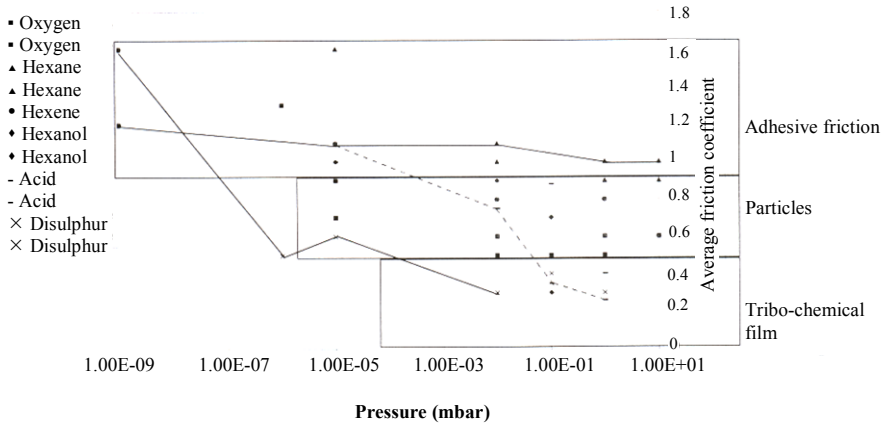

Figure I.8. *Synthetic result of the "UHV tribometer" test: Coulomb friction coefficient (gross data) with respect to the pressure from chemical species (i.e. their amount) (in [BOE 98])*

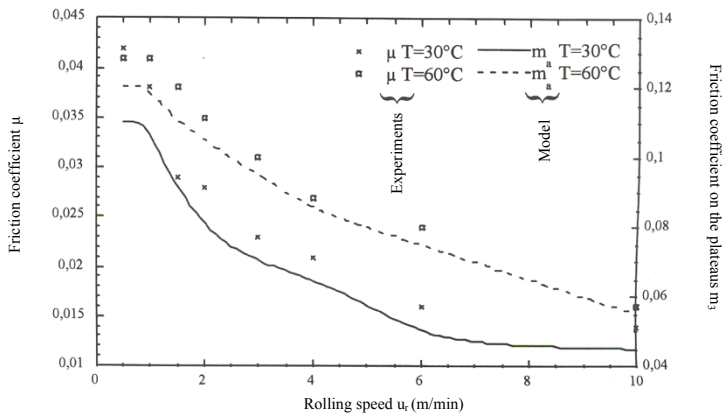

Figure I.9. *Synthetic result of "pilot rolling mill" test, Coulomb friction coefficient (in %) with respect to rolling speed (in [MON 94])*

The explanation for these variances cannot be pinned to any single parameter; we will, therefore, try to list some differences between devices that could cause them:

– The rolling machine, unlike the rolling mill, does not generate large quantities of "fresh surfaces", bare metal surfaces that are highly reactive.

Therefore, the adhesion of the lubricant is certainly worse. In contrast, solid–solid interfaces, if they are present, are probably less reactive.

– The UHV tribometer simulates the presence of lubricant by injecting a gas consisting of active elements of the lubricant. The effects of hydrodynamic lift are, therefore, non-existent. Similarly, interactions between molecules cannot take place and the dimensional effects of the molecular chains are impossible to characterize.

Thus, the validity of each experiment cannot be contested, but the circumstances of each of these experiments are different, even if the measured quantity is the same. Despite its widespread use and practical importance, the friction coefficient is the result of complex microscopic interactions, for which no overall modelling exists. The identification of the friction coefficient is particularly difficult because this parameter is theoretically ill-founded. To obtain a usable figure, all the assumptions and operating conditions must be strictly reproduced experimentally.

NOTE.– Aside these comparisons, it is particularly difficult to identify the friction coefficient using a pilot rolling mill: no device records the friction and the basic data available is the applied load and torque. To isolate the friction, it is necessary to use a rolling model. Montmitonnet [MON 94] identified the friction values from the same experimental data set using different models from the literature (Figure I.10) where not only the values, but even the patterns themselves were different. This shows the crucial importance of understanding *and correctly modeling a physical phenomenon before quantifying it.*

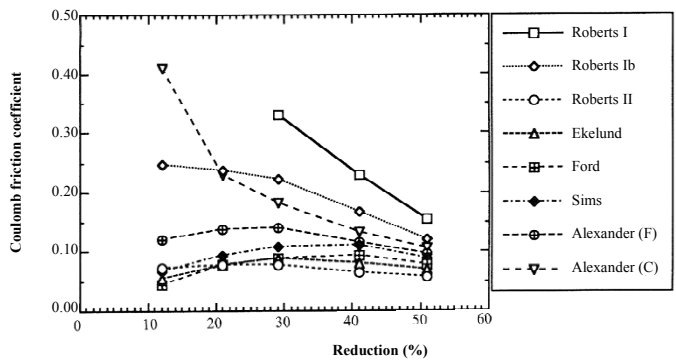

Figure I.10. *Identification of friction from various rolling models for similar basic experimental data (in [MON 94])*

I.2. Construction of an experimental model

I.2.1. *Addressing experimental difficulties*

In an experimental procedure, difficulty often arises from physical complexity: a successful experiment can reproduce a physical model only if all other variables present could be discounted (which include, in most cases, effects of temperature and history of materials). This is the first condition for an identification or inter-comparison process.

The elimination of interfering conditions is a rigorous process. For example:

– in a tensile test, bending effects are eliminated by a specific alignment of the jaws;

– in order to eliminate effects related to the history of a material, test pieces were taken from the same batch and stored in the same conditions.

In addition, the quality of measurements made is also related to the measurement system. An experimental result, such as a numerical result, is only valid if accompanied by a confidence interval. Finally, to compare the measured quantities, the experimental protocols must be written and validated.

I.2.2. *Experimental model*

Very often, mechanical testing is viewed as a purely technical field of work. The above examples indicate, however, that to develop and operate mechanical tests requires us to make choices leading to an experimental model. It is based on simple assumptions with regard to load borne by the system under study and its boundary conditions, under a controlled environment. This includes a controllable loading device and an array of instrumentation. Finally, effective controlling of an experimental model requires writing a protocol to ensure the reproducibility of the measurement. The experimental model must preempt an interpretation by an analytical or numerical model; and it must be properly validated before use.

I.2.3. *Overview of an experimental process*

Figure I.11 shows the various elements in a typical experimental process in a simplified manner.

Firstly, the physical world forms the center of the study. This involves designing an experimental model which is basically a physical idealization of the *real problem*. Then, the experimental model must be utilised and an *experimental plan* i.e. a coherent set of tests to obtain the desired information with the greatest possible clarity, must be defined.

In mechanics, the studied structure must be loaded, irrespective of whether it refers to dynamics, frequency, or static studies. The *loading* requires an *actuator* that converts a signal, which is often electrical, to a mechanical signal. Given the underlying physics in the excitation process, the load to be applied must be properly *conditioned* to ensure that the required control is effectively carried out. Usually, the control system is the subject of an active control, a PID (proportional–integral–derivative) loop.

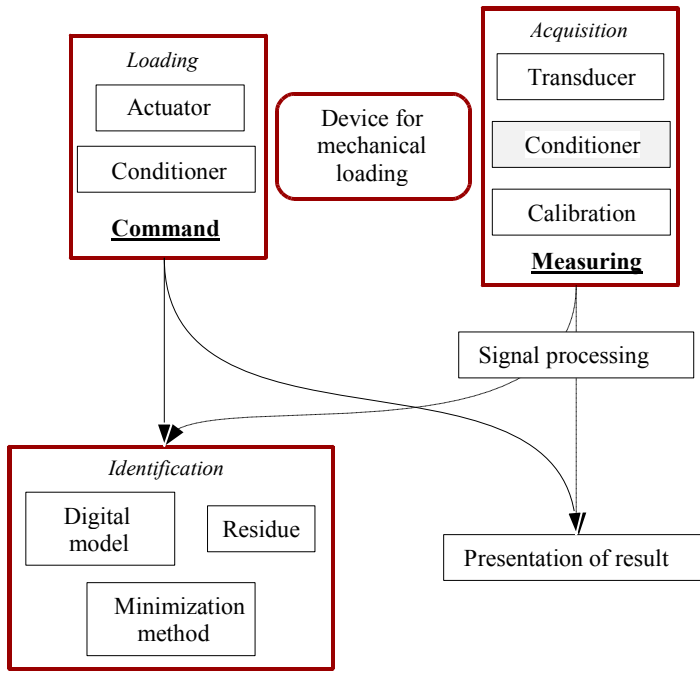

Figure I.11. *Block diagram of an experimental process*

The *acquisition* is done through a transducer such as a strain gauge, for example. The mechanical signal (elongation) is converted into an electrical signal (a change in resistance). The transducer is conditioned so as to allow the reading of the information it contains. In the case of the gauge, a Wheatstone bridge and an acquisition card are used. All elements included in the acquisition process are part of the *measurement chain*.

Then, *calibration* enables us to convert the potential difference into the desired mechanical quantity (the *measurand*). This involves using a model corresponding to the measurement system, or an experimental calibration if no effective model exists, to convert the measurement to measurand. The change in the electrical variable with the measurement (derived from the calibration curve) defines the *sensitivity* of a sensor. If the sensor is linear, the sensitivity is independent of the measured value. By definition, a measurement system is never perfect; it is essential to know the *extent of confidence* to assign to the value determined for measurand, and for that, to qualify the measurement chain (uncertainty, linearity, measurement range, influence quantities, durability, response time, bandwidth, etc.).[2]

Finally, the *signal processing* may include, for example, filtering, Fourier or wavelet transforms.

Sometimes, an active link exists between the stress and data acquisition. For example, in the case of large deformations, tensile testing is carried out at constant deformation rate and not at constant displacement speed. In this case, the closed-loop automaticity principles must sometimes be implemented in a difficult context; for example, fracture mechanics.

The objective of the study, which is to compare stress with its effect, can be reflected in two forms: the *presentation* of results followed by *discussion*, or *identification*. The latter is always based on a *mathematically expressible physical model* as a digital model. Minimizing the variance between results of numerical and experimental models requires specifying a distance function between the two (the remainder) and using *specific numerical methods*, the most well-known of them being zero order methods (Nelder–

2 Note that the above description corresponds to a *passive sensor*. In this case, an external source of energy is required; if the sensor is *active*, this means it converts the mechanical energy into an electrical energy signal, and thus no external source is used. In general, in the field of mechanics, passive sensors are used.

Mead), gradient methods (Levenberg–Marquardt), and global research methods (genetic algorithm). The most important advantage of identification is that it leads to knowing the value of one or more parameters of the observed phenomenon; however, a downside of this advantage is the significant amount of time taken for the development and implementation of digital and experimental tools. Furthermore, the main risk involves trying to identify an observed phenomenon even before it is understood or modeled the phenomenon.

Mechanical testing is based on *multidisciplinary expertise*, which is the basis of its numerous advantages but also its challenges, including solid and structural mechanics, material science and engineering, physics, automation, and signal processing. This book could not have possibly addressed all the essential insights; however, it describes, from the experimental approach, the key points of mechanical testing: the concept of the experimental model is detailed through presentation of some conventional testing devices and their instrumentation (Chapters 1 and 2), and also through synthetic presentation of some of the most promising measurement devices (Chapter 3). Furthermore, the establishment of an experimental campaign in an uncertain environment is also discussed; the organizing of tests through experimental design in a space yet to be explored is weighted against the uncertainty of measurement in order to determine the quality of information gathered during the study (Chapter 4).

IN SUMMARY.– An experimental protocol helps to understand a phenomenon, to quantify magnitude (modulus of elasticity, viscosity, etc.) or to validate a calculation. The installation of an experimental device is a process involving various scientific disciplines (mechanical, electronics, signal processing, etc.) ... and above all a lot of diligence and perseverance!

WARNING.– The measurement always changes the measured object (mass accelerometers, etc.). Therefore, a result without uncertainty has no value.

1

Mechanical Tests

1.1. Introduction

The mechanical tests performed in solid and structural mechanics have different objectives, depending on the level of knowledge sought through these tests:

– primarily, *the characterization tests* allow *understanding* of undefined mechanisms. They are particularly useful when the level of knowledge of a problem is low, such as in biomechanics and tribology. They are, therefore, essential elements of modeling and enable the development of analytical, numerical, and experimental models;

– *reference tests* can *quantify intrinsic values* (Young's modulus) and *classify technical solutions* according to extrinsic parameters (e.g. coefficient of friction). These tests should be finely described and reproduced by the scientific community in order to enable valid comparisons. This description, which increases the reliability of a test, is the standard. Various tests performed under sufficiently near operating conditions can be compared and stored in databases;

– the result of reference tests cannot be considered "as is" without verification. In particular, the actual geometry, size, or production conditions require *validation tests* scaled to a structure.

The diversity of the available standardized tests as well as tests related to a product (for example, the maximum deflection of a ski, the elasticity of a support stocking, etc.) render a comprehensive approach quite impossible. Moreover, it is more interesting to draw from certain examples how to

Experimental Mechanics of Solids and Structures, First Edition. Jérôme Molimard.

design a mechanical testing device and how to establish the test-calculation dialogue. The examples selected below are conventional tests of solid mechanics, allowing analysis using a mechanical model of beams. The approach developed for these simple cases is absolutely transposable to more complex cases, where calculation-test dialogue involves high-level tools (optical full field methods, finite element modeling).

The selected tests correspond to the simple loading of a beam: traction, bending, and shear. Fields of stress and strain in the area of analysis must be higher than in other areas so the desired phenomena (e.g. occurrence of cracking or plasticity) appear in this area. For a quantitative analysis, the fields must be described by few parameters, and they must ideally be uniform.

NOTE.– Why use all these test categories? A numerical model, however powerful, cannot describe the complexity of a real object; as it is limited by the computing capacity, imagination of designers, and especially the various assumptions. The most debatable points in any modeling are often the boundary conditions: the rigid (welding, bonding, etc.) or mobile links.

1.2. Measurable quantities

A designer may require various mechanical quantities to design a test, depending on the material and the loading mode. Here are a few examples.

Most materials are linear, elastic, and isotropic. Two parameters are required for their characterization: *Young's modulus*, which represents the proportionality of stress to strain ($\sigma = E \in$) and *Poisson's ratio*, which describes the cross-sectional reduction during unidirectional loading ($\mathrm{v} = -\frac{\in_1}{\in_2}$). Other representations commonly used include Lamé coefficients. In the case of an anisotropic material, the modules are dependent on the direction considered, which considerably increases the experimental protocol. Sometimes, the linear elastic model is set to default; the material may be elastic and nonlinear. In this case, the law of behavior is described by a higher number of parameters.

In most cases, elasticity is a convenient approximation of a material behavior. However, we must remember that more often, even for metals or

glasses, the materials are viscoelastic, which results in a deferred deformation over time, which can be illustrated during a relaxation or creep test. The first step is to observe the variation of force over time to a fixed deformation level, and the second is to observe the variation of deformation for fixed force. In both cases, the elastic behavior is coupled with viscous behavior, characterized by a viscosity μ reflecting the proportionality between shear stress and shear rate $(\tau = \mu \dot{\Upsilon})$.

In order to ensure the behavior of a mechanical part over the short time, the designer uses the *elastic limit* of the material under traction and/or compression, or sometimes resistance to traction. Over the long term, however, there was fracture for light loads, due of the repetition of load. An endurance test is performed to determine the *endurance limit*.

Further, during the shaping of metal parts, permanent deformation is obtained by subjecting the material to plastic deformation. The perfect elasto-plastic model is often too limited. In particular, the more the material is deformed, the greater is the yield strength. The strain hardening rate characterising this phenomenon can be described by the power law or Hollomon law $\sigma = K \in^n$, where *n* is the strain hardening coefficient.

These quantities are probably the most important however there are many others that could be added to the list. Similarly, different types of tests may sometimes lead to identical values. Thus, a static tensile or bending test, a dynamic ultrasonic test or an indentation test all enable us to determine Young's modulus. Therefore, it is more important to outline the logic leading to the selection of a test and the validity of the test selected than to review all possible tests.

1.3. Tensile test

A tensile testing machine consists of two jaws, one on a fixed cross-member, and the other on a movable crosshead. The test specimen is fixed between the two jaws. Then, two measurement systems are used, one to measure the applied force (a load cell) while the other to measure the relative displacement of the jaws (displacement sensor) or the deformation of the specimen (knife extensometer, strain gauge, etc.).

Basically, a tensile testing machine is used to apply a controlled displacement of one of the jaws while the other remains generally fixed to the frame. The process is controlled by controlling displacement and speed of displacement. It is possible on most systems to impose a force ramp via a Proportional-Integral-Derivative (PID) control loop. This feature is advantageous but presents practical difficulties due to the behavior law of the tested material: plastic deformation of the material may lead to never reaching a force set point, as the maximum force is low; fracture may result on returning of force to zero, which induces an infinite displacement set point on PID. Further, the forced displacement speed control does not mean a constant strain rate. Very specific devices have been developed for some polymer materials. They have controlled deformation speed due to optical measurement following markers placed in the area of interest of the specimen.

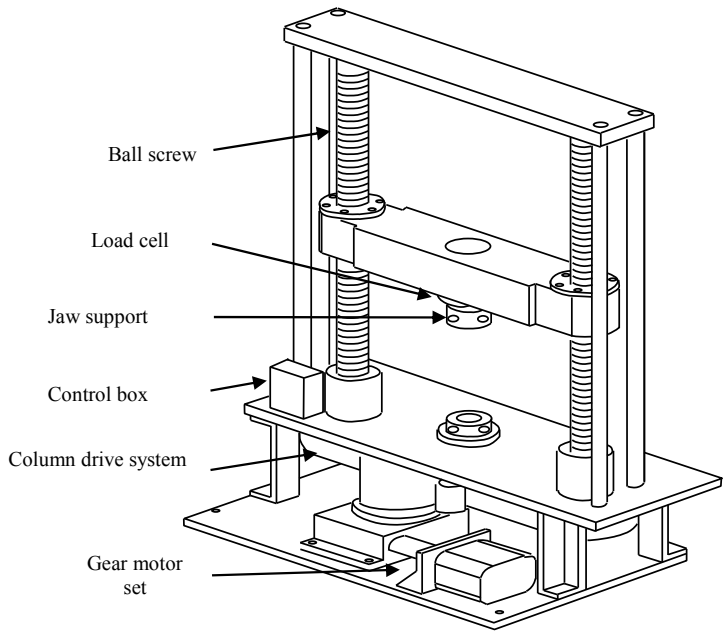

Figure 1.1. *Screw tensile testing machine*

A tensile test does not measure Young's modulus, but measures force (section 2.4) and distance or deformation. While implementing the test, the introduction of an analytical or numerical model enables to deduce the

desired value. This model is based on assumptions that we are trying to prove realistic in the test.

In the case of tensile test, model is provided by the beam mechanics which involves establishing of a uniform stress field through pure traction over the volume under consideration.

1.3.1. *Optimal testing conditions*

In order to obtain a uniform stress in the measurement area, a certain number of precautions must be taken. The shape of the test piece must allow for a well-founded mechanical modeling: its slenderness must be compatible with the rules of the beam mechanics. The ends must be shaped in such a manner that the maximum stress and therefore, the breakage appear in the useful area of the test piece – where the beam mechanics allow correct estimation of the stress.

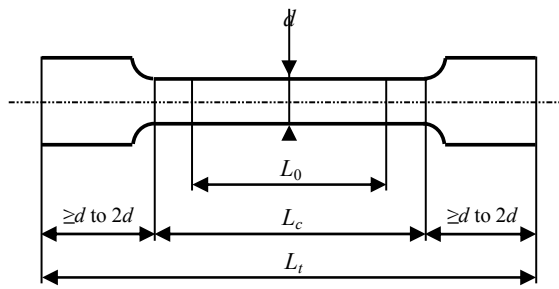

Figure 1.2. *Example of test specimen shape (according to [GOË 92])*

The shape criteria of the test specimens and the selection of anchorages are given by the standards, but an engineer must understand the provenance of these selections. For example, Figure 1.2 shows a test specimen used for determining the elastoplastic characteristics of a metal. The length L_c is the length of the specimen between the jaws; the useful area L_0 corresponds to the area where approximation of stress field by beam mechanics is acceptable. When the test specimen is held between the jaws, the length measurement taken varies from d to $2d$, according to the case. Its cylindrical shape and the presence of large corner radii near the edges provide a break in the relevant area with such consistency that this rupture can occur anywhere

in the area. The heads are in a “dog bone” shape to prevent slippage of the specimen into the jaws during the tensile test. And, the ratio of diameter and length allows establishing a uniform stress field in the useful zone.

However, the anchoring and the length of the test specimen may differ depending on the material and the desired target. For example, in the case of composite materials, the specimen is flat, as the material consists of stacked plies. Therefore, the edge effect is reduced through sealing of wedges whose rigidity is controlled rather than using a dog bone shape, which is difficult to achieve and is less effective. Further, because of anisotropy, the shape of the test specimen can move from one composite to another. The length – width ratio of the specimen depends on the anisotropy of the material, but the width – thickness ratio determines “membrane” or “plate” behavior, as the thickness is not an adjustable parameter; a product is defined specifically by the number of folds it comprises and therefore its thickness: depending on the case, the interpretation model to be used will be different.

For the test to be a tensile test, the movable crosshead displacement vector must be along the axis of the specimen, otherwise the stress field is modified by bending or twisting which disturb the determination of the stiffness of the material and its final properties. However, guidance cannot be linear over a wide range: therefore, it is necessary to take into account the defects in the machine. To minimize these problems, it is a common practice to work along the axis of symmetry, in a known displacement zone. A control and validation protocol is required before running a test campaign: the settings of the jaw position exist on most traction devices. The protocol includes purely geometrical controls, with comparators to check the kinematics of the assembly. It concludes with a test on a test specimen which must be instrumented in order to measure the undesired effects of bending or twisting (for details refer to section 2.2). The test specimen itself must be properly inserted in the tensile testing machine along the axis of traction of the machine. It must not slip into the jaws, especially if the only estimate of the deformation is based on the movable crosshead displacement, a method which is often not recommended for this reason.

Furthermore, in order to approach the conditions set by the test operating model, it may be important to take a number of precautions to prevent the occurrence of undesired phenomena. For certain classes of materials, such as polymeric materials or biological materials, controlling temperature or humidity conditions is a necessity imposed by the high sensitivity of

mechanical properties to these parameters. Similarly, the choice of the speed of displacement of the mobile jaw may change the apparent elastic modulus of the viscoelastic materials: depending on the purpose of the experimental study, tests will be carried out at different speeds so as to explore this behavior, or deliberately placed in a specific location corresponding to the instantaneous or long-term behavior.

All these precautions are intended to have the healthiest possible picture of the intrinsic properties of the material to be studied by freeing approximations related to analytical model used in testing.

EXERCISE 1.1.– Approximate the criteria given in Figure 1.2 using Bernoulli conditions.

1.3.2. *Result of a standard tensile test*

The typical stress–strain curve of a metallic material is given in Figure 1.3. While carrying out a tensile test on a specimen, the stresses are reduced to the axial component and they are assumed to be constant over a section. Hence, $\sigma = \frac{F}{S}$. On the other hand, if the deformation is small compared to other dimensions, we can approximate $\sigma = \frac{F}{S_0}$. Similarly, if the deformation is low if compared with the other dimensions over a length ΔL, then $\varepsilon_{11} = \frac{\Delta L}{L_0}$. However, at the beginning of loading, it is common that parasitic phenomena such as slack recovery may occur. This results in a nonlinear area in the stress-strain curve at the beginning of loading. This area, which is commonly called "toe of the curve" is not representative of the material and must therefore be rejected. Finally, the estimate of the modulus is made in an area defined by the toe of the curve and by early onset of plasticity. Thus, we obtain the equation:

$$E = \frac{\Delta\left(\frac{F}{S_0}\right)}{\Delta\left(\frac{\Delta L}{L_0}\right)} \qquad [1.1]$$

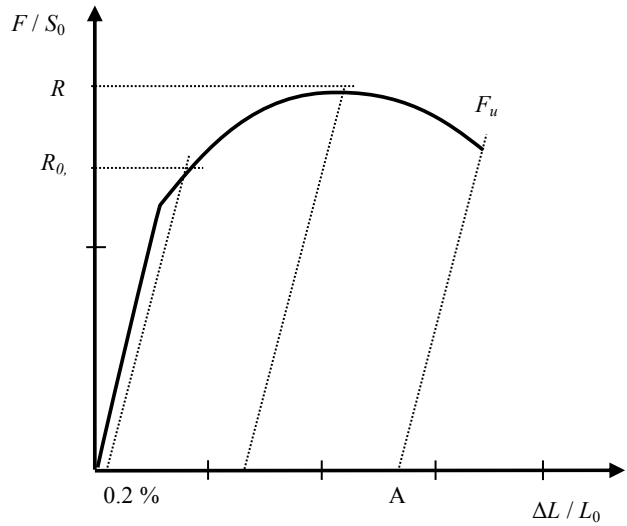

Figure 1.3. *Typical traction curve of a metallic material*

The tensile curve provides other essential information for dimensioning of structures. It is noted that the *apparent elasticity limit* R_e corresponding to the end of the reversibility area of the force/displacement curve, in general, is also the end of the linear area. As this limit is difficult to estimate, we use the *residual elongation limit* $R_{0,2}$ corresponding to an elongation of 0.2%. The *tensile strength limit* R_m is also a determining quantity in mechanics as it characterizes the maximum stress that can be tolerated by the material – and therefore the ultimate limit before failure – whereas the yield point determines its use limit. It must be remembered that the mechanical engineer systematically uses a safety coefficient to take into account the approximations and uncertainties related to operation and production procedures. Lastly, the *percentage elongation after fracture A* corresponds to the variation of ultimate length of the specimen. The interpretation of this data as longitudinal strain would be very hazardous, due to strain localization in the area of striction.

The above curve is that of a hardenable metal; for others, the plastic area can be totally absent. This is the case of brittle materials, the failure limit is then guided by the probability of existence of a defect of sufficient size for a given level of force.

1.3.3. *Stiffness of a tensile testing machine*

The support structures of the machine are not infinitely rigid; they give way to deformation under load, thus changing the movement of the movable jaw. If u is considered as the total displacement, $u_{machine}$ the displacement due to deformation of the tensile testing machine and $u_{specimen}$ is the displacement due to deformation of the test specimen, then

$$u = u_{machine} + u_{specimen} \quad [1.2]$$

or, if F is the force measured by the load cell, K is the rigidity of the tensile testing machine, then S and L_0 respectively are the section and initial length of the sample and ε is the deformation, then

$$u = \frac{F}{K} + \varepsilon L_0 \quad [1.3]$$

The strain rate is an important factor in the study of visco-elastic-plastic materials and must be controlled; many tests are ideally performed at constant strain rate. By deriving the expression [1.3] with respect to time, the relationship between transverse displacement rate and strain rate is given by:

$$\frac{\dot{u}}{L_0} = \left(1 + \frac{S}{KL_0}\frac{d\sigma}{d\varepsilon}\right)\dot{\varepsilon} \quad [1.4]$$

where $\dot{u}$ is the movable crosshead displacement rate and $\dot{u}$ is the strain rate of the material.

There is a difference between apparent strain rate, $\dot{u}/L_0$ which is a constant for controlling a conventional tensile testing machine and the average strain rate $\dot{\varepsilon}$. The condition $\dot{u}/L_0 \approx \varepsilon$ is fulfilled only if K i.e. the rigidity of the frame is sufficiently large. In addition, the value $d\sigma/d\varepsilon$ represents the hardening of the material. In many cases, the material has several consolidation stages; therefore, hardening is not a constant with respect to deformation level and consequently with respect to the strain rate.

In the elastic range, the stiffness of the test device has no influence; however, in the plastic range, the stiffness disturbs the strain rate of the specimen, thus complicating the interpretation of the test results. It is therefore necessary to have an estimate and make the necessary corrections.

1.4. Bending test

1.4.1. *Test principle*

In the case of particularly soft materials, the degradation of the surfaces in the jaw leads to another test, the bending test. The application presented here is a three-point bending test for the characterization of unidirectional composites[1]. The bending test involves placing a rectangular bar on two supports and applying "punctual force" in the center, as shown in Figure 1.4.

The load and the resultant deflection are recorded until the occurrence of damage on one side of the specimen. During the operation, the flexural modulus and admissible maximum load are the two main results considered.

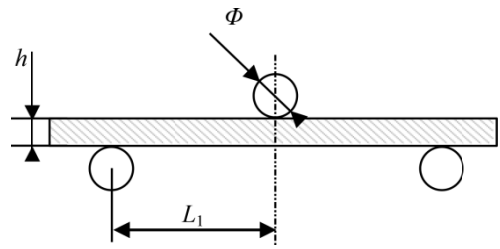

Figure 1.4. *Three-point bending*

1.4.2. *Optimal realization conditions*

The main parameters to be adjusted are summarised in Figure 1.4. This primarily involves ensuring the conditions of a typical beam pattern, by creating conditions of small disturbances. The load should be as close as possible to pure bending. However, for a three-point bending, the bending moment increases linearly from zero to its maximum value between the first and second point, and then decreases from the maximum value to zero between the second and the third point. However, the shear force is equal to and opposite to the bending moment gradient. In a three-point bending test, bending is always combined with shear. In order to approach the pure bending condition, it is necessary that the bending gradient is negligible. For this, the sample must be sufficiently slender. In other words, the ratio L_1/h must be greater than a limit value, usually set at 8. A test with close edges

1 NF EN 2562 standard.

will induce shear stresses and inter-laminar shear failure. This possibility is also used in the "short beam shear test"[2]. In this case, $L_1/h \leq 2.5$.

In this test, the *support structure* plays an important role. On the one hand, it must not generate too much local pressure, and thus damage the surface; secondly, the contact must remain "punctual", i.e. must be of the smallest possible width. A "punctual" contact in the model becomes in reality a contact area on a given depth, called a "linear" contact. It is therefore necessary that both lower and upper supports are parallel. It is also necessary to ensure sample faces are parallel to each other. Finally, the force applied in the form of a translational movement of the upper cylinder, must be normal to the plane formed by the lower contacts. In practice, these conditions are guaranteed by some design precautions: one of the two lower supports is mounted on a pivot connection, so that it can tilt back and forth; and similarly for the upper supports.

As previously stated for a tensile test, the test specimen shall be placed in the machine's plane of symmetry to avoid any undesirable effect.

1.4.3. *Determination of flexural modulus*

In order to determine the flexural modulus, we must find a mathematical model representing the mechanical phenomenon reproduced experimentally during the test. Here, the test conditions are selected such that the assumptions of the beam mechanics are valid. If $(\vec{x}, \vec{z})$ is the reference of the beam, where $\vec{x}$ is the longitudinal axis, M_f the bending moment, E the Young's modulus of the beam and I_f the bending inertia, the transverse displacement W along the beam axis is given by the equation:

$$\frac{\partial^2 W(x)}{\partial x^2} = -\frac{M_f(x)}{EI_f} \qquad [1.5]$$

For each section at position x, the strain $\sigma_x(x, y)$ is given by: $\sigma_x(x,z) = \frac{zM_f(x)}{I_f}$, where y is the distance to the neutral axis. The bending

2 NF EN ISO 14130 standard.

moment is $M_f = \frac{Fx}{2}$ before the central cylinder and $M_f = \frac{F(L_1 - x)}{2}$ after (F is the applied force). The maximum stress is, therefore, given by $x = L_1$ and z = $h/2$.

$$\sigma_{\max} = \sigma_x\left(L_1, \frac{h}{2}\right) = \frac{FL_1 h}{4I_f} \qquad [1.6]$$

Similarly, the deflection can be calculated using the tools for beam mechanics. Thus, by integrating equation [1.5], and considering that at $x = L_1$, slope is zero, as the fixed jaws are on the exterior,

$$W(x) = \frac{FL_1^3}{12EI_f}\left(3 \times \frac{x}{L_1} - \left\{\frac{x}{L_1}\right\}^3\right) \text{for } x \le L_1 \qquad [1.7]$$

The maximum deflection corresponding to $x = L_1$, given by:

$$W_{\max} = \frac{FL_1^3}{6EI_f} \qquad [1.8]$$

From the measurement of deflection and the force applied, it is easy to estimate a flexural modulus of elasticity. Note that the standard recommends the use of the central part of force/deflection curves. This means that larger values must be discarded to eliminate the loosening due to the onset of defects ("pseudo-plasticity" of composites). The *toe of the curve* must also be ruled out.

Furthermore, the model described above assumes that a section normal to the neutral axis remains normal during loading, which neglects the shear (Euler–Bernoulli hypothesis). For some anisotropic materials, whose shear stiffness is significantly lower than other rigidities, this assumption is no longer valid and the deflection is due both to bending and shear. A beam model must be used to turn the right sections during the deformation which leads to the expression of a constant shear in the section (Timoshenko hypothesis).

1.4.4. *Damage to the structure*

In this bending test, three types of damage may be encountered (Figure 1.5), of which only two are admissible: tensile damage and compressive damage. They are related to the effect of bending and therefore enable to quantify the maximum stress with the above-stated assumptions. If shear damage is observed, then this quantification is not possible, and it is observed that the test assumptions are not met.

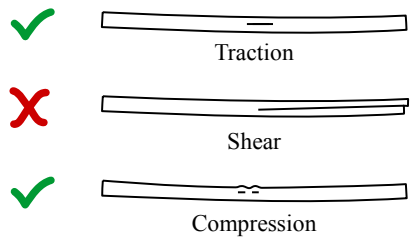

Figure 1.5. *Types of damage during a 3 point bending test. Damage due to traction and compression are consistent; inter-laminar shear damage is non-consistent*

From the force, the maximum stress is known, which allows estimation of the bending resistance of the material. However, it is notable that the resistance values for bending are always higher than those for traction. The reason is the cause of failure, which is always related to the presence of a defect. In tensile test, the entire volume is subjected to maximum stress, whereas in bending only the skin is at maximum stress. The probability of finding a fault in a volume increases therewith. It is described using Weibull distribution law: $F(x) = 1 - \exp\left\{-\left(\frac{x-d}{\eta}\right)^{\beta}\right\}$.

NOTE.– We often speak of "flexural modulus" or "tensile modulus" or "compression modulus". These modules are unique and often confused with the elastic modulus or Young's modulus. If this practice exists, it is reflected as a reality difficult to circumvent: *in most cases, the result depends on the test methods*. A designer therefore must adapt the test carried out to the load type experienced by the actual structure.

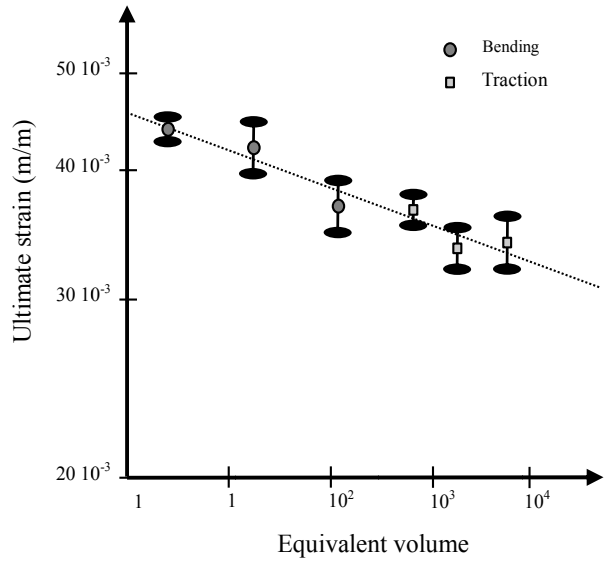

Figure 1.6. *17 Variation of ultimate strain with volume (according to [WIS 97])*

EXERCISE 1.2.– A four-point bending test also exists (refer to Figure 1.7).

Prepare the model for the test. What are its advantages? What are the specific precautions required for this testing? In particular, how to measure the deflection using this method?

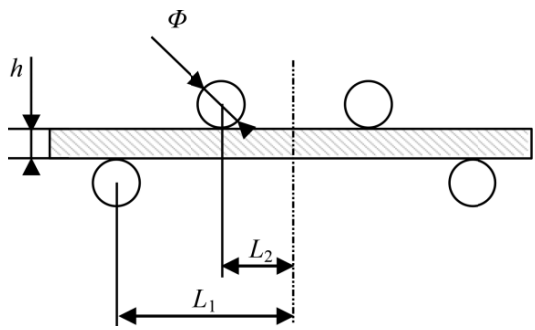

Figure 1.7. *Four-point bending*

2

A Few Sensors Used in Mechanics

2.1. Introduction

The conventional sensors used in solid and structural mechanics essentially allow the measurement of displacement, strain, force, and acceleration. Though other measurements such as speed, temperature, and humidity are also possible, these are not discussed in this chapter. Again there is no possible way to measure stress: it can only be accessed using a model or previously-acquired data.

The measurements of displacement, strain, force, and acceleration can be obtained using various different technologies. However, only a few that are described below. These technologies are very commonly used and also allow discussion on the metrological quality of the sensors and the criteria for the most common choice.

2.2. Strain measurement

2.2.1. *Principle*

The most common method used to measure strain is the strain gauges. The physical principle is as follows: the resistance of a conductor R is a function of the length of the wire L, its cross-section A and resistivity ρ:

$$R = \frac{\rho L}{A} \qquad [2.1]$$

Experimental Mechanics of Solids and Structures, First Edition. Jérôme Molimard.

by applying the differential logarithm, we get:

$$\frac{dR}{R}=\frac{dL}{L}+\frac{d\rho}{\rho}-\frac{dA}{A} \qquad [2.2]$$

Under conditions of simple traction, there is a relation between section change and length change. By introducing the Poisson ratio of the metal used υ,

$$\frac{dA}{A}=-2v\frac{dL}{L} \qquad [2.3]$$

therefore:

$$\frac{dR}{R}=\frac{dL}{L}(1+2v)+\frac{d\rho}{\rho} \qquad [2.4]$$

The sensitivity of the gauge is the ratio of relative change in resistance and relative change in length. By introducing the modulus of elasticity E, the equation is given as:

$$\frac{dR/R}{dL/L}=(1+2v)+E\left(\frac{1}{E}\frac{d\rho/\rho}{dL/L}\right) \qquad [2.5]$$

The term $\Pi=\frac{1}{E}\frac{d\rho/\rho}{dL/L}$ is sometimes referred to as *piezoresistivity coefficient*. Note that this ratio is pertinent only in the linear elastic region of the wire gauge.

2.2.2. Gauge factor

The sensitivity of the gauge $\frac{dR/R}{dL/L}$ is referred to as the gauge factor (GF). It is given by the manufacturers, and is highly dependent on Poisson's ratio of the material used. For the most common gauges $v\approx 0.3$ and $\frac{dR/R}{dL/L}\approx 2$ so the resistivity is virtually unchanged with strain $\left(\frac{d\rho/\rho}{dL/L}\approx 0\right)$. Various gauge factors are given for illustrative purposes in Table 2.1.

Material	*Gauge factor*
Steel	2
Tungsten platinum alloy	4.1
Nickel, steel alloy (Elinvar)	2.5
Chromium, nickel alloy (Nichrome)	2.5
Nickel copper alloy (Constantan)	2.1
Iron copper chromium nickel alloy (Karma)	2.1
Nickel manganese copper alloy (Manganin)	0.5
Semi-conducters	100 to 200

Table 2.1. *Gauge factor for various materials*

The sensitivity of a gauge (the gauge factor) is established for specific conditions. Its use can be complicated and corrections may be necessary at times [AVR 74]. These corrections are required due to interactions between the gauge and its environment. For example, if the structure on which the gauge is placed is not in a situation locally similar to a simple traction, or the Poisson ratio of the structure is different from that of the gauge, undesirable cross effects may occur. They induce an error which can be expressed as:

$$e_L = \frac{K_t \left(\varepsilon_L / \varepsilon_a + v_{po} \right)}{1 - v_{po} K_t} * 100 \qquad [2.6]$$

Where ν_{po} is Poisson's ratio of the support material, K_t is the coefficient of transverse sensitivity of the gauge, ε_L is axial strain and ε_a is transverse strain ε_a.

2.2.3. *Description of a gauge*

The typical architecture of a gauge is reproduced Figure 2.1. In order to increase the resolution of the acquisition system linked to the gauge, the latter comprises of a frame and two lugs for connection to the conditioning system. The metal frame is placed on a resin film for electrical protection and isolation. The glue and resin play an important role in transmitting strain. Both these elements should be treated with caution: *defective gluing* may cause an incorrect response on the gauge. On the other hand, the

application range of the gauge and the glue is limited in terms of temperature. It ranges between -270°C and 290°C, depending on the materials used.

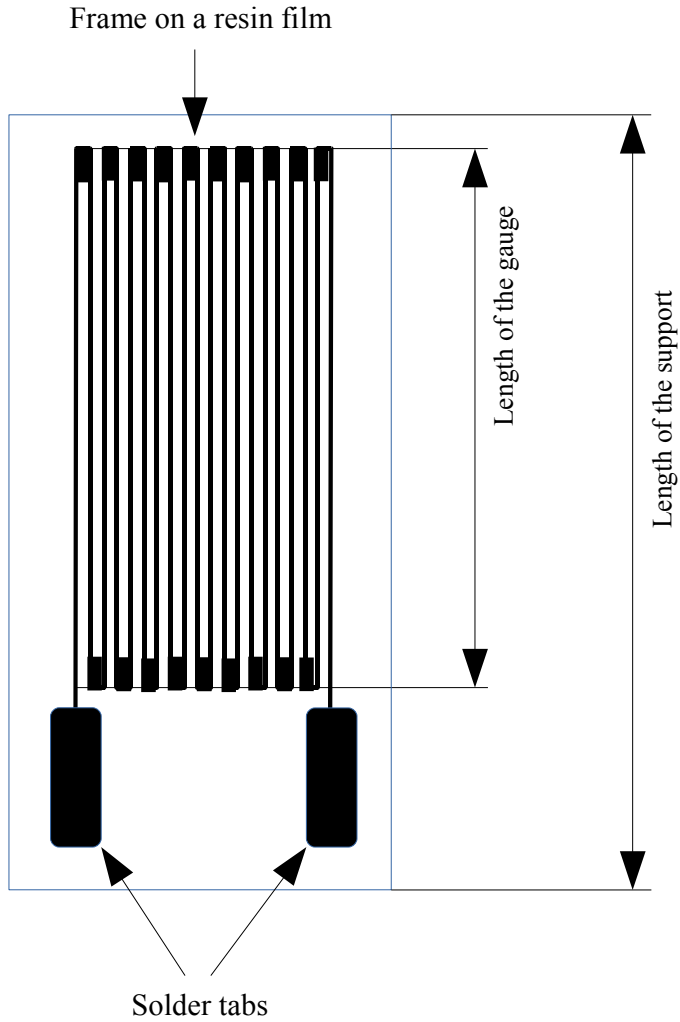

Figure 2.1. *Representation of the main elements of a strain gauge*

The shape of the gauges can be varied depending on the required application type: bending, torsion, tension, concrete, etc.

During the practical application of a gauge, various points must be taken care with precision:

– the gauge is sensitive in the *direction* of its conducting wires. The orientation of the gauge with respect to the studied strain must be achieved with precision;

– the *size of a gauge* provides the *spatial resolution* of the sensor. This point must sometimes be treated with caution. At maximum strain, the size of the sensor will limit the apparent maximum, depending on the strain gradient;

– on the other hand, in the case of a *heterogeneous material*, the size of the gauge must be relevant to the size of heterogeneities.

QUESTION.– Since the gauges are often made of Constantan (55% Copper and 45% Nickel), whose resistivity is $\rho = 1.7 \times 10^{-8}\ \Omega$m, what is the length required to obtain a resistance of 120 Ω, given that the minimum diameter is 0.025 mm?

2.2.4. *Conditioning*

The *conditioning* of a strain gauge is effected by means of a *Wheatstone bridge*. Figure 2.2 shows the simplest installation, a "quarter bridge" circuit. If the resistance R_1 varies by δR, then the potential difference δV_0 is related to the variation of resistance and the power supply voltage V_a, given by the following equation:

$$V_0 + \delta E_0 = V_a \frac{(R_1 + \delta R) R_4 - R_3 R_2}{(R_1 + \delta R + R_2)(R_3 + R_4)} \qquad [2.7]$$

If the various resistances are equal (R_1=R_2=R_3=R_4=R), the voltmeter indicates a difference of zero potential (V_0 = 0). Insofar as the variation in resistance is very small compared with the resistance itself ($\delta R/R << 1$), equation [2.7] is given as:

$$\frac{\delta V_0}{V_a} = \frac{\delta R / R}{4 + 2(\delta R / R)} \approx \frac{\delta R / R}{4} \qquad [2.8]$$

The Wheatstone bridge balancing hypothesis is fulfilled in practice by using a variable resistor either on one of the branches of the bridge, or simultaneously on both the branches. This technique remains valid only if the resistance variations are low.

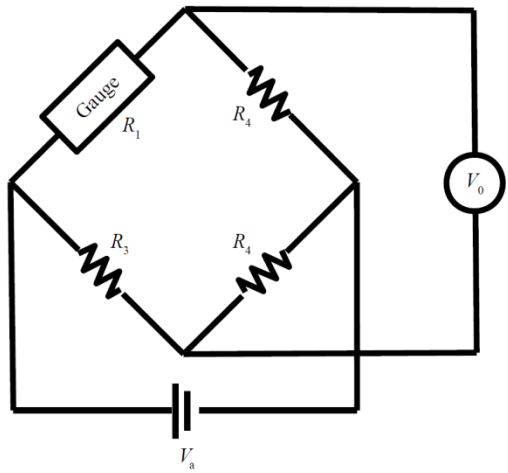

Figure 2.2. *Quarter bridge assembly*

2.2.5. *Multi-gauge assemblies*

Mounting gauges on the different branches of a Wheatstone bridge can lead to more interesting results than the simple quarter-bridge assembly, especially in the case of load cells. The electrical analysis of resistance changes on each of the branches of the Wheatstone bridge indicates:

In general,

$$V_0 = V_a \left[\frac{R_1}{R_1 + R_2} - \frac{R_3}{R_3 + R_4} \right] \qquad [2.9]$$

the sensitivity V_0 related to the change in each resistor is given by:

$$dV_0 = \sum_{i=1}^{4} \frac{\partial V_0}{\partial R_i} dR_i \qquad [2.10]$$

$$\text{or } dV_0 = V_a \left[\frac{R_2 dR_1 - R_1 dR_2}{(R_1 + R_2)^2} + \frac{R_3 dR_4 - R_4 dR_3}{(R_3 + R_4)^2} \right] \qquad [2.11]$$

assuming $dR_i << R_i$ and introducing the deformation associated with each strain gauge by the corresponding gauge factor or $dR_i = GF_i \varepsilon_i$, we obtain:

$$\frac{\delta V_0}{V_a} = \left[\frac{R_1 R_2 (\varepsilon_1 GF_1 - \varepsilon_2 GF_2)}{(R_1 + R_2)^2} + \frac{R_3 R_4 (\varepsilon_4 GF_4 - \varepsilon_3 GF_3)}{(R_3 + R_4)^2} \right] \qquad [2.12]$$

If the gauges are identical (and therefore, $R_i = R$, and $GF_i = GF$, for all i in [2.12]), we obtain:

$$\frac{\delta V_0}{V_a} = \frac{GF}{4} (\varepsilon_1 - \varepsilon_2 + \varepsilon_4 - \varepsilon_3) \qquad [2.13]$$

This is the basic equation for bridges with several gauges. It is observed that the gauges on opposite arms are summed whereas the gauges on adjacent arms are subtracted. This property will be used below to perform thermal compensation or to remove unwanted deformations.

2.2.6. *Compensation of bending effects*

In tensile testing, adverse effects due to sample bending may occur. In order to remove these effects, two identical gauges are bonded to either side of the specimen in the direction of traction. When the gauges are connected to opposite arms of the bridge (1 and 4 positions), the potential variation is given as:

$$\frac{\delta V_0}{V_a} = \frac{GF}{4} (\varepsilon_1 + \varepsilon_4) \qquad [2.14]$$

A beam of Young's modulus E, cross-section S and bending inertia I_f simultaneously subject to traction F and to parasitic bending M_f undergoes a distressed axial deformation. According to the conventional notation used, the deformation on each side is:

$$\varepsilon_1 = \frac{1}{E} \times \left(\mp M_f b / I_f + \frac{F}{S} \right) \quad [2.15]$$

$$\varepsilon_4 = \frac{1}{E} \times \left(\pm M_f b / I_f + \frac{F}{S} \right) \quad [2.16]$$

b is half the thickness of the specimen. Combining [2.14] with [2.15] and [2.16], leaves behind only the membrane effects. The reading value is not disturbed by bending effects:

$$\frac{\delta E_0}{E_1} = \frac{GF}{4} \frac{F_N}{Ebh} \quad [2.17]$$

QUESTION.– What would we do to remove the membrane effects and record the effects of bending?

2.2.7. *Effect of temperature*

Temperature is a factor that strongly influences the response of a gauge. It is sometimes necessary to remove its effect (*in situ* monitoring, aging cycles, etc.). An appropriate assembly enables to retain the mechanical stress component while supressing thermal expansion. A gauge is placed on the structure to be tested while another one with similar characteristics is placed on a mechanically non-loaded sample of the same material. The gauges are placed at adjacent positions, for examples 1 and 2. In this case,

$$\frac{\delta E_0}{Ea} = \frac{GF}{4}(\varepsilon_1 - \varepsilon_2) = \frac{GF}{4}(\varepsilon_{mechanical} + \varepsilon_{thermal} - \varepsilon_{thermal}) = \frac{GF}{4}\varepsilon_{mechanical} \quad [2.18]$$

Similarly, any identical gauge torque shall compensate the temperature effects if they are mounted on adjacent arms. More generally, Figure 2.3 reproduces the various standard configurations for compensation.

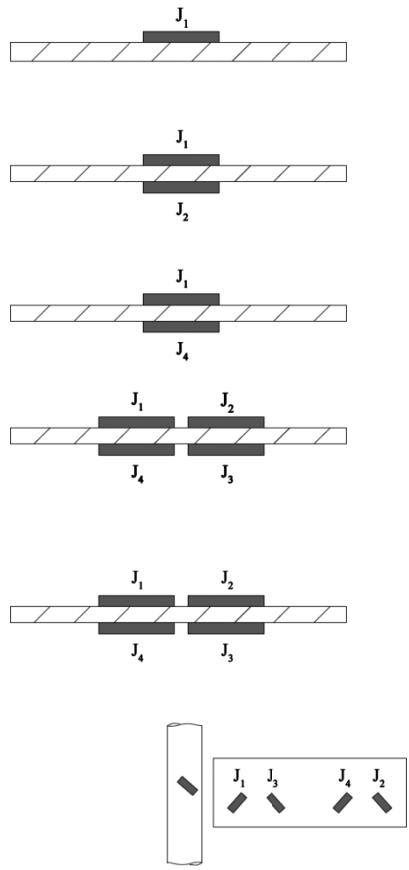

Figure 2.3. *Various assemblies and compensations*

2.2.8. *Measurement of a surface-strain tensor of an object*

A Rosette Mounting is a mount with three gauges that helps in assessing the state of strain of a plate. The gauges can be arranged at 45°, 60°, or 120°. In this section, however, we shall consider only the last case. We shall consider the classical assumption of planar stresses.

The strain in the plane is given by: $\begin{Bmatrix} \varepsilon_{11} & \varepsilon_{12} \\ \varepsilon_{12} & \varepsilon_{22} \end{Bmatrix}_R$. ε_{33} exists but it is not operated in planar stresses; moreover, it would not be accessible experimentally. The questions to be addressed by the mechanic are:

– What are the main directions?

– What is the value of the principal strain?

The problem with the Rosette Mount is that it has three unknowns: orientation of the main frame Φ_P and two principal strains ε_p and ε_q based on three available pieces of information ε_A, ε_B, and ε_C. To put it correctly, consider the rotation in the plane of the strain tensor; each of the gauges constituting the Rosette has a known rotation to a constant with respect to the main frame. The strain in the direction of each of the gauges can be easily expressed in terms of Φ_P, ε_p, and ε_q. Therefore:

$$\begin{Bmatrix} \varepsilon_A \\ \varepsilon_B \\ \varepsilon_C \end{Bmatrix} = \begin{bmatrix} \cos^2\Phi_P & \sin^2\Phi_P \\ \sin^2\left(\Phi_P + 2\frac{\pi}{3}\right) & \cos^2\left(\Phi_P + 2\frac{\pi}{3}\right) \\ \sin^2\left(\Phi_P + 4\frac{\pi}{3}\right) & \cos^2\left(\Phi_P + 4\frac{\pi}{3}\right) \end{bmatrix} \begin{Bmatrix} \varepsilon_p \\ \varepsilon_q \end{Bmatrix}_{princ.} \quad [2.19]$$

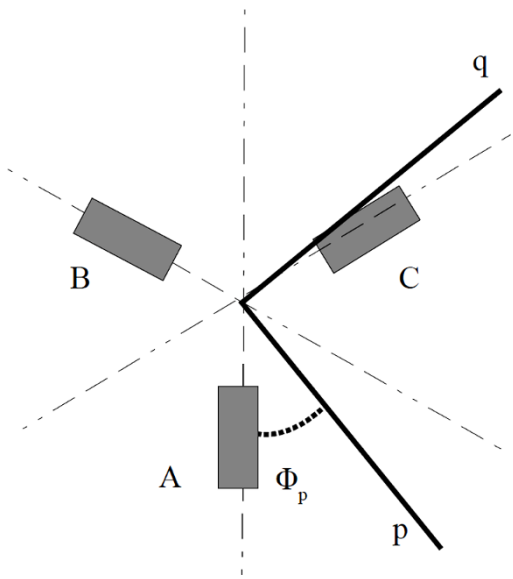

Figure 2.4. *Rosette mounting at 120°*

This system is nonlinear and the values of Φ_P, $\varepsilon_{p,}$ and ε_q are significant. By carefully recombining the deformations, we obtain:

$$\varepsilon_{p,q} = \frac{\varepsilon_A + \varepsilon_B + \varepsilon_C}{3} \pm \sqrt{(\varepsilon_A - \varepsilon_B)^2 + (\varepsilon_A - \varepsilon_C)^2 + (\varepsilon_B - \varepsilon_C)^2} \qquad [2.20]$$

and

$$\text{if } \varepsilon_A > \frac{\varepsilon_B + \varepsilon_C}{2} \text{ then } \Phi_p = \frac{1}{2}\tan^{-1}\left(\frac{\sqrt{3(\varepsilon_B - \varepsilon_C)}}{(\varepsilon_A - \varepsilon_B) + (\varepsilon_A - \varepsilon_C)}\right)$$

$$\text{if } \varepsilon_A = \frac{\varepsilon_B + \varepsilon_C}{2} \text{ then } \Phi_p = \frac{\Pi}{4} \qquad [2.21]$$

$$\text{if } \varepsilon_A < \frac{\varepsilon_B + \varepsilon_C}{2} \text{ then } \Phi_p = \frac{1}{2}\tan^{-1}\left(\frac{\sqrt{3(\varepsilon_B - \varepsilon_C)}}{(\varepsilon_A - \varepsilon_B) + (\varepsilon_A - \varepsilon_C)}\right) - \frac{\Pi}{2}$$

If $\varepsilon_A - \varepsilon_B - \varepsilon_C$, all directions of the plane are the main directions and the angle Φ_P cannot be determined.

2.2.9. "*Measurement" considerations*

– The theory developed above assumes a linear response of the gauge. Unfortunately, this is not always the case, and here, the quality of the gauge-structure transmission is essential. There may be a drift and hysteresis during the first loading. Generally, the nonlinearity error must be of 0.1%.

– The dynamic response of a gauge poses no problem in general because of its very low inertia. A limitation with respect to the size of the gauge appears for large loading rates in case of periodic stresses: if the size of the gauge is three times smaller than the mechanical wavelength, it cannot give any indication in accordance with the Shannon theorem. For a standard gauge (10 mm) glued onto a steel structure, the minimum accessible period is 6 μs.

– Because of their low inertia, gauges are capable of following dynamic strain, even at very high frequencies. However, since the strains are

phenomena which occur in the speed of the wave, a smaller frontal wave or the one with the same dimension of the gauge will not provide any indication. In general, the gauge should have 1/10 the size of the wavelength.

– The resistance of a strain gauge causes a local heating due to Joule's effect. This heating is dissipated by the tested specimen. For polymeric materials, whose thermal conductivity is low and the dependence of the mechanical properties to the temperature is pronounced, the resistance is limited to 120 Ω. For metallic materials which are less sensitive to temperature and top conductors, the resistance of the gauges is 250 Ω.

– *The gauge allows values only on the surface of a sample* thus volume strain remain inaccessible through the experiment.

– When we know a priori the shape of the deformation field undergone by the specimen, a single gauge can be sufficient, but in the general case, three gauges are required to record the status of full biaxial deformation. In this case, the presented-previously Rosette Mountings are used.

Note that the deformation measurements can also be made using other methods, though they are very rarely employed:

– these include strain gauges made of semiconductor materials (silicon crystals) whose resistivity changes with deformation. They are the basis of force or pressure sensors, but do not have direct application as strain sensors;

– optical methods are also used (interferometry, image correlation, optical fibers, photoelasticimetry, etc.). Some of these are discussed in detail in Chapter 3.

IN SUMMARY.– Gauges are sensitive to strain and temperature. Size and position of a gauge must always be considered with respect to the set objective. And *there are no methods available for measuring stress*.

Furthermore, the semiconductor gauges are made of a semiconducting material, usually single silicon crystal (N-type) doped with P-type impurities. Under the effect of stress, the density of the charge carriers and their mobility varies anisotropically. The resistivity is given by the equation:

$$\rho = \frac{1}{en\mu} \qquad [2.22]$$

where e is the charge of an electron, n is the number of charge carriers per unit volume and μ is the average carrier mobility. The current gauge factors are much higher than for conventional piezoresistive gauges (π = 160-180).

2.3. Displacement measurement

There are various possible displacement measurement methods. By derivation, or more precisely by comparing the variation length to the length, it is possible to have a rough image of the strain. However, this method is not recommended because the spatial resolution is very bad. The LVDT (Linear Variable Differential Transformer) sensor is currently one of the most popular displacement measurement methods available.

2.3.1. *Principle*

This sensor works on the principle of induction variation in a conductor coil linked to magnetic field variations. The diagram of the principle is represented in Figure 2.5. A primary coil is surrounded by two secondary coils. The primary coil is subjected to alternating current; the two secondary coils are connected in series and receive only the current induced by the first coil. The movement of the magnet disturbs the induced field.

If the displacement is sufficiently small, that is to say, if the magnet is not pulled from the coil space, then the amplitude of the voltage reading at the terminals of the secondary coils varies linearly with the displacement. By symmetry, this amplitude is zero when the magnet is centered with respect to the coils (x = 0). The direction of movement is given by 180° phase change at x = 0.

2.3.2. *Key characteristics*

As the information recorded is the amplitude of the induced current, the frequency of the signal sent to the primary circuit should be at least 10 times greater than the highest frequency of the phenomenon to be measured. The maximum permissible signal is commonly less than 2.5 kHz. The LVDT sensors show measurement error less than 0.05% and a repeatability of 0.0001 mm.

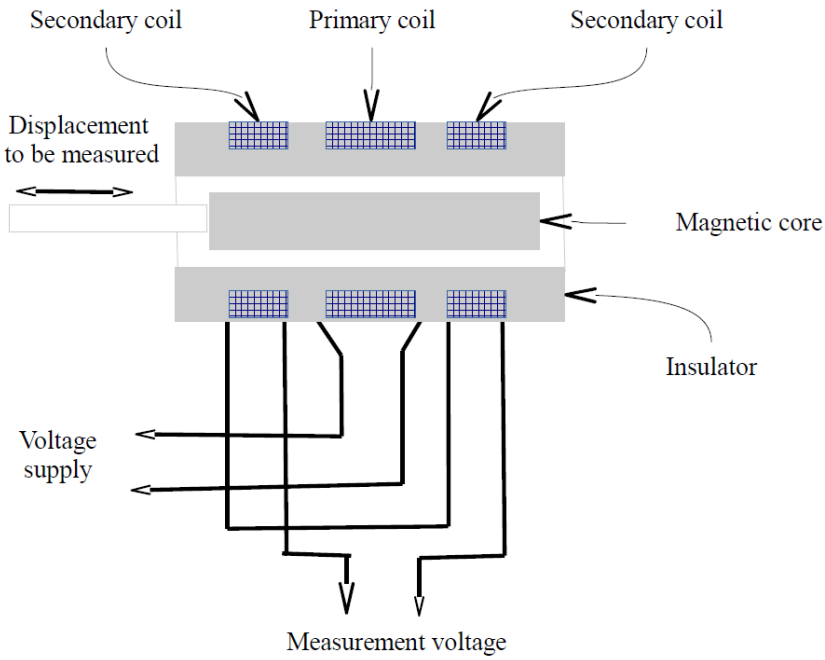

Figure 2.5. *Schematic diagram of a LVDT sensor (according to [FIG 00])*

QUESTION.– There are other measurement methods based on optical or mechanical principles. Imagine a mechanical system based on the strain gauge technology for measuring a displacement of a few tenths to a few tens of millimeters.

2.4. Force measurement

2.4.1. *Strain gauge load cell*

A first set of force sensors is based on the deformation of a test body. This deformation is measured by a set of strain gauges. The relationship between the voltage reading at the terminals of the Wheatstone bridge and the force varies with respect to the geometry of the test body. Various types of sensors are shown in Figure 2.6. It shows the locations of strain gauges required to estimate the force for each sensor. Because of the bending of these two sensors, strain gauges placed on either side of the blades are subjected to most of the deformation.

It is very common to use a bending test body. Insofar as the maximum strain does not exceed the elastic limit, the deformation ε is proportional to the applied force F, according to the standard material resistance formula:

$$\varepsilon = \frac{xb}{EI_f} F \qquad [2.23]$$

where x is the distance between the measuring point and the point of application of force and b is the distance of the sensor at the neutral axis, E is Young's modulus of the material and I_f the inertia of bending of test body.

The selection of geometry of test body depends on the desired sensitivity, force type, or desired stiffness. Another selection criterion is the robustness of the sensor: some are equipped with stops for limiting their deformation and thus ensure that the test body remains in the elastic domain.

The nature of the material used to make the test body has an important influence on the measurement. In order to obtain a linear response of the sensor, it is necessary to use a linear elastic material. The measurement range is limited by the yield strength of the sensor. The sensitivity, in turn, is related to the value of Young's modulus: a soft material amplifies the deformations and allows the measurement of small forces. However, it must be noted that sometimes the deformation of a sensor inserted in a mechanical system is detrimental to its operation. This is the case for any mechanical system controlled in position (tribometers, rolling mills, etc.).

2.4.2. *Piezoelectric gauge load cell*

Certain materials are polarized with respect to the force applied to them – this is the principle of quartz watch oscillator. The intensity of the load is proportional to the force produced, and it follows the sign of the force.

Two metal plates are placed on either side of the sensor to accumulate the charge; the resulting assembly constitutes a capacitor which, however, is unfortunately flawed so that only dynamic phenomena can be measured easily.

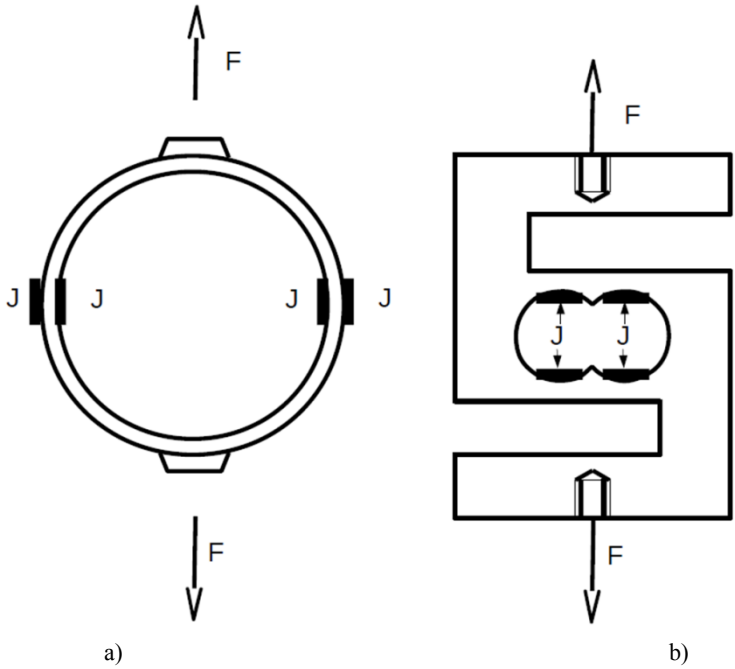

Figure 2.6. *Example of strain-gauge force sensor; a) Force washer with low load, b) S sensor*

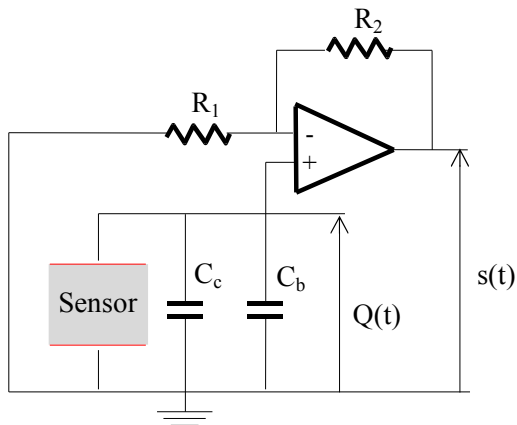

Figure 2.7. *Assembly of a voltage amplifier*

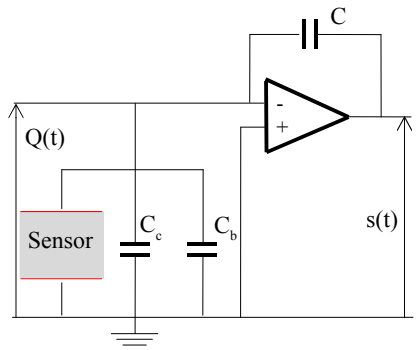

Figure 2.8. *Assembly of a load amplifier*

The charge emitted by a crystal is low, such that it is necessary to *amplify the signal*. Two possible arrangements are shown Figures 2.7 and 2.8. The capacity C_b corresponds to the capacitance of the coaxial cable whereas C_c is the capacitance of the sensor. In addition, the sensor delivers a charge $Q(t)$. The output voltage $s(t)$ is given respectively in each case, by the following equations:

$$s(t) = \left(1 + \frac{R_2}{R_1}\right) \frac{Q(t)}{C_c + C_b} \qquad [2.24]$$

$$s(t) = -\frac{Q(t)}{C_c} \qquad [2.25]$$

While in the first case (*voltage amplifier*), the output voltage depends on the capacitance of the coaxial cable (and therefore on its linear capacitance and length), the voltage of the second circuit (*charge amplifier*) does not depend on the length of the cable, even though its resistance is negligible. The first assembly which is easier to install, requires a major precaution: it must be calibrated with the cable in place. In the second case, it must be ensured that no charge can be created in the cable, especially the original triboelectric charges related to friction from various parts of the cable. Furthermore, the cable insulation and connection must be done correctly to ensure proper load transfer in the circuit.

So there is a choice between a robust assembly, whose sensitivity depends on the cable length, and a sensitive assembly, where each element must be installed carefully to ensure the quality of the measurement.

From a mechanical point of view, the piezoelectric sensor must be considered dynamic, and therefore, as a mass-spring-damper system. Due to its high stiffness (as compared to previous assemblies), its natural frequency is very high so that this assembly is intended for very high frequency applications (up to tens of kilohertz). In practice, the crystal is pre-stressed between two plates whose function is to distribute the force over its entire surface. The pre-stress enables measuring the tensile and compressive forces. Increasingly, however, several systems based on of piezoelectric sensors adapted for static measurements are available in the market nowadays.

From the measurement point of view, this type of sensor has several advantages:

– great adaptation to dynamic phenomena (to be compared with the mass of the sensor and the necessary connecting parts!);

– maximum temperature of 200°C;

– good linearity (less than 1%);

– good sensitivity (0.05 to 10 mV/N);

– large rigidity (E_{quartz} = 75 MPa);

– resolution ranging up to 10^{-6} of the measurement scale;

– permissible overload up to 300% of rated capacity.

However, the sensor has a disadvantage of a *higher transverse susceptibility*, related to poor distribution of the mechanical load on the crystal surface:

QUESTION.– This section concentrates exclusively on the problem related to force measurement. However, there is also another very important mechanical problem: torque measurement. With the insights obtained through this chapter, imagine how to construct a torque-meter, and what will its performance be? It is your turn!

2.5. Acceleration measurement

2.5.1. *Principle*

The acceleration measurement is based on the principle of a "seismic mass" acting on a spring, either in tension or bending or shear. In the case illustrated in Figure 2.9, the displacement x of the mass is proportional to acceleration.

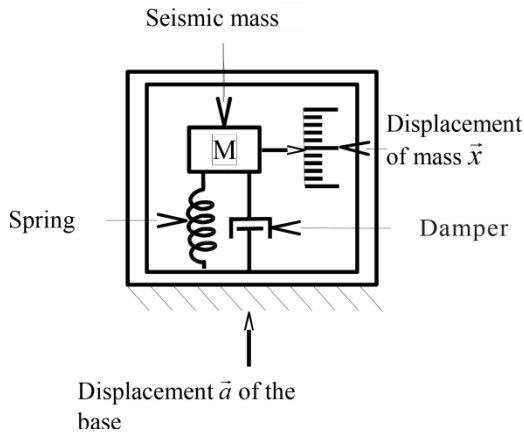

Figure 2.9. *Basic principle of an accelerometer (according to [FIG 00])*

If the base position, i.e. the structure to be analysed, is denoted by a, the behavioral equation of a damped seismic-based system can be written as:

$$m\frac{\partial^2 \vec{x}}{\partial t^2} + c\frac{\partial \vec{x}}{\partial t} + k\vec{x} = -m\frac{\partial^2 \vec{a}}{\partial t^2} \qquad [2.26]$$

if the natural frequency $\omega_r = \sqrt{\frac{k}{m}}$ and the damping rate $\xi = \frac{c}{2\sqrt{km}}$, then the permanent response to a periodic oscillation $a = A\sin(\omega t)$ is given as:

$$x_{perm}(t) = \frac{(\omega/\omega_c)^2 A\cos(\omega t - \phi)}{\sqrt{\left(1-(\omega/\omega_c)^2\right)^2 + \left(2\xi(\omega/\omega_c)\right)^2}} \qquad [2.27]$$

Like any dynamic system, the natural frequency of the assembly represents a large nonlinear area. If the Q factor $\left(x_{perm}^{\max} / A\right)$ is represented as a function of the relative angular frequency $\left(\omega / \omega_c\right)$, it is observed that the sensor works well for frequencies "sufficiently lower" to the natural frequency. In addition, the system must be "properly damped".

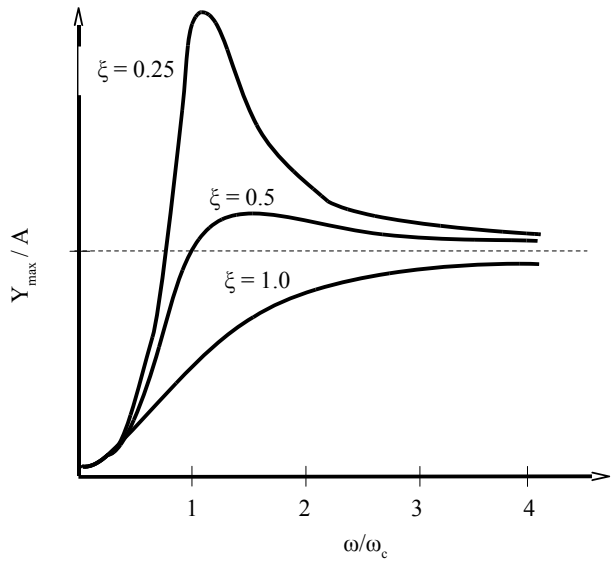

Figure 2.10. *Dynamic response of an accelerometer for different damping coefficients*

From the perspective of the dynamics of systems, the accelerometers with inertia, stiffness, and damping are systems of second order. Their response to an interval is as follows:

$$x(t) = KA - KAe^{-\xi\omega_c t}\left[\begin{array}{l}\dfrac{\xi}{\sqrt{1-\xi^2}}\sin\left(\sqrt{1-\xi^2}t\right) \\ +\cos\left(\sqrt{1-\xi^2}t\right)\end{array}\right] \text{ if } 0 \le \xi < 1 \qquad [2.28]$$

$$x(t) = KA - KAe^{-\omega_c t}\left[1+\omega_c t\right] \text{ if } \xi = 1 \qquad [2.29]$$

$$x(t) = KA - KAe^{-\xi\omega_c t}\left[\begin{array}{l}\dfrac{\xi+\sqrt{\xi^2-1}}{2\sqrt{\xi^2-1}}e^{\left(-\xi+\sqrt{\xi^2-1}\right)\omega_c t} \\ +\dfrac{\xi-\sqrt{\xi^2-1}}{2\sqrt{\xi^2-1}}e^{\left(-\xi-\sqrt{\xi^2-1}\right)\omega_c t}\end{array}\right] \text{ if } 1<\xi \qquad [2.30]$$

The term KA corresponds to the steady state response where the other data is previously defined. Here the damping rate is of utmost importance: if the damping rate is less than 1, the system is under-damped, and the transient oscillations appear. If it is greater than 1, the system is over-damped; it becomes aperiodic and the time taken to establish a steady rate may increase. The optimum for structural damping is $\xi = 1$. Figure 2.11 shows the response of an underdamped system. The key variables characterizing this system are indicated in the figure: the response time is set to 90% of time taken for steady state response, the settling time corresponding to oscillations lower than 10% of the nominal KA value and finally the period T_d.

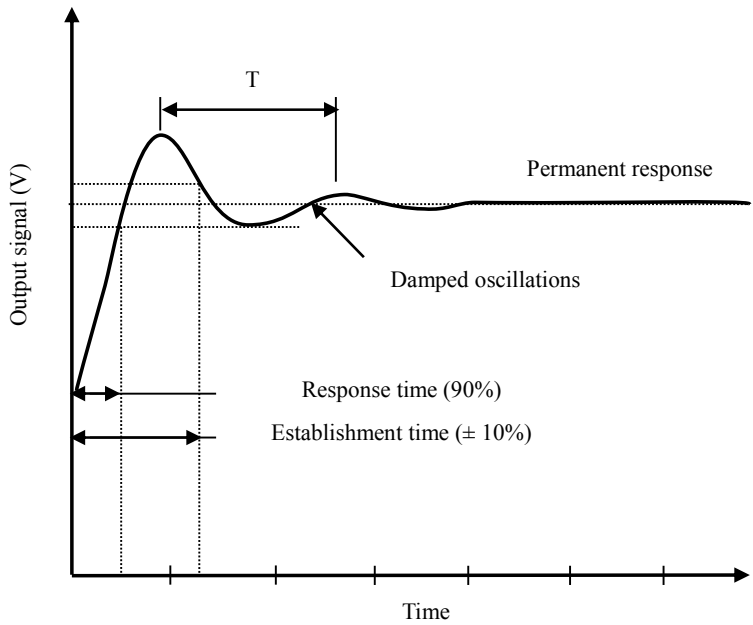

Figure 2.11. *Sample response of a sensor*

Recording the displacement of the Seismic mass is a standard problem, that can be addressed either using a gauge system (bending blade, Figure 2.12(a)) or a piezoresistive sensor (moveable under compression, Figure 2.12(b)). This involves the systems already mentioned above; as well as other rare accelerometers functioning according to capacitive, inductive, or optical principles.

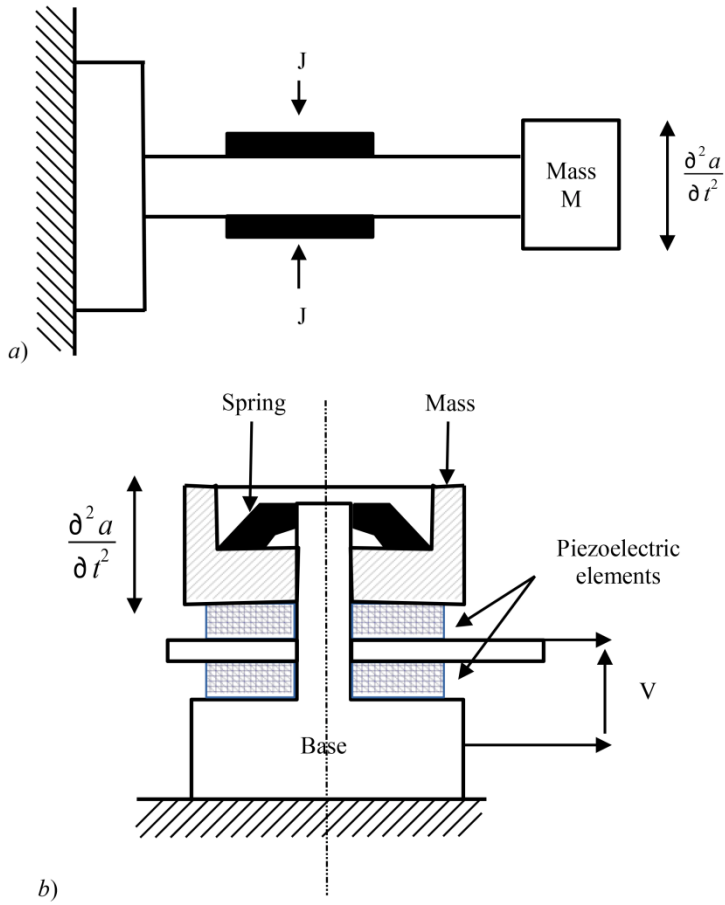

Figure 2.12. *a) Piezoresistive accelerometer (according to [MOR 92]) b) Piezoelectric accelerometer*

2.5.2. *Selection criteria*

In this particular installation, the *selection* of engineer is done based on the following criteria:

– *cost*, much higher for a piezoelectric sensor;

– *frequency range*: a piezoelectric sensor has a very high cut-off frequency (up to 10 kHz) but does not work for a continuous acceleration due to leakage currents. In contrast, a piezoresistive sensor does not allow accelerations greater than 100 Hz;

– *temperature range*: 300°C for the piezoelectric sensor with regard to 100°C for the piezoresistive sensor. Further, piezoelectric sensor drifts with temperature whereas piezoresistive sensor is self-compensating;

– *size*: the piezoelectric sensor is smaller. Therefore, it is less likely to change the frequency measurement than the piezoresistive sensor. In order to fix the orders of magnitude, the mass of a piezoresistive sensor must range between 0.5 and 50 g;

– *measuring performance*: the piezoresistive accelerometer enables to achieve accelerations ranging from 50 $m.s^{-2}$ to 50,000 $m.s^{-2}$. Sensitivity of the sensor is 0.1% of full scale, which leads to an accuracy of 0.5%; whereas the piezoelectric accelerometer has a measurement range of 10^{-4} $m.s^{-2}$ à 10^{4} $m.s^{-2}$ with a lower accuracy ranging from 1 to 2%.

QUESTION.– A dampened seismic system is used as an accelerometer. Find the spring/damper torque required to obtain an amplitude measurement accurate to 95% where the signal has the following characteristics: amplitude of 1.3 mm and a frequency of 15 Hz. What is the phase difference between the transmitted signal and its measurement, given the mass of the Seismic system is 5 g?

3

Optical Full-Field Methods

3.1. Overview

All the sensors described in the previous chapters are *electrical sensors*; these are the sensors in contact with the mechanical systems and are called *point sensors*. However, it is sometimes necessary to have either non-contact sensors or sensors insensitive to electromagnetic fields, or sensors that are capable of determining a quantity over an entire field. There are solutions for all these three types of applications. Inductive or capacitive displacement sensors, or those using laser triangulation, allow for contactless point measurement. The sensors on the optical fibres (Fibre Bragg gratings, Fabry-Perot cavities) are insensitive to the most common electromagnetic environments. Lastly, mechanical methods (nano-indentation, AFM, etc.), electronic methods (pressure sensors layers, SEM, etc.) or optical methods (X-rays, visible light, infrared, etc.) allow for full-field measurements. The latter family of methods is discussed in detail in this chapter.

Optical full-field methods enable non-contact measurements insensitive to electromagnetic radiation as well as full-field measurements. These methods combine an imaging principle, sometimes a very simple one (camera), sometimes more elaborate (interferometer-based laser light), with signal processing strategies for extracting information useful to an engineer (such as displacement, strain, etc.). They have led to a renewed approach to mechanical testing, with an abundance of information available in order to overcome the usual limitations as described in Chapter 1. In a test-calculation dialogue, the result of a test using optical full-field method is naturally set against a result from a finite element model. Optical full-field methods have led to the development of an original practice of

Experimental Mechanics of Solids and Structures, First Edition. Jérôme Molimard.

experimentation in solid and structural mechanics known as photomechanics.

Four of the most common methods are described here and illustrated by some examples. Then, key processing tools of maps obtained are analyzed from a metrological angle. This main objective of this chapter is to enable the reader to imagine the original and wide-range of mechanical tests and to provide necessary insights to make an informed choice of the most appropriate method.

3.2. Selection of a field optical method

3.2.1. *Factors governing selection*

The methods in the research phase are often very diverse, and sometimes commercialized. When the measured quantity is definite, the measurement range, accuracy and ease of implementation will guide the selection.

The measured quantity can be one of the following:

– *temperature*, current microbolometers allow for the study of increasingly complete fields (currently 256 × 256);

– *in-plane displacement* (in the plane tangent to the observed surface);

– *out-of-plane displacement* (normal to the observed surface);

– *three-dimensional displacement* of surface (“2½D”);

– *volume displacement* (3D) based on tomographic images;

– *shape*;

– *deformation* in the plane $\left(\frac{\partial u}{\partial x}, \frac{\partial v}{\partial y}, \frac{1}{2}\left(\frac{\partial u}{\partial y}+\frac{\partial v}{\partial x}\right)\right)$;

– *slope* $\left(\frac{\partial w}{\partial x}, \frac{\partial w}{\partial y}\right)$.

This measured quantity sometimes requires more thought than it would seem initially as it is often illusory to consider using a method which provides many different outcomes. For example, for the effective control of

shape defects, the measurement of shape has been less efficient than the measurement of slope and its derivation of a curvature [SUR 06].

The ease of use is related to the marking of surfaces and the working environment. For measuring displacement, the markers used to analyze the surface or the volume must be strictly adhered to. These markers may be spaced points, high density dots or line networks, derived from geometric or interferometric markings. Furthermore, the difficulty of marking is often an important practical limitation and explains the frequent use of image correlation and diffuse light interferometry methods. The working environment itself may, in turn, limit or exclude certain methods: for example, interferometric methods do not function well in a vibration environment.

Further still, the measuring range and accuracy favor the selection of either a geometric or an interferometric method. As a matter of fact, accuracy is a fraction of coverage for a geometrical method whereas it is a fraction of wavelength for interferometric methods. Therefore, in case of measurement of very low amplitude (10 nm ~ 10 µm) over a wide field (10 mm ~ 100 mm), interferometric methods are the most effective. However, if the covered field decreases, both methods are equally effective and, moreover, if the amplitude increases, geometric methods become more efficient. Typically, an analysis of vibration modes is conducted using the interferometric method and a study of the metal forming is carried out using the geometrical method. Each of these methods must be considered in detail and their performance must be explained.

3.2.2. *Fringe projection*

3.2.2.1. *Geometric model*

Fringe projection is used in the measurement of "out-of-plane" displacement. This method works on one of the simplest methods. A periodic pattern is projected onto a diffuse surface (matte white) and is observed in another incidence (Figure 3.1). Due to the angle θ, the pitch p of the grid seen by an observer depends on the variation with respect to a reference plane, denoted by z:

$$\frac{z}{p} = \tan\theta \qquad [3.1]$$

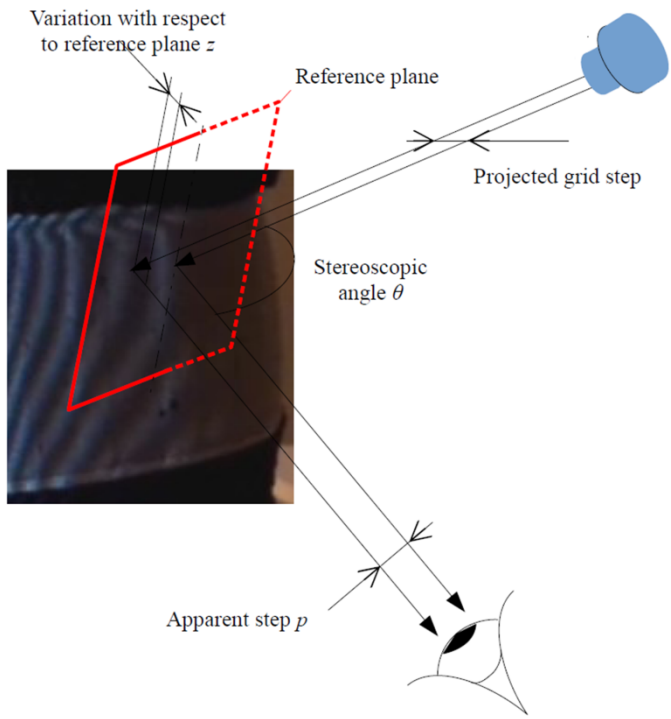

Figure 3.1. *Principle of fringe projection*

The method involves periodically recording signals (fringes) in a slightly disturbed manner, such that it can be described as a carrier with information. Thus, the light intensity I at any point is described as follows:

$$I = I_0 \times \lfloor 1 + \delta\, frg(\phi) \rfloor \qquad [3.2]$$

I_0 is the average intensity, δ is the contrast, often referred to as fringe visibility and φ is the periodic signal containing the carrier and the disturbance containing information, the phase term Φ. The periodic function *frg* is often equated to a sinus.

The phase term is given by:

$$\phi = 2\pi \frac{[y + \tan(\theta) z]}{p} \qquad [3.3]$$

NOTE.– In equation [3.3], the angle θ and the pitch p are only constants if the beams are collimated to infinity. If not, the set-up must be calibrated either empirically or based on a modeling of beam divergence.

3.2.2.2. *Phase extraction principle*

A camera only allows to measure light intensity and not phase. This information must, therefore, be extracted, i.e. determine I_0, δ and φ in equation [3.2]. For this, at least three different light intensities are required. They can be selected in two ways:

– by observing the variation in intensity for points closer to the point under observation; this is known as *spatial phase shift*;

– by changing the nature of the projected grid, for example by successively introducing an arbitrary and known phase shift over the entire field; this refers to *temporal phase shift*. This is the method elaborated for fringe projection.

Phase extraction φ can be performed in various ways, for example by Discrete Fourier Transform (DFT). If N images of the same object are acquired for N phases spread over $2\pi/N$, then:

$$\phi = -\arctan \frac{\sum_{k=0}^{N-1} I_k \sin(2k\pi / N)}{\sum_{k=0}^{N-1} I_k \cos(2k\pi / N)} \qquad [3.4]$$

Formula [3.4] states the "N-pass" algorithm.

However, the DFT method assumes the *periodicity* and *continuity* of the signal to be processed. Therefore, the terminals of the function must have the same value. To ensure this condition, which is rarely met, an additional function, called the window function, is introduced. Its simplest form is a triangle function, as shown in Figure 3.2. This case is better adapted if there is no adequate control over the carrier. The introduction of a window function naturally imposes a large number of points.

The phase obtained using the "2N-1" algorithm is given by the equation:

$$\phi = -\arctan \frac{\sum_{k=0}^{N-1} k\left(I_{k-1} - I_{2N-k-1}\right) \sin\left(2k\pi / N\right)}{N\, I_{N-1} + \sum_{k=0}^{N-1} k\left(I_{k-1} - I_{2N-k-1}\right) \cos\left(2k\pi / N\right)} \qquad [3.5]$$

Equation [3.4] and equation [3.5] correspond to the extraction of the first and second arguments of the Fourier series respectively, representing the periodic function.

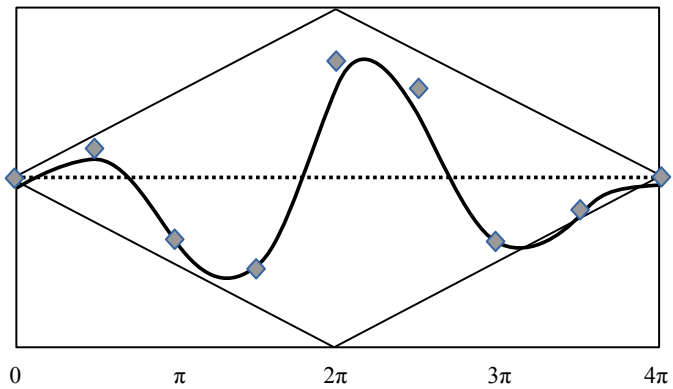

Figure 3.2. *Discrete Fourier Transform and window function*

3.2.2.3. *Mechanical applications*

The fringe projection method is very robust and well-suited to a mechanical environment. The sample size as well as the measuring range in this method is widely adaptable.

A fringe projection assembly can be used for dimensional control, for example, teeth correction. It assumes a comprehensive modeling of the various interference phenomena, or accurate calibration and use of a reference surface [BRÈ 04]. Currently, a few systems allow for a complete reconstruction of an object (reverse engineering[1]). Analysis of deformations

1 For example, the manufacturer 3D-Shape (http://www.3d-shape.com).

could also be performed using fringe projection in the study of thermomechanical stresses in the manufacturing composites [GIG 09].

There are several applications of fringe projection in biomechanics and in the domains of physiotherapy (postural study [GOM 10], study of certain medical devices [PIE 15]), anatomy (anatomical volumes of body parts [LEA 10]), dentistry (imprints of prostheses [KUH 07]) or dermatology (wrinkles, scabs [LAG 01]). Figure 3.3 shows the result of a skin texture measuring device, with fringe image and reconstruction of the topology of a forearm. The advantage of the temporal phase shift is apparent in this case: each pixel contains information independent of the adjoining pixels, which allows an accurate description of wrinkles and fine lines.

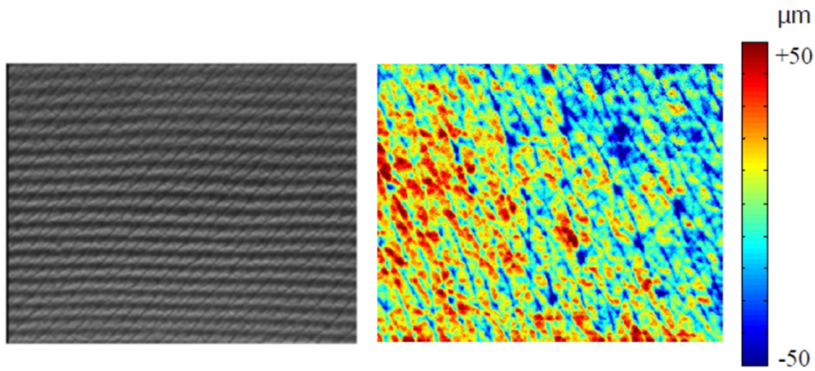

Figure 3.3. *Texture of human skin obtained by fringe projection (forearm)*

However, interpreting the data requires close attention: though there is development in the shape, it is, generally, difficult to distinguish the out-of-plane displacement vectors, due to planar displacement which cannot be detected using this method.

3.2.3. *Grid method*

3.2.3.1. *Geometrical optics*

The grid method allows for the measurement of displacements along the plane of the object. A periodic pattern is transferred onto the surface of the object under study. When the object is deformed, the grid follows the deformation, as does an electric gauge. The pitch p_{ref} of a grid, whose

characteristics depend on the y-axis, vary if the displacement u_x of the grid varies along orthogonal x-axis according to:

$$p = p_{ref}\left(1+\frac{\partial u_x}{\partial x}\right) \qquad [3.6]$$

However, this property is used very rarely. The estimate of pitch variation at the local level involves large strain, often incompatible with mechanical applications. By contrast, the grid phase, at the local level, varies with displacement.

3.2.3.2. *Signal processing*

The signal received by the camera is analyzed using equations [2.29] to [3.5]. But the phase term is changed as follows, in the case of smaller displacements:

$$\phi = -2\pi\frac{u_x}{p} \qquad [3.7]$$

In a problem related to structural mechanics, displacements are generally small. The spatial phase extraction is, therefore, well adapted for this problem. The influence, if any, of an out-of-plane displacement is noticeable. The usual lenses have a finite focal length, which means that the image is formed on a spherical portion, and not on a plane, which would be the case for a telecentric lens. The further the object moves, the more its apparent size (the size in the image plane) decreases. Therefore, the apparent pitch p varies with a displacement along the optical axis: it decreases if the object moves away and increases if the object approaches, resulting from a contraction (negative homogeneous deformation) or expansion (positive homogeneous deformation), of the object respectively. Figure 3.7 illustrates this effect.

If the coding is vertical, then the horizontal displacement can be easily known. Similarly, if a horizontal coding is performed, the vertical displacement is measured. But in the case of a cross grid, some lines (e.g. axis lines) have no contrast (see Figure 3.4). One way to address this problem is to average the information over a period along the direction of fringes. The spatial resolution is thus uniform in both directions and the information is dispersed in a reliable and reproducible manner across the image.

Finally, the transferred network is not very regular. The 2N-1 algorithm is best suited to this situation as it tolerates a linear phase drift.

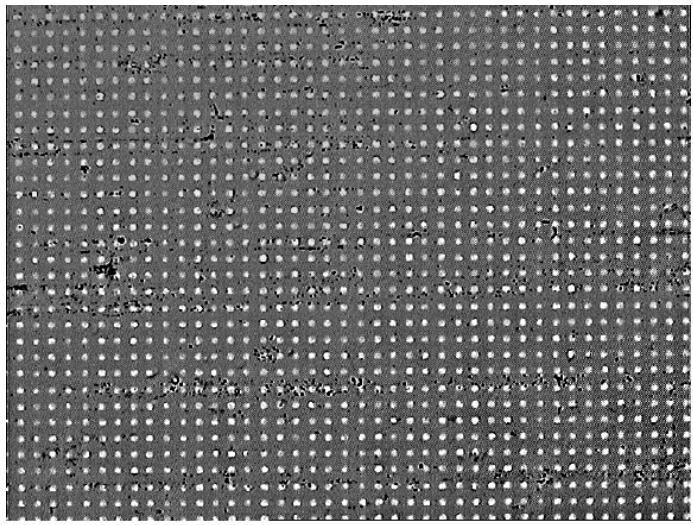

Figure 3.4. *Cross grids for a measurement along x and y (no 30 µm grid)*

3.2.3.3. *Mechanical applications*

There are several mechanical applications of this device. They involve studies to increase general understanding and validation of hypotheses (embedding conditions in an off-axis tensile test [PIE 98]) and studies to monitor damages (repair of a cracked beam [AVR 04], damage around a bore of composite plates [PIE 12]). The identification of properties of composite materials has been conducted based on measurements using the grid method (Iosipescu shear test [GRÉ 94], T specimen [GRÉ 99] and perforated plate [VAU 09]). The identification, which is a broad and complex process, is not discussed here. However, the reader may refer to [GRE 11] for more information. The most intuitive method is to compare an experimental map with a map obtained from an analytical or numerical model (Finite Element model, in particular) associated with a minimization process, for example Levenberg-Marquardt or Simplex, leading to optimal parameter values [MOL 05, SIL 07] (Figure 3.5). Other micromechanical studies describe the behavior of metallic materials (single or poly aluminium crystals [BER 11] – Figure 3.6) or bitumen [BAD 09].

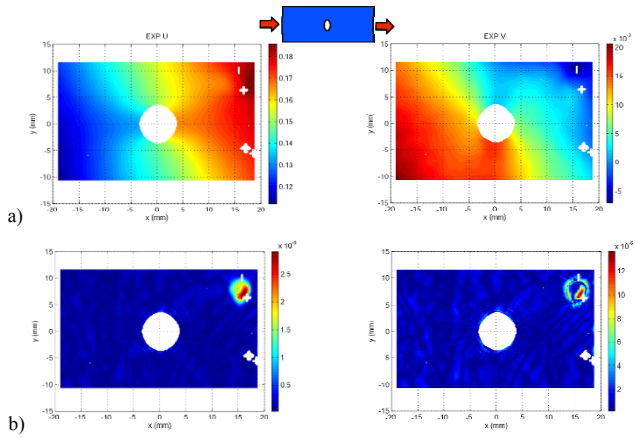

Figure 3.5. *Identification of mechanical properties of a composite material. a) Fields of displacement measured in the direction of traction (EXP U) and transversely (EXP V) (in mm). Asymmetry is visible: it has been analyzed during identification. b) Function of variation between numerical and experimental expansions: illustration of a defect and identification of effective properties of the damaged area in [VAU 09]. For a color version of the figure, see www.iste.co.uk/molimard/mechanics.zip*

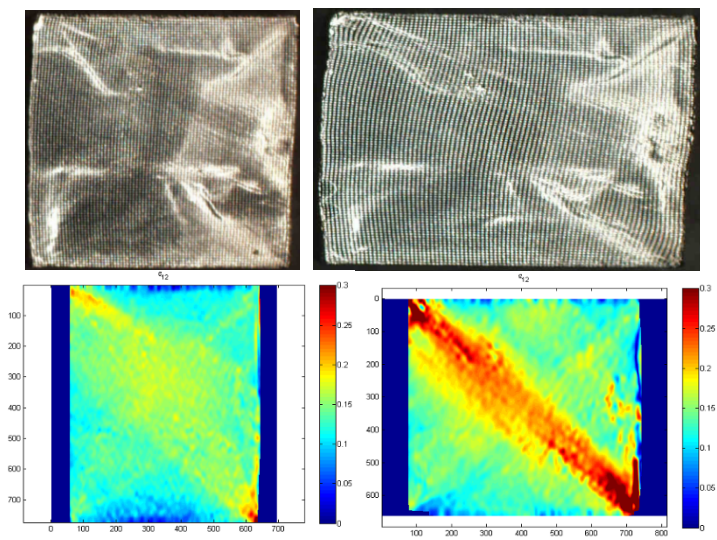

Figure 3.6. *Monitoring the planar compression of aluminum single crystal along Gauss orientation. a) Grids after a deformation of 15% and of 30%. b) Main shear for step 0–15% and for step 15%–30 %. Location of the deformation at mesoscopic scale is clearly identified (in [MOL 09]). For a color version of the figure, see www.iste.co.uk/molimard/mechanics.zip*

3.2.4. *Digital image correlation*

Since the first publication of Sutton [SUT 83] in 1983, Digital Image Correlation (DIC) has become the most popular photomechanic method. It has been applied to all types of materials (wood, metal, composites, bone, etc.), of varying scales: from SEM [ALL 94] tests to monitoring of geophysical structures [DEB 11]. The first planar implementations have evolved to non-planar surfaces [SUT 98] and, following the development of laboratory tomographic systems, to volumes [GER 07]. DIC is described in great detail by Scheier *et al*. [SCH 09]; only basic principles of this method are described in this chapter.

3.2.4.1. *Principle of Digital Images Correlation*

Consider an object whose reference image im_0 is described by the function $f(x, y)$ and an actual image im_1 described by $g(x, y)$ obtained after the disruption of the object. Assuming the optical signature of the object did not change between the two situations, then:

$$g(x,y) = f\left(x-\delta_x, y-\delta_y\right) + b(x,y) \qquad [3.8]$$

where δx and δy are displacement components of im_1 relative to im_0 and $b(x, y)$ the measurement noise.

It is possible to determine δx and δy by maximizing the function h defined by:

$$h(x,y) = (g * f)(x,y) = \int_{-\infty}^{+\infty}\int_{-\infty}^{+\infty} g(\xi,\eta) f(\xi - r, \eta - s)\, d\xi d\eta \qquad [3.9]$$

The sign * represents the cross-correlation product, and the values r and s are the maximum probability values for the displacement (the notation represents the optimal value obtained *for a given methodology*). This method can be used in Fourier space. If FFT2D is the fast Fourier transform, then the equation [3.9] becomes:

$$g * f = FFT2D^{-1}\left(FFT2D(g)\, FFT2D\left(\tilde{f}\right)\right) \qquad [3.10]$$

This represents the complex conjugate and $\tilde{f}(x,y) = f\left(L_x - x, L_y - y\right)$, where L_x and L_y are the dimension of the domain.

Insofar as there is high spatial density information (a speckle), equations [3.9] and [3.10] may be used on a local scale, typically for 32 × 32 thumbnail images. By repeating the operation on the whole image, a complete displacement field is reconstructed.

The approach presented here assumes that (i) the images im_0 and im_1 have similar light characteristics and (ii) the local transformation of the object can be equated locally to a translation. The first point can be solved by reducing the light intensity to contrast or medium intensity, either upstream, or by changing the expression of the inter-correlation product. The second point based on the deformation of the im_0 thumbnail according to a certain hypothesis of processing and comparing it with the corresponding im_1 thumbnail. The processing may be a rigid body mode (2 translations + 1 rotation), which can be associated with a constant strain (2 translations + 1 rotation + 2 dilations + 1 shear). This approach requires a quick search method of six variables, but also a sub-pixel interpolation method of the image. A more recent method has been proposed to write the overall processing of the work piece based on a mechanical approach (analytical solution and finite element mesh) [BES 06]. All this leads to several sources of errors that could be analyzed in [AMI 13] and [BOR 09]. In the end, in proper conditions, an image correlation method allows for movements with a resolution close to $1/100^{th}$ of a pixel and in the same order of magnitude. As in the case of the grid method, the bias increases in areas of high gradient with selection of thumbnails acting as a low pass filter.

3.2.4.2. *Determination of sub-pixel displacement using phase analysis*

A sub-pixel displacement is conventionally achieved through interpolation of the cross-correlation peak or interpolation of the grey levels of the images. Here, however, a different approach is described: achieving displacement through generalized phase analysis. This accentuates that optical methods presented are not isolated from one another, but are all based on common concepts of signal processing.

The speckles of image correlation is a random two-dimensional signal across a thumbnail. Considering its decomposition into a Fourier series, it is the superposition of a large number of periodic signals (grids) which may be horizontal, vertical or oblique. As before, their phase will encode displacements of the object in the direction normal to the grid. If the contrast associated with a particular periodic signal is not zero, all the phase changes between the reference state and the current state can be associated with displacement by the following equation:

$$\left\{\Delta\phi_\theta^i\right\} = \underbrace{\begin{bmatrix} \frac{2\pi}{p_\theta^i}\cos\theta^i & \frac{2}{p_\theta^i}\sin\theta^i \end{bmatrix}}_{A} \begin{Bmatrix} \delta_x \\ \delta_y \end{Bmatrix} \quad [3.11]$$

To the extent that the matrix A is invertible, i.e. there are at least noncollinear frequencies containing phase information, it is possible to estimate the displacement using following formula:

$$\begin{Bmatrix} \delta_x \\ \delta_y \end{Bmatrix} = \left(A^t A\right)^{-1} A^t \left\{\Delta\phi_\theta^i\right\} \quad [3.12]$$

A phase in case of a random signal can be extracted under the same conditions as for a periodic signal: as the frequency at the edges is not ensured, each thumbnail is multiplied by a bi-triangular windowing function (pyramidal, 2D), then the phase is extracted from the whole Fourier transform.

Usually, a sub-pixel algorithm is used in addition to the classic correlation pixel; equation [3.11] is, therefore, still valid, as no phase jump is possible for sub-pixel displacements.

3.2.4.3. *2D½ correlation*

The correlation given here is used to obtain the apparent displacement along the camera object plane. If the necessary precautions are taken, this information is sufficient for testing a flat specimen (tensile, bending and shear). In this case, however, a displacement of the out-of-plane test object typically results in a variation in the apparent size of the object, where the current objectives are not telecentric. This influence is characterized by the camera's angle of view. In the absence of information on out-of-plane displacement, the variation in apparent size is equivalent to a dilatation of the object.

Furthermore, a flat specimen biased in a plane is significant but too specific; most structures have non-planar surfaces and their displacements are three-dimensional.

The measurement of displacements $u_x(x, y, z)$, $u_y(x, y, z)$, $u_z(x, y, z)$ on a surface $S(x, y, z)$ by image correlation combines the 2D correlation technique and the shape measurement technique, either by stereovision [SUT 06] or by fringe projection [MOL 10]. From the shape of the part before and after the biasing and project displacement on the object plane, it is easy to reconstruct the three-dimensional displacement by ray tracing (Figure 3.7).

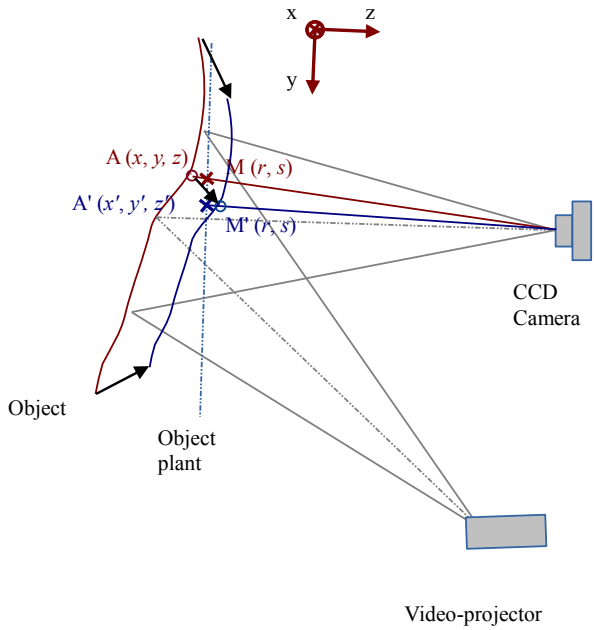

Figure 3.7. *Reconstruction of three-dimensional displacement fields on the surface of a non-planar object by projecting coupling fringes and image correlation [MOL 10]. For a color version of the figure, see www.iste.co.uk/molimard/mechanics.zip*

Figure 3.8 shows an example of results from the study of knee braces [PIE 15]. The study showed that these braces do not slide on the thigh for short periods of time and that the strain of the skin close to the brace during a bending motion was 5.9% in men and 15% in women.

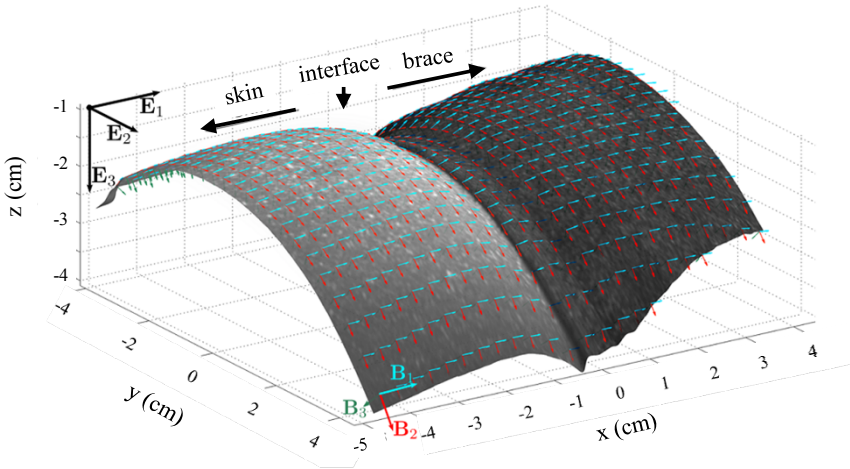

Figure 3.8. *Three-dimensional displacement fields on the surface of a leg covered with textile brace [PIE 15]. For a color version of the figure, see www.iste.co.uk/molimard/mechanics.zip*

3.2.5. *Speckle interferometry (ESPI)*

3.2.5.1. *Interferometric assembly*

Speckle or diffused light interferometry is an interferometric method requiring the usual conditions for formation of interference: spatial and temporal coherence of the light beams. A surface is illuminated by a laser sheet obtained by a spatial filter with or without a lens for collimating the beam to infinity. The surface diffusing the light can be observed by an optical system (naked eye, photographic plate or more usually a digital camera). Part of the laser beam is intercepted by a beam splitter and directly illuminates the optical system via a set of mirrors: thus an interferometer is formed; and when one of its arm is scattered by the surface, it contains information on the surface. Various types of arrangements are possible using this basic principle. The two main assemblies are those used in measuring out-of-plane and in-plane displacements of the surface. In the first case, the illumination of the surface is normal to its plane (see Figure 3.9(a)), whereas in the second the surface is illuminated simultaneously in two opposite directions (see Figure 3.9(b)).

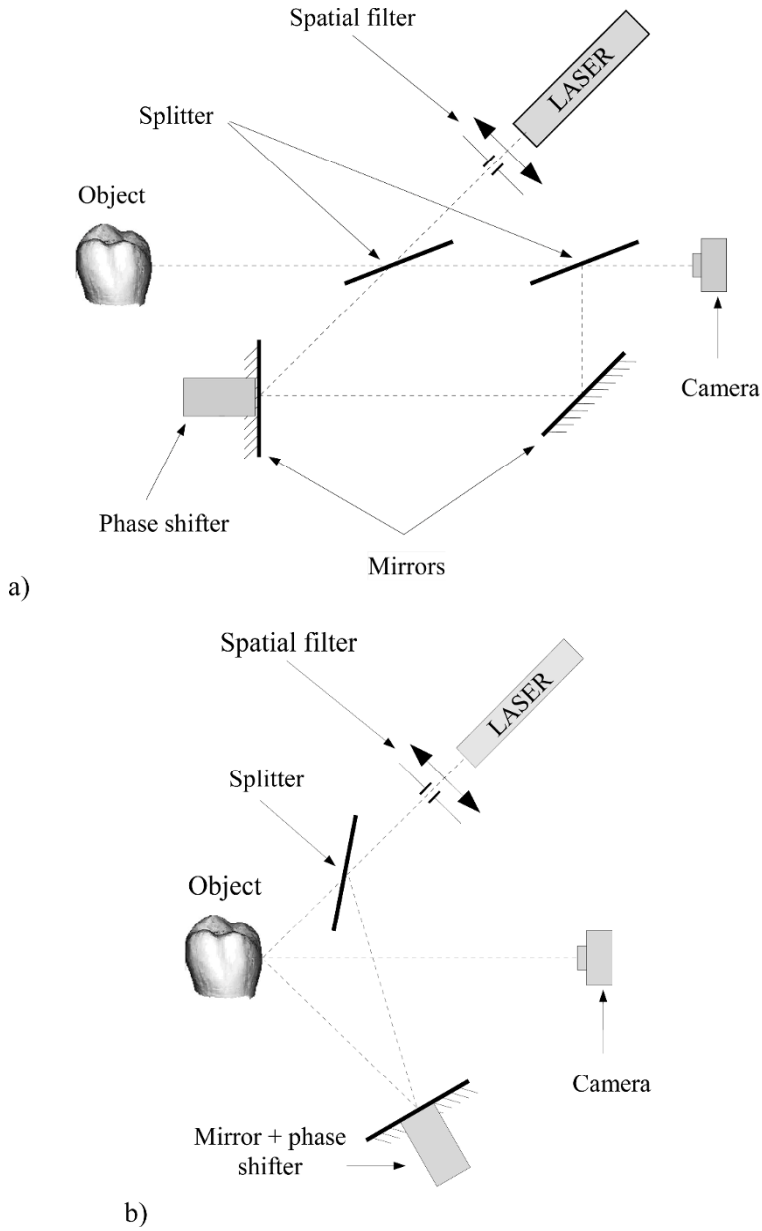

Figure 3.9. *Main speckle interferometry assemblies: a) out-of-plane assembly; b) in-plane assembly*

The interpretation of the interferogram obtained is directly derived from the optical path variation induced by an infinitesimal displacement. Therefore, in speckle interferometry, the useful information is the variation between two states of the optical path, as measured by a phase shift:

$$\Delta\phi(x,y) = \frac{2\pi}{\lambda}(\vec{e}_i - \vec{e}_0)\cdot\vec{u} \qquad [3.13]$$

where $\vec{e}_i$ and $\vec{e}_0$ are the unit vectors defining the direction of illumination and observation and λ is the wavelength of light.

Equation [3.13] using a phase variation is therefore necessary to use a phase extraction system. Usually, it is based on a temporal shift and applying equation [3.5]. In practice, the temporal variation of the phase is obtained by changing the optical path of one of the arms of the interferometer. A piezoelectric actuator placed on one of the mirrors ensures a sufficiently small micro-displacement to obtain a phase variation by a fraction of 2π.

3.2.5.2. *Correlation of speckle patterns*

The phase field obtained is a random field: each grain of material from the surface of the object studied is randomly diffused in all directions of space and the light beams thus formed locally interfere with each other to give light and darker areas called *objective speckle*. The opening of the imaging optical system transforms this target speckle into *subjective speckle*[2]. This randomness is specific to the speckle interferometry; this is a significant difference when compared with other interferometric systems used in photo-mechanics (Moiré interferometry, holographic interferometry).

In most mechanical applications, the speckle signature of a surface does not change over time. Insofar as the measured displacements are largely smaller than the size of the subjective speckle, equation [3.13] is valid. It ceases to be so if the speckle signatures of the reference state and the current state are not completely superimposed, at which point a random term representing speckle noise should be added.

2 This transformation is the convolution of objective speckle (white noise) by a door function characterizing the opening of the imaging system.

Various strategies of re-correlation of speckle signatures have been proposed; however the most interesting ones are used over small areas. They can be based on the correlation of intensity images [BRU 00], on maximization of signal to noise ratio of phase differences [MOL 08] or on a correlation of complex image intensity and phase [SVA 06]. Figure 3.10 shows a simple tensile test on a composite based on carbon fabric as observed using speckle interferometry. Without the use of a re-correlation algorithm of speckle grains locally, the information contained in the phase difference is very noisy and unreadable. However it appears clearly if each area (here 32×32 pixels) is adjusted so that the signal to noise ratio is maximized.

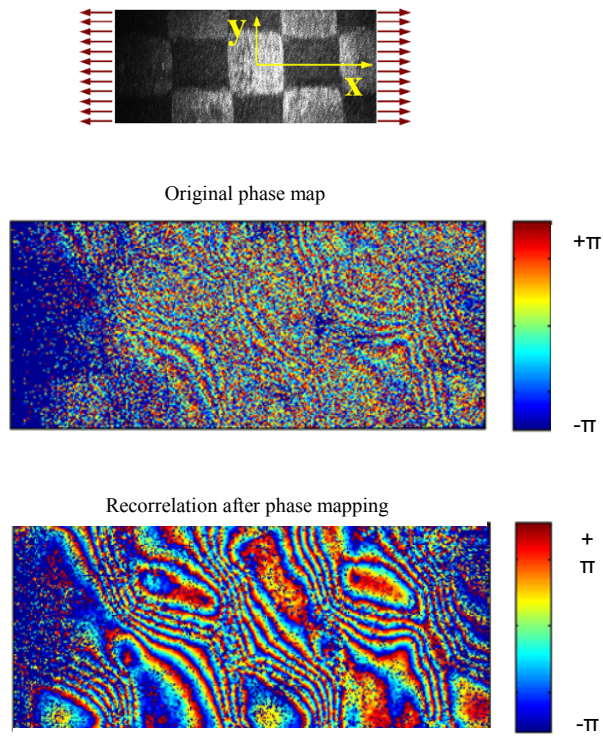

Figure 3.10. *Result of a tensile test on a carbon composite cloth, with or without principle of local re-correlation of speckle pattern [MOL 08]. For a color version of the figure, see www.iste.co.uk/molimard/mechanics.zip*

3.2.5.3. *2D½ speckle interferometry*

The installations illustrated in Figure 3.9 provide access only to a part of information on surface displacement (in a direction of the plane, out-of-plane). However, they are limited to flat surfaces; despite this, they have the advantage of simplicity and speed. A natural application field of this kind of installation is the vibration mechanics, for examples see [NIS 15].

When the displacements are more complex, provided that the situation is quasi-static, it is possible to combine three interferometers to obtain all displacements u_x, u_y, and u_z at any point M of the visible surface in a pixel (i, j) of the camera. In the Figure 3.11, the reference beam (1) may be combined successively with a set of plates with each of the illumination beams (2), (3) or (4). All beams are obtained from the same source, using semi-reflecting beam splitters. The phase shifter is positioned on one of the mirrors of the reference beam. A green laser (λ = 532 nm) is used on a 18 mm × 18 mm illuminated surface.

Considering equation [3.13], the vector observation reference is given as $\vec{e}_0 = (0,0,-1)$. Two interferometer arms are placed symmetrically in a horizontal plane; then the illumination vectors $\vec{e}_1 = (\sin\gamma_1, 0, \cos\gamma_1)$ and $\vec{e}_2 = (\sin\gamma_2, 0, \cos\gamma_2)$ respectively, where $\gamma_2 \approx -\gamma_1$. The last arm of the interferometer is in the vertical plane. The corresponding illumination vector is thus written as $\vec{e}_3 = (0, \sin\gamma_3, 0, \cos\gamma_3)$. Considering these conditions in equation [3.13], we obtain:

$$\begin{Bmatrix} \Delta\phi_1^{DSPI} & (i,j) \\ \Delta\phi_2^{DSPI} & (i,j) \\ \Delta\phi_3^{DSPI} & (i,j) \end{Bmatrix} = \frac{2\pi}{\lambda} \begin{bmatrix} \sin\gamma_1 & 0 & (1+\cos\gamma_1) \\ \sin\gamma_2 & 0 & (1+\cos\gamma_2) \\ 0 & \sin\gamma_3 & (1+\cos\gamma_3) \end{bmatrix} \begin{Bmatrix} u_x & (i,j) \\ u_y & (i,j) \\ u_z & (i,j) \end{Bmatrix} \quad [3.14]$$

Equation [3.14] is reversible, provided that the angles are selected carefully; this is sufficient if the angles are constant, i.e. if the beams are collimated to infinity. Otherwise, the divergence of the beams must be taken into account [MOL 09]. In this case, the shape of the object has an impact on local sensitivity and must also be measured: this is the role of video projector in Figure 3.11.

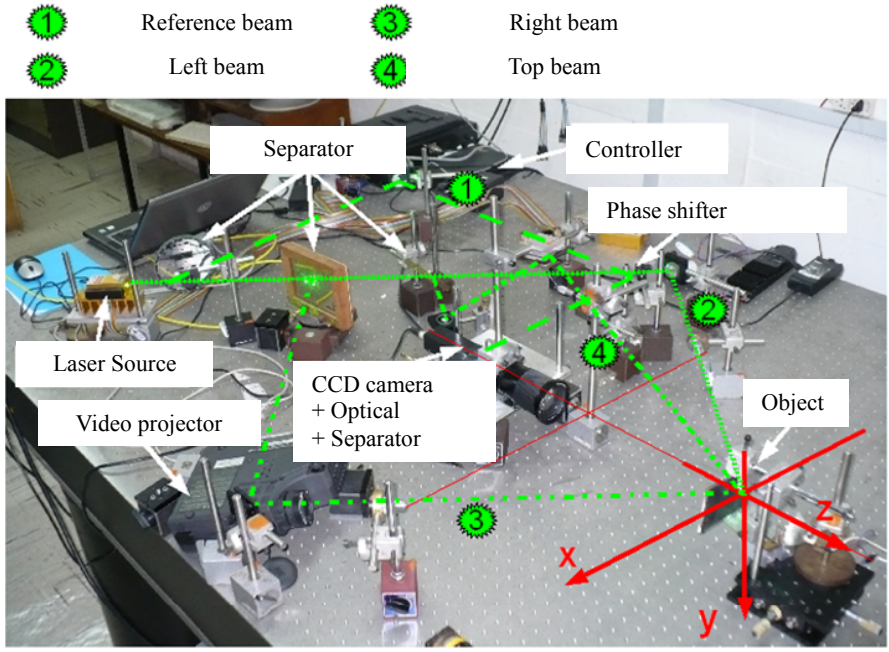

Figure 3.11. *ESPI 2D½ interferometric assembly (according to [MOL 09]). For a color version of the figure, see www.iste.co.uk/molimard/mechanics.zip*

The previous installation was used to study the dimensional stability of thick composite plates (9 mm) subjected to a variation in temperature. Such a situation induces small variations in shape, which can be dangerous in aeronautics where the composite parts may be subjected to temperature variations of about 100°C. Figure 3.12 shows the displacement field obtained in the direction normal to the surface for a temperature change of 12.4°C in a curved area, which can be easily produced. The stacking sequence is $[0\ 90]_{60}$ and the inner and outer curvatures are 9 mm and 21 mm respectively. The nominal thickness is 9.5 mm. The ESPI assembly has a spatial resolution on displacement of 20 nm; after derivation, the resolution on strain is 2 μm/m.

The measurement of the displacement variation enables the *in situ* estimation of the coefficient of thermal expansion in the reinforcement plane (11.3×10^{-6} m/m/K) and the thickness (58.0×10^{-6} m/m/K). Figure 3.12

highlights the differential expansion of the layers. From this information, the authors have determined the size of each composite layer (183 µm instead of the nominal value of 152 µm), in a completely non-destructive manner. This information is very dependent on the manufacturing method used and is involved in the failure mode of the work piece.

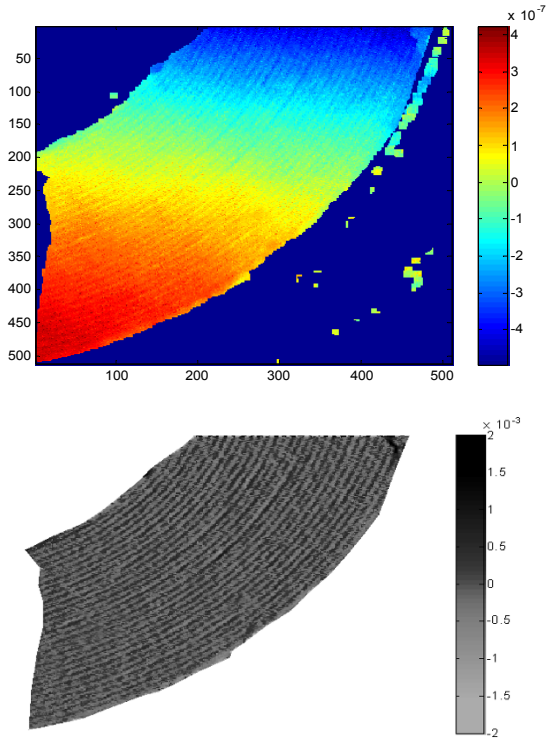

Figure 3.12. *Out-of-plane displacement and displacement gradient on a composite part subject to temperature variation. For a color version of the figure, see www.iste.co.uk/molimard/mechanics.zip*

QUESTION.– Fringe visibility and maximum displacement are accessible.

According to equation [3.14], if $\gamma_1 = -\gamma_2$, the difference of phase variations $\Delta\phi_1$ and $\Delta\phi_2$ depend only on u_x. From this, state the sensitivity defined as displacement variation u_x corresponding to a phase variation of 2π. (A.N. $\gamma_1 = -\gamma_2 = 45°$, $\lambda = 532$ nm).

In a uniform tensile test, given that the observation area of the specimen is 20 × 20 mm and is imaged by a camera of 512 × 512 pixels, what is the maximum acceptable deformation considering the limits of the Shannon theorem?

In this case, what is the maximum displacement due only to this deformation? Knowing that ESPI systems are set such that the size of a speckle grain corresponding to a pixel, is it possible to measure displacement without using a re-correlation system?

3.3. Main processing methods of photomechanical results

3.3.1. *Metrological aspects*

The photomechanical methods can be analyzed as any other measurement method; however, the detailed insights provided by these methods require the defining of the additional quantities. In particular, optical methods are characterized by their *resolution* and *spatial resolution*.

The *resolution* refers to the threshold below which the distinction between two successive random measurements has no significance. For a two-dimensional measure such as fringe projection, simply calculate the difference between two successive measurements for 10^{+6} statistically independent results. Therefore, the resolution can be quantified by a repeatability test.

The *spatial resolution* refers to the distance beyond which a local phenomenon has negligible effect on the adjacent points. The definition of the spatial resolution is therefore related to a degree of interaction. If one chooses to limit the degree of interaction to 50%, this corresponds to a Gaussian distribution (diffraction spot, high frequency filter, etc.) in defining the resolution of an optical system as used by opticians[3]. The limitations of

3 Be careful: note the semantic difficulty – in a general assumption, the resolution of an instrument is related to the noise level. In the optics domain, resolution of an optical system is linked to image sharpness. Here, the optical system is used as a measurement instrument, thus leading to “resolution” and “spatial resolution”. The spatial resolution is nothing but the resolution in the opticians’ assumption.

spatial resolution are related to optical elements (diffraction spot), discretization of the CCD cameras (pixel size), phase extraction method and, more generally, to information extraction method.

Table 3.1 shows the orders of magnitude of the resolution and spatial resolution for the different methods discussed above. Some implementations have been published with better claims, in particular for the Grid method [BAD 09] and the digital image correlation method [BES 06]; therefore, it is perfectly possible to obtain a better performance, but at a significantly higher development costs. It must be noted that specific metrology work on the method of the Grid method [BAD 13] or the digital image correlation [BOR 09]. Furthermore, the resolution is only an uncertainty component. Very few uncertainty analysis studies are published for fringe projection [MOL 13], image correlation [REU 12a, REU 12b] and speckle interferometry [MOL 09].

Fundamentally, spatial resolution is related to the discretization of the camera and the information extraction kernel, which can either be a segment or a thumbnail. For a metric spatial resolution, it is necessary to know the magnification of the optical system and the resolution of the CCD or CMOS sensor[4]. The resolution in turn is limited by the fringes in carrier methods: the smaller the fringes, the better the resolution. Specific limitations, however, prevent maximizing this parameter; the measurement range is also related to the size of the fringes. For fringe projection, equation [3.3] shows that the sensitivity of the method also depends on the projection angle.

Finally, it should be noted that for geometrical methods, the reference length is always the pixel size in object space; this is obvious to the image correlation, though maybe a little less so for grid and fringe projection methods. For speckle interferometry on the other hand, the reference length is the wavelength of light; therefore, the sensitivity does not vary in this case with the size of the field covered. When preferring high sensitivity to larger sizes, interferometric methods are much more efficient. However, for small areas (a few mm^2), the resolution of geometric methods can be as good as for interferometric methods [TRI 07].

4 The words used can be ambiguous. For CCD or CMOS frame manufacturers, the resolution refers to the amount of sensors in each direction.

	Fringe Projection	Grid Method	Digital Images Correlation	Speckle Interferometry
Measured quantity	Shape	Planar displacement	In plane or out-of-plane displacement	In plane or out-of-plane displacement
Resolution	$0.2/100^{th}$ fringe	$0.5/100^{th}$ fringe ($2/100^{th}$ pixel)	$2/100^{th}$ pixel	$10/100^{th}$ fringe (~5 nm)
Spatial Resolution	1 pixel	1 or 2 fringes (5 to 10 pixels)	1 Thumbnail image (32 pixels)	1 pixel

Table 3.1. *Commonly accepted performances of a few field optical methods*

3.3.2. *Correction of target distorsions*

The optical camera consists of lens instruments through which the resulting image may not be focused on a focal plane but on a curved surface. Due to the spherical geometry of the lenses, the paraxial rays near the optical axis and those located close to the edges of the lenses do not converge at the same focal point. Consequently, the magnification is not constant over the entire image and this causes distortion.

The various optical methods presented here have different sensitivities to the distortion. The image correlation refers to comparing the length of a part segment in two different states; this segment is imaged in different places of the image space, hence at different magnifications; therefore, distortion must necessarily be corrected [FOR 84, SCH 09].

Camera distortion is corrected by calibrating with the known geometry of targets, such as grids. The principle of correction refers to transition of apparent coordinates of a point $M_{app}(x_{app}, y_{app})$ measured on the CCD sensor to the coordinates of the corrected point $M_{corr}(x_{corr}, y_{corr})$.

Figure 3.13 shows the result of a tensile test followed by image correlation obtained under an Optem Zoom 125 at 6.0 magnification. The gross displacement does not give a clear image of traction, while the corrected displacement is acceptable.

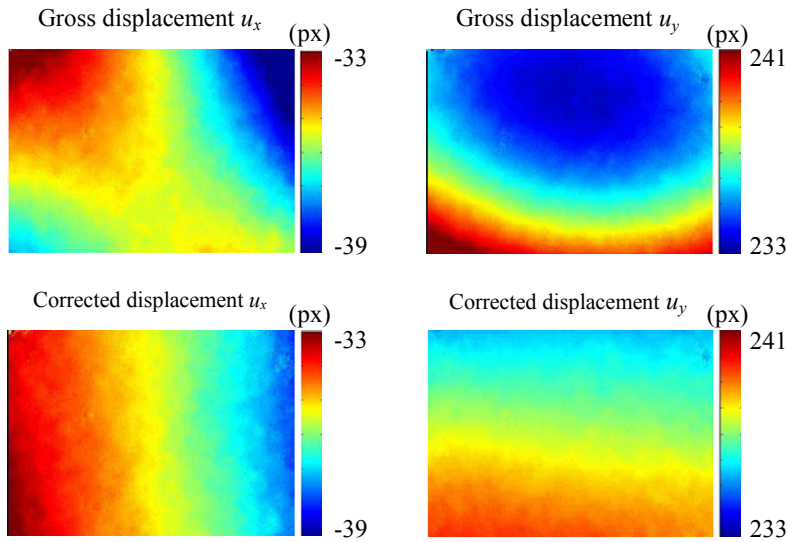

Figure 3.13. *Optical principle of camera distortion. For a color version of the figure, see www.iste.co.uk/molimard/mechanics.zip*

3.3.3. *Denoising in mapping*

3.3.3.1. *Convolution kernel with low-pass filtering*

The most intuitive noise removal method consists of replacing a value using the average of the adjacent elements in the neighborhood. In mathematical terms, this refers to convolution that may be written continuously as:

$$(f * g) = \int_{-\infty}^{+\infty} f(x-t)\, g(t)\, dt \qquad [3.15]$$

This requires consideration of the size of the adjacent elements in the neighborhood: naturally, the larger the neighborhood, the more the mapping will be denoised, but at least the details in the image will be less visible. Next, the calculation of an average is not unique: several different weightings are possible. An analysis in the frequency space of different convolution kernels among the conventional ones (rectangular, triangular, Gaussian) favors the

Gaussian kernel. The equation for a two-dimensional discretized Gaussian filter is:

$$u_{filt}(i,j) = (u * g) = \frac{\sum_{k=-2\sigma}^{k=+2\sigma}\sum_{l=-2\sigma}^{l=+2\sigma} u_{gross}(i-k, j-l)\, g(k,l)}{\sum_{k=-2\sigma}^{k=+2\sigma}\sum_{l=-2\sigma}^{l=+2\sigma} g(k,l)} \qquad [3.16]$$

where $g(k,l) = \frac{1}{\sqrt{2\pi\sigma^2}} e^{\left(k^2+l^2\right)/\left(2\sigma^2\right)}$

Linear smoothing has two very important effects: it increases the spatial resolution, which leads to fewer independent points in the image, and reduces the resolution, which increases the ability to detect even a small variation of the measurand. In a first approximation, we consider, for a Gaussian smoothing characterized by its standard deviation σ in pixels, that the spatial resolution is degraded σ and that the resolution is improved by $1/2\sigma\sqrt{\pi}$ as $4\pi\sigma^2$ points are involved in averaging. Note that this value is not strictly accurate; the respective weight of the various points involved in calculating the average must also be considered.

3.3.3.2. *Nonlinear noise removal*

Very often, some isolated points on a map raise concerns. In such cases, the displacement calculation can reasonably overlooked, and the point can be eliminated. This type of noise is known as salt-and-pepper noise. A low-pass filter such as the Gaussian convolution responds poorly to this concern. The most common strategy is to replace all the points of the mapping with the average of the neighboring points; in this case, the scope of the neighborhood is the only parameter to be adjusted. The major drawback of this filter is that it acts indiscriminately on all mapping points, e.g. a maximum displacement which can be quite relevant.

The preferred approach is an extension of 2D stochastic signals of a filter based on the probability of a given point to be very different from its neighboring points. The criterion is given as:

$$u(i,j) \text{ is admissable if } \left|u(i,j)\right| \le u\left(\overline{i},j\right) \pm t_{v,P} S_{\Delta i,\Delta j}\left(u(i,j)\right) \qquad [3.17]$$

Equation [3.17] is derived from equation [3.3]; $S_{\Delta i,\ \Delta j}$ is the estimated standard deviation over a certain surface $\Delta i \times \Delta j$ around the point (i, j). The two approaches are compared in Table 3.2: a well-controlled noise is added to a mapping; and, the result is denoised with one or the other filter. It is clear that the stochastic filter is more selective than the median filter: only 0.5% of salt-and-pepper noise is not removed and fewer points that supposedly do not create noise are not affected by the filter.

	Noise removed	Points changed without noise
Median filter	89 %	607.5 %
Stochastic filter	99.5 %	41.6 %

Table 3.2. *Comparison of non-linear filters*

3.3.4. *Phase unwrapping*

Fringe projection, the grid method or Speckle interferometry work with the information on a phase, necessarily determined in a space $[-\pi, +\pi]$. The continuity of the phase field must be restored before using the gross result, such as displacement or shape. Various strategies can be adopted for this purpose:

– temporal phase unwrapping: the final phase is obtained by cumulating the intermediate states such that each phase difference remains within the interval. This strategy is very effective in the case of the grid method, where recording videos is easier than photographs at specific moments [BER 11];

– fringe coding: a pixelwise identification of each fringe gives an assignment of fringe order at each point. The phase is rewritten as the sum of the phases extracted in the interval $[-\pi, +\pi]$ plus 2π times the fringe order. Identification of the fringe order for each pixel is obtained in fringe projection by the successive projection of binary images together constituting an identification code [LEA 11];

– spatial phase unwrapping: the spatial unwrapping would be trivial in the absence of noise. Just browse through each line or each column of the image and add or subtract 2π whenever there exists a phase variation between two successive pixels of $\pm (2\pi - \varepsilon)$. The presence of noise makes the procedure difficult and sometimes dependent on the method followed. In

fact, a few robust comprehensive methods for minimizing the phase gradient have been proposed and they most often provide satisfactory results [VIO 06].

3.3.5. *Derivation of a displacement map*

3.3.5.1. *Introduction*

More often than not, the strain is of greater importance than the displacement. Therefore, the calculated field must be derived experimentally. However, the derivation always substantially increases the noise. Point by point derivation is ineffective. For example, an image correlation method has a resolution of $2/100^{th}$ of a pixel on displacement; considering that the measurements are made on thumbnails of 32 × 32 pixels, the point-by-point derivation leads to a resolution on the deformation of $2/100\times\sqrt{2}/32 = 0.910^{-3}$ m/m.

The strategies to reduce noise and to approach an acceptable resolution for solid or structural mechanics have only recently piqued the interest of researchers. One class of methods is to combine a low-pass filtering with a derivation obtained from a least-squares formulation. Avril and Feissel [AVR 08] compared a derivation by diffuse approximation to a derivation based on of finite elements. Similarly, Berge-Gras [BER 09] used a low pass filter coupled to a derivation by least squares and discussed the outcome for resolution as well as for spatial resolution. The second type of methods consist of using images to directly extract the displacement gradient. A variant of the speckle interferometry allows one to obtain deformations directly and slopes with a resolution of 0.05 10^{-3} m/m and a spatial resolution of a few pixels [MOL 99]. The grid method may also be modified to obtain a phase directly susceptible to strain [BAD 09]. This method has recently been adapted to digital image correlation [MOL 11]. However, only two of these derivation methods are described in detail in this book.

3.3.5.2. *Obtaining deformation through filtering/derivation*

In the filtering/derivation approach, each displacement function u_x or u_y is approximated locally to the field by its mean plane in the least squares sense. This requires us to define an area on which the approximation can be made, usually a square of n by n points. The *spatial resolution* is naturally changed by this derivation and becomes n pixels in each direction.

The mean plane is represented by:

$$\overline{u}_i = a_0^i + a_x^i x + a_y^i y \quad \text{for } i \in \{x, y\}$$

The vector values $\{a^i\} = \{a_0^i, a_x^i a_y^i\}^t$ are given by the equation:

$$\{a^i\} = \left(\left(A^t A \right)^{-1} A^t \right) \{u_i(x, y)\} \qquad [3.18]$$

where matrix A is defined as $\begin{bmatrix} 1 & x_1 & y_1 \\ \vdots & \vdots & \vdots \\ 1 & x_n & y_n \end{bmatrix}$.

As the deformations are linear combinations of derivatives $\frac{\delta u_x}{\delta x}$, $\frac{\delta u_y}{\delta y}$, $\frac{\delta u_x}{\delta y}$ and $\frac{\delta u_y}{\delta x}$, the values of the first derivatives correspond to the parameters a_y^i and a_j^i for each direction of derivation and each displacement.

In general, under the assumptions of statistical independence and homoscedasticity of the experimental variable u_i, the covariance matrix is used to find the dependency of parameters a_j^i with the variance of the experimental variable u_i.

$$[V]_a = V_{u_i} \left(\left(A^t A \right)^{-1} A^t \right) \left(\left(A^t A \right)^{-1} A^t \right)^t \qquad [3.19]$$

Finally, the *resolution on the derivative term* is given by:

$$\sigma_{a_j} = \sigma_{u_i} \sqrt{\frac{N}{N \sum_{k=1}^{N} x_k^2 - \left(\sum_{k=1}^{N} x_k \right)^2}} \quad \text{for } i, j \in \{x, y\} \qquad [3.20]$$

where N is the total number of points used for the least squares formulation.

3.3.5.3. *Direct extraction of the displacement gradient by derivative kernel*

Rather than having to extract a phase and then derive it, it is possible to directly extract the gradient [BAD 09, MOL 11]. This procedure avoids the propagation of noise during the process of derivation. Consider the Fourier transform index ψ_θ of a signal $s(x,y)$. This term corresponds to the wavelength P_θ and direction θ. With the grid method, the wavelength is given as the grid pitch and the direction θ takes the values 0 or 90°; using sub-pixel correlation method described in section 3.2.4, P_θ and θ correspond to all contrast non-zero situations. The mathematical expression is:

$$\psi_\theta(x,y) = (R_\theta + iJ_\theta) = \int_{-\infty}^{+\infty}\int_{-\infty}^{+\infty} s(\xi,\eta)\times g(\xi-x,\eta-y)\times\exp\left(-i\frac{2\pi}{P_\sigma}(\xi\cos\theta+\eta\sin\theta)\right)d\xi\,d\eta \quad [3.21]$$

where s (ζ, η) is the signal, g (x-ζ, η-y) is a Gaussian windowing function. R_θ and J_θ are the real and imaginary part of the Fourier transform respectively. The phase displacement according to θ is defined as:

$$\varphi_\theta(x,y) = \arg(R_\theta + iJ_\theta) = a\tan_{2\pi}\left(\frac{R_\theta}{J_\theta}\right) \quad [3.22]$$

$$U_\theta = -\frac{P_\theta}{2\pi}(\Delta\varphi_\theta + 2k\,\pi) \quad [3.23]$$

where k is the fringe order.

The equation of the displacement derivative U_θ according to $\vec{x}$,

$$\frac{\partial U_\theta}{\partial x} = -\frac{P_\theta}{2\pi}\Delta\left(\frac{\partial\varphi_\theta}{\partial x}\right) \quad [3.24]$$

$$\frac{\partial\varphi_\theta}{\partial x} = \left(\frac{\frac{\partial J_\theta}{\partial x}\times R_\theta - \frac{\partial R_\theta}{\partial x}\times J_\theta}{J_\theta^2 + R_\theta^2}\right) \quad [3.25]$$

Finally, the derivation of J_θ or R_θ according to x is summarized according to the derivation of g (ζ, η). By selecting the Gaussian function, we obtain:

$$\frac{\partial R_\theta}{\partial x} = \int_{-\infty}^{+\infty}\int_{-\infty}^{+\infty} \frac{(x-\xi)}{2\pi\sigma^4} s(\xi,\eta)\, g(\xi-x,\eta-y) \cos\left(\frac{2\pi}{P_\theta}(\xi\cos\theta+\eta\,\sin\theta)\right) d\xi d\eta \qquad [3.26]$$

$$\frac{\partial J_\theta}{\partial x} = \int_{-\infty}^{+\infty}\int_{-\infty}^{+\infty} \frac{(x-\xi)}{2\pi\sigma^4} s(\xi,\eta)\, g(\xi-x,\eta-y) \sin\left(\frac{2\pi}{P_\theta}(\xi\cos\theta+\eta\,\sin\theta)\right) d\xi d\eta \qquad [3.27]$$

Equations [3.26] and [3.27] highlight a convolution kernel modified by the term $(x-\xi)/(2\pi\sigma^4)$. This linear term is a derivative kernel.

Figure 3.14 shows an example of a result using the derivative kernel on a random signature. Each thumbnail is of 64 × 64 pixels. The deformation maps were filtered with a salt-and-pepper stochastic filter and a low-pass Gaussian filter, σ = 9 pixels. Finally, the resulting spatial resolution is of 13 pixels, which is very low compared to other methods such as strain extraction by filtering/derivation. The result is obtained on a composite consisting of a woven carbon single-ply of 8 × 8 mm^2 subject to traction of 200 N. The deformation maps in Figure 3.14 show periodic variations due to local bending effects in the microstructure as described in [LEE 04].

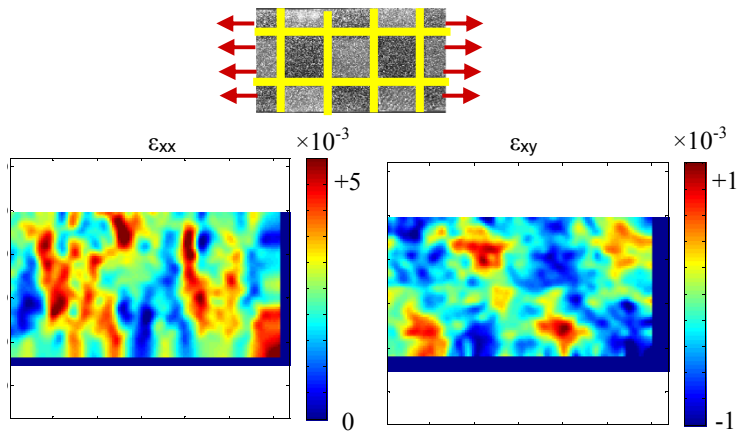

Figure 3.14. *Deformation maps of a composite comprising a woven carbon fold subjected to traction. For a color version of the figure, see www.iste.co.uk/molimard/mechanics.zip*

QUESTION.– Resolution of a map contains spatially correlated points.

The resolution following filtering or a derivation is given in the case of statistically independent data. What is it in the case of coupled data? Consider the reasoning leading to equations [3.18] and [3.19], incorporating the additional parameter of a noise reduction using Gaussian convolution kernel (i) expressing the variance on the result of a low-pass Gaussian filtering based on statistically independent data and (ii) expressing the variance on the combined result from the low-pass filtering and derivation in the least squares sense. Does the order of operations have an influence on the result?

4

Basic Tools for Measurement Methods

4.1. Introduction

It is common for mechanical training to include notions of signal processing. However, proper data extraction is only one topic on which mechanics should reflect when devising tests. Despite all the efforts that can be made to increase measurement quality – and incidentally the associated signal processing – the measurement result is inevitably tainted with error; it is an imperfect representation of reality. It is necessary to be able to estimate this error to produce an experimental result and no result should be given without its uncertainty range and the level of probability accorded to it. This vision is even more necessary when focusing on differences between one situation and another. Tools for processing information statistically provide the appropriate methodology and, in particular, enable the likelihood of variation occurring to be confirmed.

EXAMPLE 4.1.– A cosmetics laboratory suggests an anti-aging cream with a "proven effect" on skin. To prove this effect, an indentation test is carried out. A panel of subjects is chosen and tests are carried out for different levels of treatment. The results obtained are very broad, due to the great variability between individuals, which is due in part to their very different lifestyles, among which can be cited exposure to sunlight, pollution, cigarettes and, of course, age. However, variation has been demonstrated according to the level of treatment. Is this significant?

Experimental Mechanics of Solids and Structures, First Edition. Jérôme Molimard.

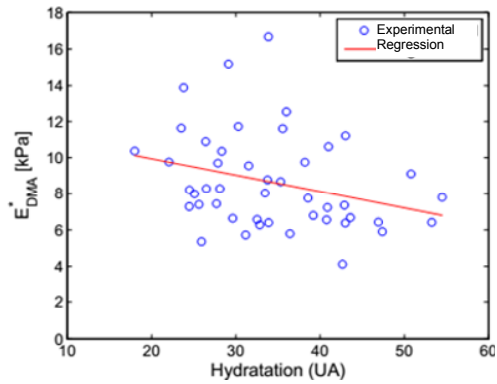

Figure 4.1. *Results from cosmetic tests with a markedly dispersed character [BOY 10]*

To go further, as seen above in the introductory examples, it is sometimes difficult to place different parameters' influence on a response variable. In many laboratories or design offices, it is usual to alter each parameter independently and to deduce its sensitivity. However, this method is not very effective: it provides little data when a large number of tests are considered. The remainder of this chapter will provide a method that will enable a minimum number of tests to obtain a maximum amount of information. The quality of the information obtained will be discussed, depending on the quality of the descriptive model and also by comparing the results with an experimental dispersion. These two approaches are generally known as "design experiments", or "ANOVA".

4.2. Measurement and precision

4.2.1. *Calibration*

Calibration aims to provide a correspondence table or a function between the value read (in general, a potential difference) and the measurand (for example, a distortion). Here, we are interested in experiment calibrations, which are often necessary due to the complexity of modeling a complete acquisition chain and the number of variables that must be known if the modeling is to be carried out. For example, a load cell can very often be modeled using a mechanical beam model, such as the bending blade described in section 2.4.1. However, there are many reasons to move away

from the analytical model. These can relate to the model's limits (the installation quality, small transformation hypotheses) or to the test conditions (uncertainties in positioning the gauges in the blade section).

This calibration can be made at the sensor level or along the entire measuring chain. Before calibration, it is important to identify influence quantities and to take them into account in the context of a multi-variable calibration. A calibration will be valid within a known range of influence and measurand variables. More simply, the calibration can be carried out in the conditions in which the sensor is used. The temperature and degree of hygrometry are the environment parameters to follow, especially, for example, for a pressure mapping system, which is built from polymeric elements and foam. Similarly, time is a critical parameter, as a sensor's sensitivity is often linked to its excitation frequency. Above a critical frequency (the cut-off frequency) the sensor will not be capable of returning information.

Figure 4.2 shows a typical calibration. On the graph we can see several important elements. First of all, the *measurement points* appear "reasonably *dispersed*". To quantify this dispersion, it is necessary to provide a reference curve (*calibration curve*), obtained by smoothing the previous values. This operation is carried out correctly if the form of the smoothing function chosen is correct. Is it necessary to take a straight line? Must it pass through zero or not? On what theoretical or practical consideration can we rely? A form defect in the smoothing function automatically leads to a *systematic error* on the subsequently measured values. The average difference between the points and the curve therefore becomes a *dispersion* in the direction of the measurement. Finally, the slope $K(x)$ at any point on the calibration curve corresponds to the measurement system's *sensitivity*.

The International Bureau of Weights and Measures provides definitions for the concepts described below. As precision in the wording is particularly important in metrology, the definitions below follow the reference document from the International Bureau of Weights and Measures as closely as possible [BIP 12]:

– *measurement error* is the difference between the measured value of a quantity and a reference value;

– *measurement accuracy* is the closeness of the agreement between the average of an infinite number of repeated values measured and a reference value. Accuracy in itself cannot be expressed numerically. It varies in an

inverse direction to the *systematic error*, a component of the measuring error which, in repeated measurements, remains constant or varies predictably. Systematic error is estimated by a *bias*;

– random error is a component of the measuring error which, in repeated measurements, varies unpredictably. Measurement precision takes account of random error, depending on the method chosen, the conditions of *repeatability*, conditions of intermediary precision or conditions of *reproducibility*. Precision is usually expressed by a standard deviation, a variance or a variation coefficient.

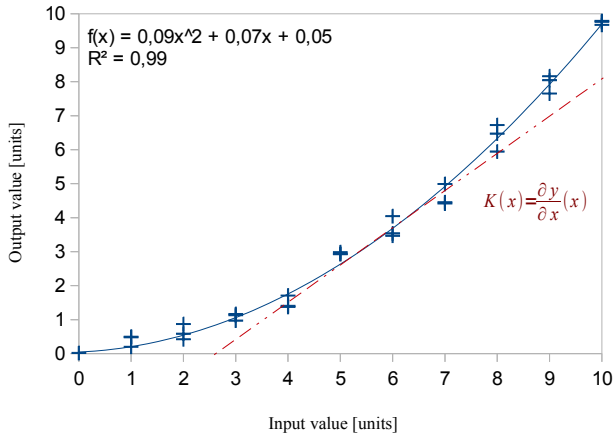

Figure 4.2. *Typical calibration curve*

Accuracy and precision can be illustrated using the arrows on Figure 4.3 as an example.

In the first instance, the launcher is extremely precise (the arrow tips meet), but there is an error in accuracy (they are not centered). In the second instance, the precision is middling, although the arrows are generally well-centered. Both these cases give a measuring error in the same order of size, but the reality is very different in a statistical sense, and of course in an underlying, physical sense. Evidently the third situation is best, however, this case is not always desirable, as it can make the cost of instruments too high.

These definitions should not be confused with the definition of *uncertainty*. Uncertainty quantifies, using the errors defined above, the reasonable range of variability in a specific measurement. Finally, the

definitions of errors given above classify them as mathematical modeling, but another more physical classification is necessary to comprehend errors in measurement. This classification is envisaged below in the form of either sequential or random metrological tests, depending on whether a characterization of accuracy or precision is required. All these tests help to establish the *instrument's total error*, estimated as the quadratic mean of all the errors identified.

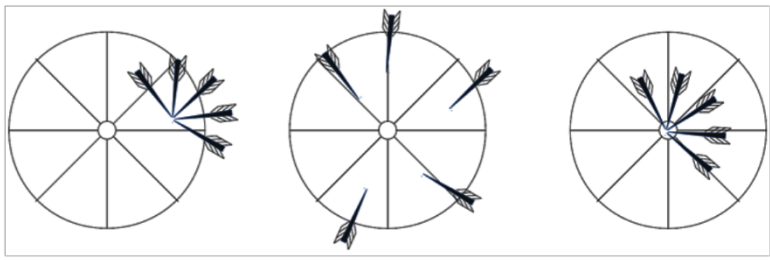

Figure 4.3. *Illustration of repeatability and systematic error*

4.2.2. *Tests*

4.2.2.1. *Sequential tests*

Sequential tests are tests that aim to reveal historical phenomena in measurement; this effect can be linked directly to time, or to the load level at the previous level.

A measuring system's *drift* is quantified by maintaining a load level over time and by observing the slow variation in the indicator. It is necessary, if we need to observe an instrument's drift, to confirm that no other element could account for the drift measured, and more specifically for the load mode.

There is often a gap between the ascending and descending curves, called a *hysteresis*. This indicates that the current value depends on the previous value. This is particularly the case in measuring systems that rely on mobile items (dry friction, backlash) or viscoelastic materials; electrical phenomena can also produce hysteresis, in the case of electrostatic charges for example. The surface of the zone thus delimited corresponds to the energy dissipated during the cycle. The test for hysteresis consists of successively running through the entire range of measurements recording the measurand's value as

a function of the output value, from the smallest to the greatest, then from the greatest to the smallest. Figure 4.4 shows a hysteresis test for foam-based pressure sensors. Since this foam has a relaxation time, the return route is not the same as the initial route.

From a measurement perspective, a hysteresis error is defined as the maximal gap Δy between the values found in each direction over the maximal value y_{max}:

$$e_{h_{\max}}(\%) = \frac{\Delta y}{y_{\max}} \times 100 \qquad [4.1]$$

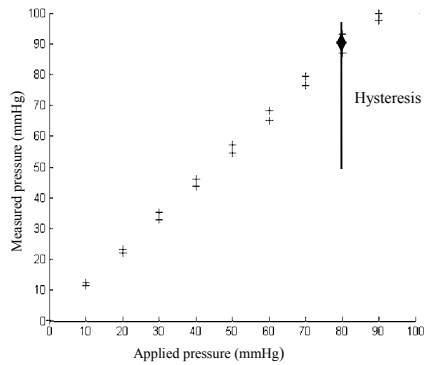

Figure 4.4. *Hysteresis effect: the case of a pressure sensor*

4.2.2.2. *Random tests*

Other tests should be carried out on measurements for points taken at random, which randomizes the historic effects and renders them undetectable. The defects characterized in this way are defects in linearity, sensitivity or the zero and the measuring instrument's precision.

The defect in *linearity* is only relevant if we assume an affine relationship linking the signal measured and the measurand. In this case, it is usually defined by:

$$e_{lineartiy} = \frac{\max\left(y - \hat{y}_{lin}\right)}{y_{\max}} \times 100 \qquad [4.2]$$

As seen previously, this definition reveals the maximal error reported on the equipment's range. One notable difficulty lies in defining the line passing ideally through all the points, represented in [4.2] by $\hat{y}_{lin}$.

Figure 4.5 shows the force/strain relationship in the case of a force cell with strain gauges. The calibration curve shown does indeed seem linear, but has shifted slightly in relation to zero, whereas theoretically it should pass through zero. Depending on the case (noise level, instrument design) this phenomenon can be analyzed in two ways:

– if we consider a curve passing through zero and trace the different lines passing through the point cloud. A sensitivity error is therefore detected;

– it may be that the zero is not fixed, but the sensitivity is known. The different lines passing through the point cloud constitute an error on the zero, which is most often taken into account by frequently adjusting the sensor.

Linear regression and the associated uncertainty will be expanded upon in section 4.3.2.

Precision can be defined by different conditions, corresponding to different experimental concerns, using a repeatability or reproducibility test.

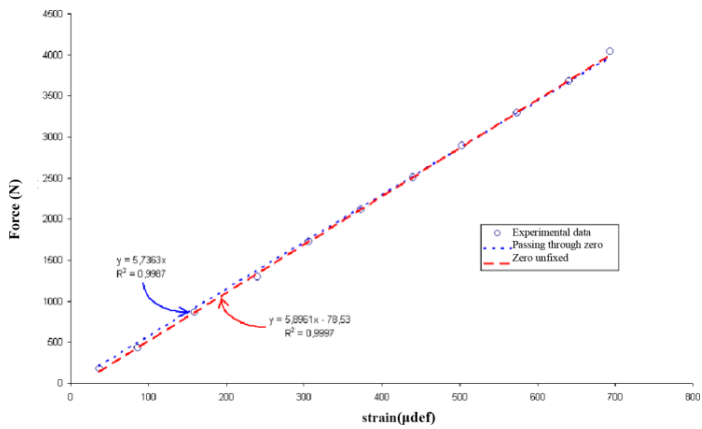

Figure 4.5. *Zero and sensitivity error. The case of a force cell*

In the first instance, *repeatability* is defined in the measuring conditions as "the same measurement procedure, same operators, same measuring system, same performance conditions and same location, and replicate

measurements on the same or similar objects over a short period of time" [BIP 12]. We thus obtain a standard deviation characterizing the measurements' dispersion. *Repeatability* is defined in a standard fashion as:

$$e_{repeatability}^{\max} = \frac{2.\sigma}{y_{\max}} \times 100 \qquad [4.3]$$

This size does not take account of all the measurement parameters and, notably, the proper procedures for each laboratory, or long time periods. A notion synthesizing the different repeatabilities is introduced: *reproducibility*. The measuring conditions "include different locations, operators, measuring systems, and replicate measurements on the same or similar objects".

4.2.2.3. *Resolution and discrimination threshold*

A measuring system has a detectable minimum, linked to a graduation for the oldest systems or a digital sampler for the most recent. This detectable minimum is the *discrimination threshold*. However, all researchers have experienced a numerical display whose last figures vary at random and to which they attach no importance. The last significant figure is defined by the *resolution*. This is the smallest value between two measurements that can be perceived significantly. The resolution can be characterized by a repeatability test. It must be noted that the discrimination threshold corresponds to a monotone variation in the measured data, whereas the resolution corresponds to a random variation. The discrimination threshold can therefore be, depending on the choices made by the apparatus's designers, greater or smaller than the resolution, without there being any systematic rule.

4.2.3. *Evaluating uncertainties*

4.2.3.1. *Introduction*

Statistical analysis for measurements is an essential tool for describing uncertainties but is not sufficient on its own. In fact, to establish uncertainty, all the sources of uncertainty should be taken into account. The uncertainty budget includes, in the first place, estimations of uncertainties in the quantities involved in the measurements; links between the quantities are included since they change the overall balance (in the form of covariance);

the type of probability density functions used should be mentioned: generally speaking, Student law (or Normal law, for large amounts) can be applied to continuous data. For discretized data, a uniform law is preferable.

The current objective of uncertainty analysis consists of "characterizing the dispersion of values that could, reasonably, be attributed to the measurand". Sources of uncertainty, such as those mentioned in *Guide to the Expression of Uncertainty in Measurement*, published by the International Bureau of Weights and Measures (GUM) [BIP 12] can be linked to:

– the measurand, either because it is not completely defined or because the practical test is itself incomplete. For example, this is the case for problems with friction;

– the choice of measurement sample. Typically, this is what occurs in biomechanics, during clinical studies;

– the test conditions (temperature, hygrometry). There are numerous examples, once again, from biomechanics (tests on soft tissue), but also from any test on polymeric materials;

– the measuring instrument and how it is used: the user can introduce bias or the system can be imperfectly calibrated. Both these possibilities are common in optical systems. The measuring system, as we saw in detail previously, has a finite resolution and the measurand's repeated observations give different results in apparently identical conditions.

– the data handling algorithm: the calculation approximations and hypotheses create uncertainties, as may the retiming values (correspondence tables for example) used or the signal's pre-processing condition (filtering). Measuring temperature by thermal camera illustrates these difficulties very well.

Uncertainty analysis can only be developed profitably when the objectives of the tests carried out are well-defined, when the experiment procedure is written and validated, when the data are established for pertinent experimental values (see section 4.3) and when the experimentalists have some experience with the system components.

The uncertainty evaluation can result from repeated tests (type-A evaluation), but this methodology is not always possible. In other cases, we speak of type-B uncertainty evaluation.

EXAMPLE 4.2.– We wish to check the mean diameter of a shaft using classic calipers. The shaft is measured; its diameter is ideally constant. How does one identify the possible sources of error at work in the uncertainty of the measurement for the diameter?

APPLICATION.– The mounting on Figure 4.6 is of a micro-indentation system. The impedance head is made of a force sensor and a piezoelectric accelerometer; this impedance head enables a movement cycle with controlled amplitude to be applied and the resulting effects to be recorded. The turntable and the frame enable the measuring system to be placed at the site to be analyzed. Finally, the micro-metric platinum, used with the camera, enables it to be placed precisely:

– what are the measurands here?

– what are the dependent parameters in this test? What external parameters could influence the measurement?

– what are the possible sources of uncertainty?

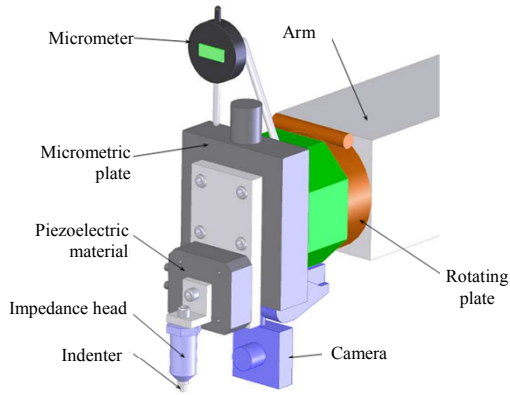

Figure 4.6. *Micro-indentation mounting*

4.2.3.2. *Evaluating type-A uncertainty*

Different types of errors have been described above, notably system errors (biases) and random errors. If these errors can be characterized experimentally, depending on the suggested tests, then the systematic error can be compensated, for example by using a calibration table. However,

random error is sustained. In the case of a measurement where the systematic error is null, the value measured can be described as:

$$x = x \pm u_x \ (p\%) \qquad [4.4]$$

where x is the average value, u_x is the confidence interval and P the probability level. This presentation of the result is recommended. The whole question is one of giving a correct value to the confidence interval and the associated probability value, using some tests that characterize accuracy. The result of these tests is a group of measurement results for which it is easy to estimate a variance, then a standard deviation. To obtain an uncertainty range at a given confidence level (in general 95%), the statistical distribution of the measurements is required. The relationship [4.4] can be rewritten in the form:

$$x = x \pm E_{v,P} S_x \quad (P\%) \qquad [4.5]$$

where $E_{\nu, P}$ is a function of the number of statistical degrees of freedom for the accuracy tests ($\nu = N–1$, with N the total number of tests) and the confidence level P. $E_{\nu, P}$ is called the coverage predictor.

If the number of measurements is infinite, using normal law, the confidence interval and probability level would indeed be known. They correspond to the reciprocal of the distribution function taken between two geometric terminals z_1:

$$P(z_1) = \frac{1}{\sqrt{2\pi}} \int_{-z_1}^{z_1} e^{\frac{-\beta^2}{2}} d\beta \qquad [4.6]$$

A spreadsheet or programming software such as Scilab, R or MATLAB® enables the desired values to be obtained easily; some are given in Table 4.1.

P	$E_{+\infty, P}$
90 %	1.64
95 %	1.96
99 %	2.58

Table 4.1. *Coverage predictors for normal law*

QUESTION.– The mean value for an electrical signal is 8.5 V. The variance (the square of the standard deviation) of the measurement is 2.25 V². What is the probability of having a signal between 10 and 11.5 V?

Normal law is most often inapplicable, the number of tests enabling accuracy to be characterized being limited. For a finite number of tests N, the expression of the sample's mean value x remains unchanged:

$$\overline{x} = \frac{1}{N}\sum_{i=1}^{N} x_i \qquad [4.7]$$

The variance S_x^2 should take account of the fact that a statistical degree of freedom is used in calculating the mean. It is therefore:

$$S_x^2 = \frac{1}{N-1}\sum_{i=1}^{N}\left(x_i - \overline{x}\right)^2 \qquad [4.8]$$

It is always possible to define a random variable's standard deviation using a finite number of embodiments of the variable, independently of the statistical law considered. However, its use differs depending on the case. For a finite number of runs, the statistical distribution is no longer entirely a normal law but a Student law, whose coverage predictor, usually written $t_{v,P}$, depends on the number of tests and the confidence level sought. If the number of tests tends towards infinity, Student law tends towards normal law.

Some values of the student coverage predictor are given in Table 4.2 and the probability density function in Figure 4.7. It will be noted, in particular, that when three tests have been carried out, as many norms recommend for mechanical tests, the standard deviation measured should be multiplied by 4.3 to have an uncertainty of 95%. Here, using normal law would lead to the uncertainty range being under-estimated by a predictor of 2. The evolution of predictor $t_{v,\ 95\,\%}$ with the number of degrees of freedom is not linear: from 13 tests, the variation of predictor $t_{v,\ 95\,\%}$ is less than one percent. There is therefore only a very limited advantage in carrying out a large number of tests to reduce the coverage predictor.

♦	$t_{90\%}$	$t_{95\%}$	$t_{99\%}$	♦	$t_{90\%}$	$t_{95\%}$	$t_{99\%}$
1	6.314	12.706	63.657	8	1.860	2.306	3.355
2	2.920	4.303	9.925	9	1.833	2.262	3.250
3	2.353	3.182	5.841	10	1.812	2.228	3.169
4	2.132	2.770	4.604	11	1.796	2.201	3.106
5	2.015	2.571	4.032	12	1.782	2.179	3.055
6	1.943	2.447	3.707	13	1.771	2.160	3.012
7	1.895	2.365	3.499	14	1.761	2.145	2.977

Table 4.2. *Student distribution -t*

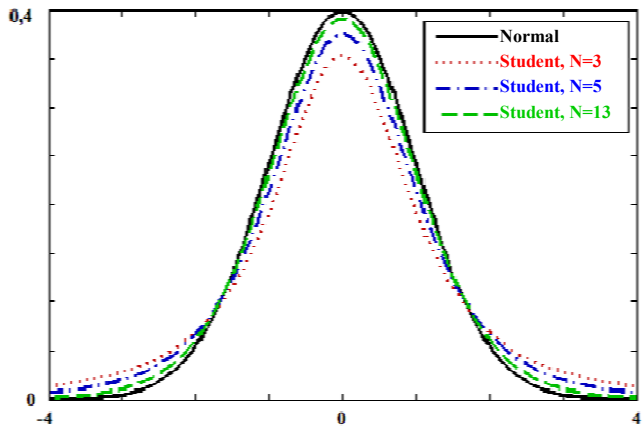

Figure 4.7. *Probability density function for normal law and Student law. For a color version of the figure, see www.iste.co.uk/molimard/mechanics.zip*

A large number of measurement points, however, enable averages to be calculated and an average's standard deviation is naturally less than the standard deviation for each test.

The sample's mean value u_x should be disassociated from the expected value of the random variable x'. When the sample size tends towards infinity, $\overline{x} \to x'$, the standard deviation on the average of the sample u_x

evolves depending on the number of experiments carried out, N according to the relationship:

$$S_{\bar{x}} = S_x / N^{1/2} \qquad [4.9]$$

Taking account of the discussion above on the representiveness of the chosen range, we obtain an estimate of the true mean, obtained from a finite data set:

$$x' = \bar{x} \pm t_{v,P} S_{\bar{x}} \quad (P\%) \qquad [4.10]$$

NOTE.– Just as it is possible to determine the uncertainty of the mean value determined using a finite data set, a similar analysis can be carried out on the standard deviation.

NOTE.– The statistical tool has other applications in mechanics, especially for analyzing life span, or describing roughness.

QUESTION.– Let us consider 20 data samples. The sample's standard deviation is 0.16 and the average value is 1.02. What is the confidence range corresponding to the mean value for a probability of 95%?

4.2.3.3. *Evaluating type-B uncertainty*

A type-B uncertainty evaluation should only be used when the first method is impossible. This approach is based on scientific judgement using available data: the makers' specifications for equipment, the calibration certificate, the designer's experience or knowledge gleaned from literature. When it is only possible to estimate a random variable's lower limit a^- and upper limit a^+, a statistical law must be given to obtain standard uncertainty, that is to say the uncertainty for a standard deviation. The most robust approach consists of assuming that the value can take absolutely any of the values in this range (uniform law). To go a little further, the external values are less probable; a statistical law showing a central zone of equiprobability and lateral zones heading linearly towards zero at their boundaries could be the most pertinent. This law is a trapezoidal law parametered by the proportion of the equiprobable zone β. If parameter β tends towards zero, the law becomes triangular. Table 4.3 gives the uncertainty types associated with each of the statistical laws.

Statistical law	*Uncertainty-type*
Uniform law	$u = \sqrt{\left(a^+ - a^-\right)/12}$
Trapezoidal law	$u = \sqrt{\left(1+\beta^2\right)\left(a^+ - a^-\right)/24}$
Triangular law	$u = \sqrt{\left(a^+ - a^-\right)/24}$

Table 4.3. *Standard uncertainty for different statistical laws*

QUESTION.– A watch with a resolution of 0.01s and a drift of 1 min/month is used as a chronometer for phenomena whose duration ranges from a few seconds to a few minutes. What is the predictable uncertainty for a probability level of 95%? What phenomena could come into account in a more complete analysis of the measurement?

4.2.3.4. *Expanded uncertainty*

Standard uncertainty is the uncertainty expressed for a standard deviation. In the case of normal law, the standard uncertainty $\pm 1 \times u_c$ corresponds to a probability level of 68%. This probability level is most often unsatisfying. A level of 95% is often retained; it is therefore necessary to multiply the standard uncertainty by a coefficient called a coverage predictor to move from a confidence range of 68% to a confidence range of 95%. In the case of normal law, this coefficient is 1.96. This coverage predictor has already been used previously in the description of Student. It must be noted that it depends on the statistical law considered.

4.2.3.5. *Combining uncertainties*

The different quantities influencing the measurement chain can be shown in a mathematical model, represented by a function *f*. By using a Taylor series for the function *f* and ignoring the higher order terms, equation [4.14] is

made linear, and it becomes possible to separate the average value and the random component. It becomes:

$$\bar{y} = f\left(\bar{x}\right) \qquad [4.11]$$

$$u_y = \sqrt{\left(\frac{\partial y}{\partial x}\right)_{\bar{x}}^2} \times u_x \qquad [4.12]$$

In general cases, where the function f depends on the different random variables, the uncertainty is written as the square root of the variance:

$$u_c^2 = \sum_{i=1}^{L} \left(\frac{\partial f}{\partial x_i}\Big|_{\bar{x}} u_{x_i} \right)^2 \qquad [4.13]$$

When the model representing the measurement chain cannot be specified, sensitivity values are often estimated by the perturbation method, each one of the random values is altered slightly at the nominal position, which gives an idea of the average value of the local partial derivative. A more instructive method requiring fewer tests consists of an experimental test plan.

NOTE.– When the input data are correlated, it is necessary to take account of their interactions, which is what the extra-diagonal terms of the covariance matrix describe:

$$u_c^2 = \sum_{i=1}^{L} \left(\frac{\partial f}{\partial x_i} \right)^2 u^2\left(x_i\right) + 2\sum_{i=1}^{L-1} \sum_{j=i+1}^{L} \frac{\partial f}{\partial x_i} \frac{\partial f}{\partial x_j} u\left(x_i, x_j\right) \qquad [4.14]$$

QUESTION.– Re-demonstrate relationship [4.9] using the law of uncertainty composition.

QUESTION.– An oven's average temperature is measured using a sensor whose designer gives a precision of 0.6°C. A reading is taken on a reader whose resolution is 0.1°C. The method for characterizing the temperature in the oven is well-established: it assumes there are eight measurement points in specific places. For each point, ten measurements are made, and the results are presented in Table 4.4. What is the average value and its associated uncertainty?

Location	*Average temp.*	*Standard deviation*	*Location*	*Average temp.*	*Standard deviation*
1	342.1	1.1	*5*	345.2	0.9
2	344.2	0.8	*6*	344.8	1.2
3	343.5	1.3	*7*	345.6	1.2
4	343.7	1	*8*	345.9	1.1

Table 4.4. *Temperature measurements at different points in an oven (°C)*

4.2.3.6. *Monte-Carlo method approach*

When the Taylor series development used in equation [4.14] is not possible, a digital simulation of the uncertainty propagation remains the only approach. In particular, the Taylor series development is impossible if the signal to noise ratio is weak or if the parameters' dependence is very non-linear.

The function describing the measurement chain f defined in equation [4.11] should be explained in analytic or numerical form. It would have to include the sources of uncertainty, such as the model's parameters. In other words, the simplifying assumptions often used are no longer relevant. Each source of uncertainty should be characterized, with a representative statistical law and its parameters. If there are dependencies between the input parameters, they should be described.

The Monte Carlo approach consists of launching a large number of random draws of input parameters and thus writing the probability density function of the quantity to be measured. This type of analysis leads to the most probable value – the expected value – and the range of variation for a given level of probability – the expanded uncertainty. The critical sources of uncertainty, those which most impact the measurement's uncertainty, are also very important results of this analysis. Depending on this result, a new design for the experiment equipment or the experiment protocol will enable the variability range to be improved at the lowest cost by working only on critical points.

4.3. Experimental test plans

From a scientific point of view, the previous sections (calibration, statistical analysis of measurement, uncertainty analysis, etc.) focused on a point that is very important in mechanics: knowing the value and the accuracy accorded to it. There are, however, a number of studies that lack models. It is therefore necessary to return to scientific basics: the phenomenological approach. Within this framework, experimental test plans can be very important aids.

On the other hand, from the point of view of engineering, a design office must respond in the least time at the least cost, but give an "acceptable" level of quality. If the level of quality required is overestimated, it leads to unnecessary cost. If it is under-estimated, the client is not satisfied. Optimizing the number of tests to be carried out to obtain a correct result is one step to integrate. Well-known examples include process optimization (plasturgy) or even aeronautical tests.

The principles behind design plan methods consist of analyzing a phenomenon, which produces an outcome, y depending on i *predictors* x_i. Predictors can generally be expressed in a digital form, with a given maximal value conventionally set to +1 and a minimum value to –1. In defining experimental test plans, it is sometimes possible to reduce the dimension using a-dimensional sizes such as, for example, Reynolds numbers (fluid mechanics) or Péclet (thermal) mechanics.

Unfortunately, it is sometimes very difficult to define a digital size, such as for example in sensory approaches, to define surface quality. For example, how can we reliably and reasonably sensitively characterize the surface quality of a pen cap? Is it by addressing sides with dimensional tolerances (cylindricality), the surface state at microscopic level, or the diffusion coefficient, or the light reflection on the sides? Similarly, the outcome, like the predictors, can be discreet or continuous, for example, the colors are "red" ,"green" or "blue", etc.

While Figure I.11 focused on experimental tasks, Figure 4.8 shows the process of acquiring knowledge from a broader perspective, as the "experiments" are "experimental" or "digital", which occurs when analyzing phenomena that demand vast resources in terms of calculating power (for example, car accidents or surgery).

First of all, it is necessary to pose the problem we wish to study correctly. Then, and above all, it is necessary to ensure that the solution does not already exist elsewhere (bibliography, internal notes, theory, consulting experts, etc.). Once this phase of analysis and documentation is carried out, it is necessary to define an experimental model and a design plan to be used.

The experimental model is the testing equipment, the associated instruments and the experimental protocol. The testing equipment is broadly intuitive; however, we should not neglect the secondary conditions (environmental or vibratory). The instruments should be adapted in each case; positioning distortion gauges for example, depends on the test piece's geometry and the type of load envisaged. Finally, the experiment protocol is essential since it enables the dispersion linked to the operator to be limited. It can rely on the good practice described in the norms.

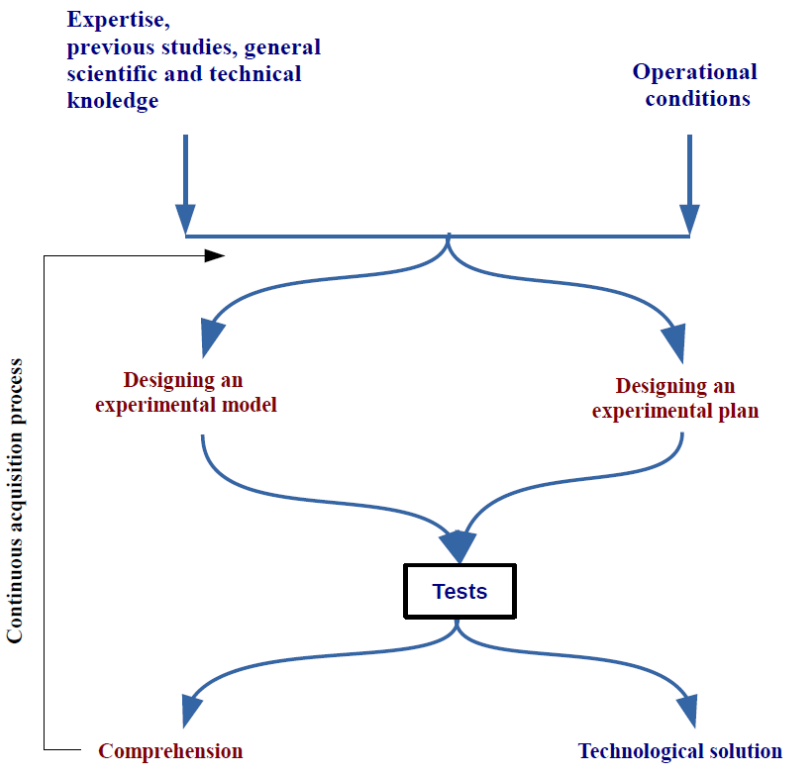

Figure 4.8. *Process for acquiring knowledge*

The theory of experimental test plans focuses more specifically on the quantity and the spatial distribution of predictors in the experimental case frame of reference. Figure 4.8 shows an iterative learning process. Even if an initial series of tests can result in a modification of the experiment model, ideally only experimental test plans can be changed in order to improve the model's relevance in describing the object studied. The corollary question is evidently that of the test enabling the model's exactitude to be checked and for data acquisition to be stopped.

4.3.1. *Preparation*

The test campaign addresses the following questions:

– what results will be recorded in each test?

– what predictors influence the process studied?

– to what field of study does each of these predictors belong?

– what systematic errors could be revealed and how can they be ruled out?

– what are the possible experiment constraints?

– can we envisage complementary tests to evaluate the experimental error committed?

This reflection should be carried out with care. It is important to *take the time* necessary to clarify the predictors and quantities that are of interest. It is also advantageous to *involve many people* (especially technicians) at this stage of the process. This culminates in choosing the design of the experiment, taking account of potential experimental errors. This experimental test plan should be made after determining the order of the tests at random, which has the effect of quietening phenomenon linked to time (an instrument's systematic drift, a material's relaxation, etc.). These still have effects, but these are randomized and appear in the analysis as additional noise. But be careful: the methodology described hereafter relies on the fact that the uncertainties are constant, especially over time. The randomization suggested does not allow this limitation to be ruled out.

Results analysis begins with a critical look at the run's quality:

– does a result seem aberrant?

– have the levels postulated at the start really been reached?

– does the supposed mathematical model represent the results correctly?

– have the risks of ambiguity been correctly avoided (coupling phenomenon)?

When the quality of the results has been validated, we can move on to calculations and interpretations. Depending on the conclusions, complementary tests will be envisaged. They can call the mathematical model into question (a first or second degree mathematical model), or eliminate ambiguity. It will be attempted, when designing later experiments, to, at best, include existing results so as to minimize the time required and maximize the wealth of information.

4.3.2. *Approach*

In the absence of scientific arguments relevant to the tests envisaged, methodology consists of turning from the simplest model to more detailed models. At each stage, the model is tested using *analysis of variance* (ANOVA). The necessary tests are therefore those that aim to establish the model, but also those enabling its robustness to be analyzed at a well-chosen additional measuring point, repeated a number of times in order to quantify the tests' dispersion. The analysis method will be described in more detail in section 4.3.6. The models that can be envisaged are linear models without interaction, then with second order of interaction and finally quadratic with interaction.

The respective formulas for the different models are:

$$f(x) = \beta_0 + \sum_{i=1}^{m} \beta_i x_i \qquad [4.15]$$

$$\forall\, x \in E, \quad f(x) = \beta_0 + \sum_{i=1}^{m} \beta_i x_i + \sum \sum_{i<j} \beta_{ij} x_i x_j \qquad [4.16]$$

$$\forall\, x \in E, \quad f(x) = \beta_0 + \sum_{i=1}^{m} \beta_i x_i + \sum_{i=1} \beta_{ii} x_i^2 + \sum \sum_{i<j} \beta_{ij} x_i x_j \qquad [4.17]$$

The advantage of this approach lies in the gradual increase in the number of unknowns and therefore in the minimum number of experiments to be carried out, as Table 4.5 shows. We will see the efficiency of the approach suggested here if we consider that the classic approach for design plans gives

a number of unknowns of 2^m (complete factorial design). However, as will be described below, the number of tests is sometimes greater than the number of unknowns in order to conserve the predictors' space symmetry. This approach, shown briefly here, is analyzed in more detail in Tinsson's work [TIN 10].

In the first instance, the experimental test plan makes it possible to class the most important predictors and reject those that do not influence the outcome (screening). The predictor's lack of dimension in the form of high (+1) and low values (–1) on a given range enables their sensitivities β_i to be compared directly with one another. But in order to do this it is necessary to ensure that the models are relevant, that is to say that they do not lead to systematic errors greater than the tests' random variability: this is the aim of ANOVA, developed in section 4.3.6.

Secondly, the experimental test plan model can be used to optimize parameters (response surface analysis). This therefore involves comprehending the model using the relationships [4.15], [4.16] or [4.17], finding an optimal value for the outcome in the experimental space, whether it is a maximum or a minimum. As in any data adjustment method, the experimental model has no value except for the limits that serve to establish it, but not more.

Model type	Number of unknowns p
Linear without interaction	$m + 1$
Linear with order 2 interactions	$(m^2 + m + 2)/2$
Quadratic with order 2 interactions	$(m + 2)(m + 1)/2$

Table 4.5. *Number of unknowns for different models*

4.3.3. *Adjusting polynomial models by least squares*

Generally, experiments have n responses available (so n equations) to identify the values of $m + 1$ coefficients. Insofar as there are more experiments than there are variables, the problem is one of minimization. Each of the n runs can be written, especially in the form of an experimental model, as shown in relationships [4.15], [4.16] and [4.17]. The group of relationships

corresponding to *n* runs can be synthesized in a standard fashion in the form of a matrix relationship:

$$Y = X \quad \beta + \varepsilon \qquad [4.18]$$

In this relationship, Y is the run's vector, X is the experimental model's matrix, containing all the experiment conditions and β is the vector for the model's parameters. The term ε covers the errors (experimental uncertainty, errors in the model's fitting) that need to be minimized, through writing in the function:

$$J(\beta) = \frac{1}{2}\|X\ \beta - Y\|^2 = \frac{1}{2}\ {}^t(X\ \beta - Y)(X\ \beta - Y) \qquad [4.19]$$

An extremum $J(\beta)$ is sought by deriving the function with respect to different variables β_i, $i \in$ N. If the approximate solution minimizing the differences in the least squares-sense is written $\hat{\beta}$, the mathematical expression is:

$$\nabla_\beta J\left(\hat{\beta}\right) = 0 \Leftrightarrow {}^t X\left(X\hat{\beta} - Y\right) = 0 \qquad [4.20]$$

By developing equation [4.20], if the matrix $({}^t X\, X)$ is invertible, that is to say if the number of independent experiments is greater than the number of unknowns; and if the conditioning for this matrix is correct the approximate solution in the least-squares sense is:

$$\hat{\beta} = \left({}^t X\ X\right)^{-1}\ {}^t\ X\ Y \qquad [4.21]$$

Consequently, it is possible to establish an estimate of the outcome written Y using the relationship [4.18].

$$\hat{Y} = X\left({}^t X\ X\right)^{-1}\ {}^t\ X\ Y \qquad [4.22]$$

The covariance matrix of $\hat{\beta}$ is given by the relationship:

$$\mathrm{Var}\left(\hat{\beta}\right) = \left[\left({}^t X\ X\right)^{-1}\ {}^t X\right]\mathrm{Var}(Y)^t\left[\left({}^t X\ X\right)^{-1}\ {}^t X\right] \qquad [4.23]$$

Under the hypothesis of a constant variance for Y (homoscedasticity), the variances on $\hat{\beta}$ and Y are simplified to:

$$\mathrm{Var}\left(\hat{\beta}\right) = \sigma_Y^2 \left({}^t X X\right)^{-1} \quad [4.24]$$

$$\mathrm{Var}\left(\hat{Y}\right) = \sigma_Y^2 \left[X \left({}^t X X\right)^{-1} {}^t X \right] \quad [4.25]$$

The optimality criteria for choosing experiment points are based on study of the matrix $({}^t X X)$. Different criteria exist. They seek to:

– minimize the global prediction error, that is to say, to minimize the determinant of the $({}^t X X)$ matrix (D-Optimality criterion);

– minimize the matrix trace (A-Optimality);

– minimize disproportionately high sensitivity (G-Optimality);

– ensure an identical error for a constant distance from the center of the domain explored (rotability).

4.3.4. *Linear factorial design without interaction*

4.3.4.1. *Linear model*

Independent of the choice of experimental points, if we consider n different runs, in the sense of the model, the j-th run is expressed by the expression:

$$y_{(j)} = f\left(x_{(j)}\right) = \beta_0 + \sum_{i=1}^{m} \beta_i x_{(j)i} \quad [4.26]$$

If we aggregate all the tests, it becomes the matrix expression:

$$\begin{bmatrix} 1 & x_{(1)1} & x_{(1)2} & \cdots & x_{(1)m-1} & x_{(1)m} \\ 1 & x_{(2)1} & x_{(2)2} & \cdots & x_{(2)m-1} & x_{(2)m} \\ \vdots & \cdots & \ddots & \cdots & \cdots & \cdots \\ 1 & x_{(n)1} & x_{(n)2} & \cdots & x_{(n)m-1} & x_{(n)m} \end{bmatrix} \begin{pmatrix} \beta_0 \\ \beta_1^L \\ \vdots \\ \beta_m^L \end{pmatrix} = \begin{pmatrix} Y_{(1)} \\ Y_{(2)} \\ \vdots \\ Y_{(n)} \end{pmatrix} \quad [4.27]$$

or, in the contracted form:

$$\left[I_n \middle| D_L \right] \{\beta\} = \{Y\} \qquad [4.28]$$

in this writing I_n is a unit vector, corresponding to the calculation of the mean β_0 and D_L the matrix of the experimental test plan containing all the states of all the predictors. X is the matrix representing the model.

X is a rectangular matrix; estimating the vector of the unknowns β is therefore impossible using simple inversion and instead requires a minimization process (see equation [4.21] and more generally section 4.3.2).

4.3.4.2. *Usual experimental test plans*

Until now, the problem of choosing experiment points has not been raised and this result remains general. The first rule we will give ourselves for constructing an experimental test plan is to meet the design's orthogonality condition. This is expressed by the matrix's diagonality (${}^tXX$), which guarantees its reversibility. However, this condition is not enough, as some quantities of influence potentially have more weight in estimating the response than others. It is therefore necessary to add an equality condition to the diagonal terms. An experiment plan is called "usual" if all the diagonal terms of (${}^tXX$) are equal to the number of tests n. In these conditions, the propagation of uncertainty is the same for all the $\hat{\beta}_L$ estimators. By applying the relationships [4.21] and [4.22], the estimators of $\hat{\beta}_0$, $\hat{\beta}_L$, and $\hat{Y}_L$ are then summarized in Table 4.6. The variable s_2 is given by $\forall i = 1,...,m$ $s_2 = \sum_{u=1}^{n} x_{(u)i}^2$. It can be seen that the variance on $\hat{\beta}_0$ is different to the variance on $\hat{\beta}_L$. This difference appears if the points are added to the center of the experiment domain. It can also be noted that with such a construction, the variance for estimating Y in a point x of the experiment space is the same whatever the direction for a given distance at the center of the experimental test plan (rotability criteria for the experimental test plan).

$\hat{\beta}_0 = Y$	$\mathrm{var}\left(\hat{\beta}_0\right) = \dfrac{\sigma^2}{n}$
$\hat{\beta}_L = \dfrac{1}{s_2}\,{}^t DY$	$\forall i = 1,\ldots,m \;\; \mathrm{var}\left(\hat{\beta}_i\right) = \dfrac{\sigma^2}{s_2}$
$\hat{Y}(x) = x\left({}^t X X\right)^{-1}\,{}^t X Y$	$\mathrm{var}\left(\hat{Y}(x)\right) = \sigma^2\left(\dfrac{1}{n} + \dfrac{1}{s_2}\|x\|^2\right)$

Table 4.6. *Estimators and variance for a usual linear experiment design without interaction*

4.3.4.3. *Factorial experimental test plans*

A factorial design plan is a design on two levels: a high level, noted as +1 and a low level noted as -1. The factorial design is complete if it includes all the combinations of all the predictors; it therefore uses all the vertices of the experimental space's hypercube. A supplementary test should be made to check the validity of the experimental test plan model and the experimental model's dispersion. It is carried out in the middle of the experiment space (0, 0). One possible name is FD, for Full Design, followed by the number of levels (2) of power, the number of predictors (m), then the number of central replications. Two examples of a design are given in Table 4.7. One easy construction method consists of alternating the +1 and -1 levels for the k-th column every 2^k terms.

	2 predictors, 3 central replications	3 predictors, 0 central replication
Name	FD(2^2, 3)	FD(2^3, 0)
Shape of the design matrix	$D_L = \begin{vmatrix} -1 & -1 \\ 1 & -1 \\ -1 & 1 \\ 1 & 1 \\ 0 & 0 \\ 0 & 0 \\ 0 & 0 \end{vmatrix}$	$D_L = \begin{bmatrix} -1 & -1 & -1 \\ 1 & -1 & -1 \\ -1 & 1 & -1 \\ 1 & 1 & -1 \\ -1 & -1 & 1 \\ 1 & -1 & 1 \\ -1 & 1 & 1 \\ 1 & 1 & 1 \end{bmatrix}$

Table 4.7. *Examples of complete factorial designs*

QUESTION.– Express the constants n and s_2 in the two cases described in Table 4.7. What is the standard uncertainty linked to $\hat{\beta}_0$ and $\hat{\beta}_L$ for a given dispersion constant σ?

QUESTION.– Show that an experimental test plan with three uncentered repetitions is not a usual design.

The design $D_L = \begin{bmatrix} -1 & -1 \\ 1 & -1 \\ -1 & 1 \\ 1 & 1 \\ \alpha & \gamma \\ \alpha & \gamma \\ \alpha & \gamma \end{bmatrix}$ will be written with $\alpha, \gamma \neq 0$.

4.3.4.4. *Regular fraction of a complete factorial design*

For a complete factorial design, the number of tests to be carried out is therefore 2^m, a series that grows remarkably fast. For example, for six predictors tested, the number of tests is 64; for two predictors more (8), the number of tests is 256. This situation enables all the interactions in a linear design to be determined, but in many cases, these interactions are not useful for comprehension and linear or rank-2 interaction model is enough. Determination of a regular fraction for a complete factorial design aims to adjust the number of tests to the number of parameters to be determined more closely. The most relevant points of the complete factorial design are selected depending on the model behavior kept, in this case the linear model without interaction.

In order to see the approximations produced by down sampling points, it is useful to introduce the complete model, with all the measurable interactions. This is an FD (2^3, 0) experimental test plan (the central replications do not change the reasoning; they are removed to avoid overburdening the equations). The complete model for this design is:

$$\begin{aligned} \forall x \in E, \quad f(x) &= \beta_0 + \beta_1 x_1 + \beta_2 x_2 + \beta_3 x_3 \\ &+ \beta_{12} x_1 x_2 + \beta_{13} x_1 x_3 + \beta_{23} x_2 x_3 \\ &+ \beta_{123} x_1 x_2 x_3 \end{aligned} \qquad [4.29]$$

For all the points in the factorial design, it therefore generates the relationship:

$$\left[I_n \left| D_L \right| D_I \right] \{\beta\} = \{Y\} \qquad [4.30]$$

with the interaction matrix D_I:

$$D_I = \begin{bmatrix} \vdots & \vdots & \vdots & \vdots & \vdots \\ x_{(i)1}x_{(i)2} & x_{(i)1}x_{(i)3} & x_{(i)1}x_{(i)3} & x_{(i)2}x_{(i)3} & x_{(i)1}x_{(i)2}x_{(i)3} \\ \vdots & \vdots & \vdots & \vdots & \vdots \end{bmatrix} \qquad [4.31]$$

Finally, the experimental model's matrix is:

$$X = \begin{bmatrix} +1 & -1 & -1 & -1 & +1 & +1 & +1 & -1 \\ +1 & +1 & -1 & -1 & -1 & -1 & +1 & +1 \\ +1 & -1 & +1 & -1 & -1 & +1 & -1 & +1 \\ +1 & +1 & +1 & -1 & +1 & -1 & -1 & -1 \\ +1 & -1 & -1 & +1 & +1 & -1 & -1 & +1 \\ +1 & +1 & -1 & +1 & -1 & +1 & -1 & -1 \\ +1 & -1 & +1 & +1 & -1 & -1 & +1 & -1 \\ +1 & +1 & +1 & +1 & +1 & +1 & +1 & +1 \end{bmatrix} \qquad [4.32]$$

The last column, which corresponds to the interaction between predictor 1, predictor 2 and predictor 3, is the multiplication, term by term, of the columns corresponding to the effect of predictors 1, 2 and 3. Of the $2^3 = 8$ tests of the complete factorial design, 4 have the interaction value ($x_1x_2x_3 = 1$) and 4 have the interaction value ($x_1x_2x_3 = -1$). By selecting the 4 points such as ($x_1x_2x_3 = 1$), it is always possible to determine the 4 variables in the linear model without interaction. As this choice has been made for a constant level of the product $x_1x_2x_3$, the design does not permit the level of this interaction to be determined.

Retaining only the points ($x_1x_2x_3 = 1$), the equalities of the columns' terms must also be noted ($x_1x_2 = x_3$), as well as ($x_1x_3 = x_2$) and ($x_2x_3 = x_1$). This means that by construction $\hat{\beta}_1^* = \hat{\beta}_{23}^*$, $\hat{\beta}_2^* = \hat{\beta}_{13}^*$, and finally $\hat{\beta}_3^* = \hat{\beta}_{12}^*$. $\hat{\beta}_i^*$, or $\hat{\beta}_{ij}^*$ refer to estimations of the predictors's effects, obtained using the information

available in this reduced space in contrast to $\hat{\beta}_i$ and $\hat{\beta}_{ij}$, which refer to the estimation of the predictors' effects obtained from information from the complete factorial design. A slightly deeper analysis enables us to establish that:

$$\hat{\beta}_1^* = \hat{\beta}_1 + \hat{\beta}_{23}$$

$$\hat{\beta}_2^* = \hat{\beta}_2 + \hat{\beta}_{13}$$

$$\hat{\beta}_3^* = \hat{\beta}_3 + \hat{\beta}_{12}$$

Insofar as the interactions are negligible, $\hat{\beta}_1^* \approx \hat{\beta}_1$, $\hat{\beta}_2^* \approx \hat{\beta}_2$, $\hat{\beta}_3^* \approx \hat{\beta}_3$.

All these relationships flow from $x_1x_2x_3 = 1$. This relationship is written symbolically in the notation to Box **I** = **1**.**2**.**3**, where each term represents a column of the experimental test plan. If it is observed that each product of a column by **I** is equal to the column itself and that the product of a column by itself is the neutral element **I**, the previous relationships can be written according to the same algebra:

I = 123 ⇔ 1 = 23 ⇔ 2 = 13 ⇔ 3 = 12

I = 123 is called an alias generator. **23** is the alias of **1**, and respectively **13** that of **2** and **12** that of **3**. Here, **1** has a single alias, but in most cases, there are as many aliases as there are possible combinations of the alias generator giving **1**.

The regular fraction of the factorial design written FD (2^{3-1}, 0, ***I*** = **123**) therefore enables an estimation of the predictors' effects in the case of a linear model without interaction. Adding an alias generator enables the number of tests to be divided by 2. The matrix of the experimental model of FD (2^{3-1}, 0, ***I*** = **123**) is written:

$$X = \begin{bmatrix} +1 & +1 & -1 & -1 \\ +1 & -1 & +1 & -1 \\ +1 & -1 & -1 & +1 \\ +1 & +1 & +1 & +1 \end{bmatrix} \qquad [4.33]$$

It must be noted that the regular fraction FD (2^{3-1}, 0, ***I*** = **-123**) would give another, equally valid estimation.

The reasoning here is acceptable, but not all the divisions of the complete design give useful results. For example, selecting a regular fraction on the basis of the interaction (x_1x_2=1) would give, in the algebraic notations already defined, the following rules: **I** = **12**, but also, **1**=**2**. This means that it is not possible to distinguish the effect of predictor 1 and the effect of predictor 2 with such a choice. This example enables the notion of the *resolution* of the regular fraction to be introduced. **I** = **12** is called resolution 2; **I** = **123** is resolution 3. To conveniently separate the predictors' linear effects the resolution for the regular fraction should be at least 3.

Table 4.8 shows the regular fractions of a complete factorial design for a linear model without interactions. As soon as the number of predictors increases, several alias generators should be used simultaneously. Comparing column FD (the number of tests to be carried out for the complete factorial design) and column Frac (the number of tests to be carried out for the regular fraction) shows how effective this approach is. Some situations are noted in italics: they correspond to *saturated* designs, that is to say designs for which the number of tests is equal to the number of unknowns in the model. Other types of design are systematically saturated. Simplex designs, which are very flexible, exist for all possible predictor numbers, but the values of the levels of each predictor are no longer -1, 0 or 1, which sometimes makes them difficult to use. The Plackett and Burman designs guarantee levels of -1, 0 or 1, but can only be adapted to a certain number of predictors. Additional information can be obtained in works that focus on experimental test plans for example [GOU 97] or [TIN 10].

QUESTION.– Express the 7 aliases of predictor 1 for the design with 7 predictors.

4.3.5. *Linear factorial design with interactions*

The most reasonable linear design with interaction is a design with order 2 interactions. The higher orders often have a negligible influence on the result. The model for this design is:

$$\forall x \in E, \quad f(x) = \beta_0 + \sum_{i=1}^{m} \beta_i x_i + \sum \sum_{i<j} \beta_{ij} x_i x_j \qquad [4.34]$$

	p	FD	Frac	Generators
2 predictors	3	4	–	–
3 predictors	*4*	*8*	*4*	*123*
4 predictors	5	16	8	1234
5 predictors	6	32	8	124, 135
6 predictors	7	64	8	124, 135, 236
7 predictors	*8*	*128*	*8*	*124, 135, 236, 1237*
8 predictors	9	256	16	125, 126, 147, 238
9 predictors	10	512	16	125, 126, 147, 238, 249
10 predictors	11	1024	16	125, 126, 147, 238, 249, 3410
11 predictors	12	2048	16	1235, 137, 1248, 12349, 1210,1311, 2346
12 predictors	13	4096	16	145, 179, 1310, 1611, 256, 2411, 2712, 367

Table 4.8. *Regular fractions for a complete factorial design for a linear model without interactions (according to [TIN 10])*

The corresponding matrix expression is:

$$\left[I_n \middle| D_L \middle| D_I \right] \{\beta\} = \{Y\} \qquad [4.35]$$

The matrix for interaction D_I and the vector β are expressed by:

$$D_I = \begin{bmatrix} \vdots & \vdots & \vdots & \vdots & \vdots \\ x_{(i)1}x_{(i)2} & \cdots & x_{(i)1}x_{(i)k} & \cdots & x_{(i)m-1}x_{(i)m} \\ \vdots & \vdots & \vdots & \vdots & \vdots \end{bmatrix} \qquad [4.36]$$

$$\beta = {}^t\left(\beta_0 \middle| \underbrace{\beta_1^L \cdots \beta_m^L}_{linear} \middle| \underbrace{\beta_{12}^I \cdots \beta_{(m-1)m}^I}_{\text{int}eraction} \right) \qquad [4.37]$$

This model therefore adds C_m^2 unknowns to the former. The usual design in this case is one in which the matrix^t (XX) is diagonal, with the same

sensitivities for linear terms, and the same sensitivities for the interaction terms. The estimators of $\hat{Y}$, $\hat{\beta}_L$, are the same as in the previous case (linear without interactions); the estimation of $\hat{\beta}_I$ is given in Table 4.9. The variable s_{22} is given by $\forall i = 1,...,m \quad s_{22} = \sum_{u=1}^{n} x_{(u)i}^2 x_{(u)j}^2$. In the case of factorial designs, it will be noted that $s_2 = s_{22}$, the levels being +1 or -1. The variance over $\text{Var}(\hat{\beta}) = \sigma_\gamma^2 ({}^t X\, X)^{-1}$ shows a term in x^4. The rotability condition is therefore no longer met, as Figure 4.9 illustrates.

$\hat{\beta}_0 = \overline{Y}$	$\text{var}\left(\hat{\beta}_0\right) = \dfrac{\sigma^2}{n}$
$\hat{\beta}_L = \dfrac{1}{s_2}\,{}^t DY$	$\forall\, i = 1,...,m \quad \text{var}\left(\hat{\beta}_i\right) = \dfrac{\sigma^2}{s_2}$
$\hat{\beta}_I = \dfrac{1}{s_{22}}\,{}^t D_I Y$	$\forall\, i = 1,...,m \quad \text{var}\left(\hat{\beta}_{ij}\right) = \dfrac{\sigma^2}{s_{22}}$
$\hat{Y}(x) = x\left({}^t XX\right)^{-1t} XY$	$\text{var}\left(\hat{Y}(x)\right) = \sigma^2\left(\dfrac{1}{n} + \dfrac{1^2}{s_2}\|x\|^2 + \dfrac{1}{2s_{22}}\|x\|^4 - \dfrac{1}{2s_{22}}\sum_{i=1}^{m} x_i^4\right)$

Table 4.9. *Estimators and variance for a usual linear design plan with interactions*

As seen previously, the complete factorial design enables a linear model with interactions to be adjusted. This design is not optimal if the number of predictors exceeds 5. A regular fraction of the complete design can be used to reduce the number of tests. However, the alias generator should separate interactions, therefore **PQ** = **KL** type situations (in Box notation), which is **KLPQ** = **I**. The alias generator should therefore be order 5, that is to say the form **KLPQR** = **I**. Table 4.10 summarizes the number of tests for a complete factorial design, for the best fractional design and gives the corresponding alias generators. Even if the optimal number of tests remains useful, the addition of interactions triggers a dramatic increase. For example, for 8 predictors, the optimal number of tests is 8 for a design without interaction and 64 for the design with order 2 interactions. This type of design should therefore be justified by the previous design's inadequacies.

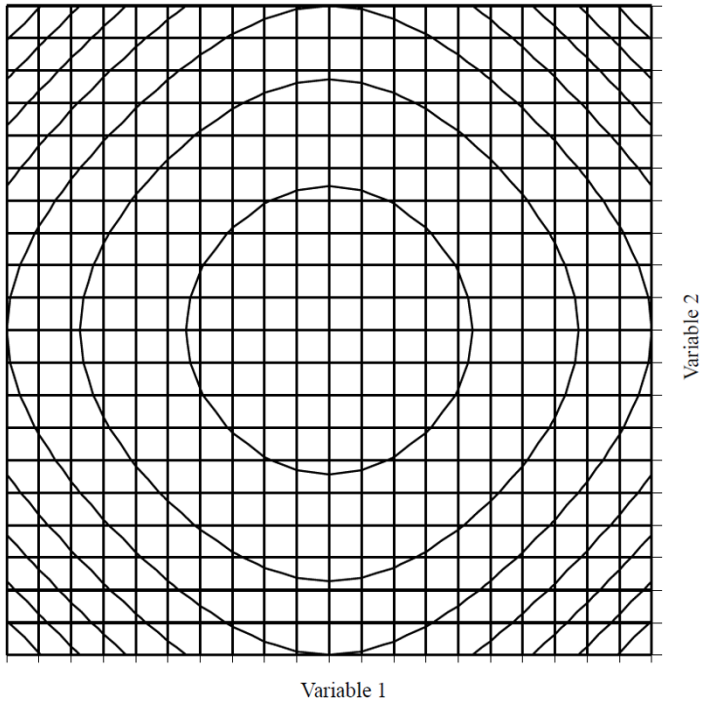

Figure 4.9. *Variance of the estimator Var* $(\hat{\beta}) = \sigma_v^2 ({}^t X\ X)^{-1}$ *for a factorial linear design with 2 predictor interactions*

	p	FD	Frac	Generators
2 predictors	4	4	–	–
3 predictors	7	8	–	–
4 predictors	11	16	–	–
5 predictors	*16*	*32*	*16*	*12345*
6 predictors	22	64	32	123456
7 predictors	29	128	64	1234567
8 predictors	37	256	64	12345, 45678
9 predictors	46	512	128	12345, 56789
10 predictors	56	1024	128	12378, 23459, 134610

Table 4.10. *Regular fractions for a complete factorial design for a linear model with interactions (after [TIN 10])*

4.3.6. *Quadratic design with interactions*

In the process of continuously acquiring experimental test plans, quadratic designs are implemented after linear designs, without, and then with, interactions. They thus naturally exploit the points that are already known. The transition from one design to another is made on the basis of statistical tests aiming to determine the model's accuracy (see sections 4.3.6 and 4.4.5). The quadratic design can also be justified by physical considerations, if an optimum is expected within the domain studied.

Quadratic design with order 2 interaction has the following as a model:

$$\forall x \in E,\ f(x) = \beta_0 + \sum_{i=1}^{m} \beta_i x_i + \sum_{i=1} \beta_{ii} x_i^2 + \sum \sum_{i<j} \beta_{ij} x_i x_j \qquad [4.38]$$

The corresponding matrix expression is:

$$\left[I_n \middle| D_L \middle| D_Q \middle| D_I \right] \{\beta\} = \{Y\} \qquad [4.39]$$

with the supplementary matrix D_Q and the vector β expressed as:

$$D_Q \begin{bmatrix} \vdots & \vdots & \vdots & \vdots & \vdots \\ x_{(i)1}^2 & \cdots & x_{(i)l}^2 & \cdots & x_{(i)m}^2 \\ \vdots & \vdots & \vdots & \vdots & \vdots \end{bmatrix} \qquad [4.40]$$

$$\beta = {}^t \left(\beta_0 \middle| \underbrace{\beta_1^L \cdots \beta_m^L}_{linear} \middle| \underbrace{\beta_{11}^Q \cdots \beta_{mm}^Q}_{quadratic} \middle| \underbrace{\beta_{12}^I \cdots \beta_{(m-1)m}^I}_{interaction} \right) \qquad [4.41]$$

The quadratic model therefore adds m unknowns to the former. It is not possible to obtain the (${}^tXX$) matrix's orthogonality. The usual design in this case is as:

$$\left({}^t XX \right) = \begin{bmatrix} n & 0 & s_2^t I_m & 0 \\ 0 & s_2 I_m & 0 & 0 \\ s_2 I_m & 0 & (s_4 - s_{22}) I_m + s_{22} J_m & 0 \\ 0 & 0 & 0 & s_{22} I_{m(m-1)/2} \end{bmatrix} \qquad [4.42]$$

with I_m a vector of m terms equal to 1, J_m a size $m \times m$ matrix of which all the terms are equal to 1. s_2 and s_{22} are given by the previous expressions and s_4 by: $\forall i = 1,...,m \quad s_4 = \sum_{u=1}^{n} x_{(u)i}^4$.

As the $({}^tXX)$ matrix is not diagonal, the expressions of the estimators and the variances are more complex (Tables 4.11 and 4.12), the other terms remaining unchanged in relation to the linear designs with interaction (Table 4.9).

$\hat{\beta}_0 = \bar{Y} + \frac{S_2}{\varphi}\left(m s_2 \bar{Y} - \sum_{u=1}^{n} \|z_u\|^2 Y_u \right)$
$\hat{\beta}_Q = \frac{1}{s_4 - s_{22}}\, {}^t D_Q Y - \frac{1}{\varphi}\left(n s_2 \bar{Y} + \frac{n s_{22} - s_2^2}{s_4 - s_{22}} \sum_{u=1}^{n} \|z_u\|^2 Y_u \right)$
with $\varphi = n s_4 + n(m-1) s_{22} - m s_2^2$

Table 4.11. *Estimators for a usual quadratic experimental plan with interactions*

$\mathrm{var}\left(\hat{\beta}_0\right) = \frac{\sigma^2}{n}\left(1 + m\frac{s_2^2}{\varphi}\right)$
$\mathrm{var}\left(\hat{\beta}_{ii}\right) = \frac{\sigma^2}{s_4 - s_{22}}\left(1 + \frac{s_{22}^2 - n\, s_2^2}{\varphi}\right)$
$\mathrm{var}\left(\hat{Y}\right) = \sigma^2\left[\left(\frac{1}{n} + \frac{m\, s_2^2}{n\varphi}\right) + \left(\frac{1}{s_2} - 2\frac{s_2}{\varphi}\right) r^2 + \left(\frac{1}{2 s_{22}} + \frac{s_2^2 - n s_{22}}{\varphi(s_4 - s_{22})}\right) r^4\right]$
$\mathrm{var}\left(\hat{Y}\right) = \sigma^2\left[\left(\frac{1}{n} + \frac{m\, s_2^2}{n\varphi}\right) + \left(\frac{1}{s_2} - 2\frac{s_2}{\varphi}\right) r^2 + \left(\frac{1}{2 s_{22}} + \frac{s_2^2 - n s_{22}}{\varphi(s_4 - s_{22})}\right) r^4 + \left(\frac{1}{s_4 - s_{22}} - \frac{1}{2 s_{22}}\right) \sum_{i=1}^{m} x_i^4\right]$

Table 4.12. *Variances for a usual quadratic experimental plan with interactions (after [TIN 10])*

The hypothesis for positioning experimental points relies on the fact that a factorial design has already been made. It is therefore necessary to add supplementary measuring points. For a composite, centered design, pairs of points are added to the axes of the variables, at a distance α from the center of the experimental test plan, as illustrated in Figure 4.10. This distribution

of points enables the curvature effects in the quadratic model to be rendered while retaining the design's symmetry.

In the framework of this design,

$$\begin{aligned} s_2 &= 2^{m-q} + 2\alpha^2 \\ s_{22} &= 2^{m-q} \\ s_4 &= 2^{m-q} + 2\alpha^4 \end{aligned} \qquad [4.43]$$

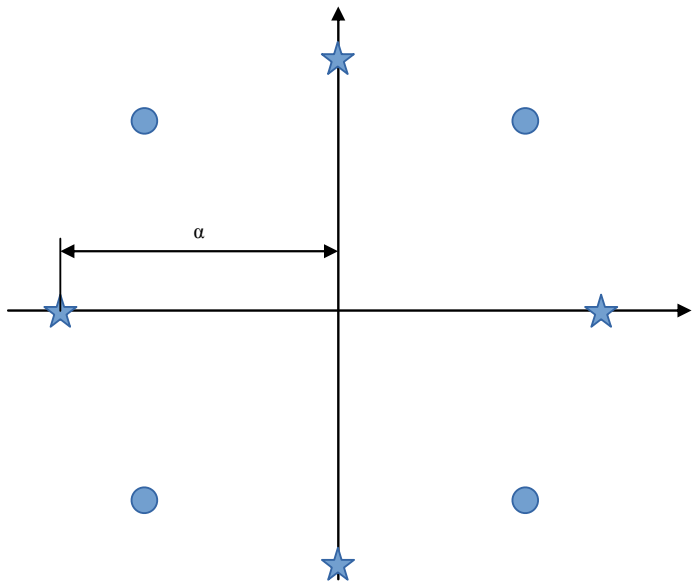

Figure 4.10. *Position of experimental points in a quadratic design (two dimensional case)*

To define parameter α, it is necessary to provide a constraint on the experimental test plan. A reasonable constraint involves conserving the isovariance in rotation with the estimator $\hat{Y}(x)$. The quality of the estimation of $Y(x)$ is therefore the same whatever the direction for a given distance at the center of the design plan. It results necessarily from Table 4.12 that $s_4 = 3\ s_{22}$, which implies, using equation [4.43], that $\alpha = (2^{m-q})^{1/4}$. In the most common situations, α varies from 1.4 to 2.8. In practice, this means, that the user of a design plan should take care and give conservative limits to the

problem they are handling, as a quadratic design leads to an enlargement of the experimental domain. If, however, this enlargement was not possible and had been poorly anticipated, other choices are possible for α, for example $\alpha = 1$, which comes to be placed on the sides of the hypercube. The isovariance condition can evidently no longer be met.

4.3.7. *Variance analysis*

Variance analysis is a very complete domain and, here, we will only tackle its most general principles. This type of analysis aims to validate the model of an experimental test plan by comparing variation sizes obtained experimentally and in the model. We thus define the sum of the squares of variances (SST) and the sum of squares linked to regression (SSR) as:

$$SST = \sum_{i=1}^{n} \left(Y_i - \overline{Y} \right)^2 \qquad [4.44]$$

$$SSR = \sum_{i=1}^{n} \left(\hat{Y}_i - \overline{Y} \right)^2 \qquad [4.45]$$

Y_i is the experimental response, $\overline{Y}$ is this response's mean value and $\hat{Y}_i$ is the response calculated with the experimental test plan model. The difference between SST and SSR demonstrates the gap between the model and the experiment. The sum of squared deviations is given by:

$$SSE = SST - SSR = \sum_{i=1}^{n} \left(Y_i - \hat{Y}_i \right)^2 \qquad [4.46]$$

But this error can originate in a bias resulting from the model not being adjusted or a dispersion resulting from the experiment's variability. By making the hypothesis that the dispersion of measures is constant in time and for different operational conditions, and by defining n^* as the number of different experimental conditions, it is possible to determine the indicators for a lack of adjustment (SSLOF) and pure error (SSPE):

$$SSLOF = \sum_{i=1}^{n^*} \left(\hat{Y}_i - \overline{Y}_i \right)^2 \qquad [4.47]$$

$$SSPE = \sum_{i=1}^{n^*} \sum_{u=1}^{c_i} \left(Y_i^{(u)} - \overline{Y}_i \right)^2 \qquad [4.48]$$

By these definitions, $\hat{Y}_i$ is the estimation of Y, $\overline{Y}_i$ is the average of the experiment's results and $Y_i^{(u)}$ is the u-th run, this for the i-th experimental condition.

However, the sums of squares SST, SSR, SSLOF and SSPE automatically increase with the number of measurement points. To enable comparison between models of different complexities, obtained by a number of different points, these indicators should be averaged, by dividing them by the number of statistical degrees of freedom associated with them. It therefore follows that (with n: the number of tests, n^*: the number of experimental conditions, p: the number of parameters):

$$MSR = \frac{SSR}{p-1} \qquad [4.49]$$

$$MSE = \frac{SSE}{n-p} \qquad [4.50]$$

$$MSLOF = \frac{SSLOF}{n^*-p} \qquad [4.51]$$

$$MSPE = \frac{SSPE}{n-n^*} \qquad [4.52]$$

Relationship [4.50] shows clearly that an estimation of error has no meaning if the number of tests is equal to the number of parameters. Similarly, it is not possible to estimate the lack of adjustment if the number of experimental conditions corresponds to the number of parameters [4.51] nor to estimate the pure error if at least one experimental condition is not repeated [4.52].

These quantities can be used to calculate the coefficient of determination R^2. However, R^2 has a tendency to increase mechanically with the number of variables in a model. It is therefore not adapted to comparing models containing a different number of variables. In this case it is better to use the adjusted determination coefficient, corrected for degrees of freedom.

$$R^2 = \frac{SSR}{SST} = 1 - \frac{SSE}{SST} \qquad [4.53]$$

$$R_{aj}^2 = 1 - \frac{\left(1 - R^2\right)\left(n - 1\right)}{n - p - 1} \qquad [4.54]$$

4.4. Hypothesis tests

4.4.1. *General principle*

How do we conclude that an alloying element has an effect – positive or negative – on a metal's mechanical properties? Or that a cosmetic product has a mechanical effect on skin? In practice, in comes down to comparing the averages of the two groups tested, for groups of results for size and dispersion that usually differ. If the difference between the two groups of tests is close to the uncertainty, it is necessary to use a hypothesis test in order to ascertain whether or not this difference is significant.

To carry out a hypothesis test, a hypothesis H_0 and its alternative H_1 must be defined. Then this hypothesis (for example, "the alloying element has no effect on the elasticity module E") should be formalized in a mathematical test (following the previous example, $T = \Delta E / \sigma(\Delta E)$). A statistic should be linked to the mathematical indicator T. A criterion for accepting or rejecting the test should be established *before* carrying the test out. Finally, the test is carried out and conclusions are drawn from it.

The way the hypothesis is formulated may appear strange, but it is justified quite easily: testing for a negative response to the hypothesis "the alloying element has no effect on the mechanical properties" requires a simple mathematical expression. Its alternative "the alloying element has an effect on the mechanical properties" would require all possible levels of effect to be tested, which is obviously too much to formulate. This type of test, therefore, enables predictors that may have an effect to be distinguished from predictors whose effect is not shown. However the effect's intensity is not indicated.

The result for a statistical test is "I can certainly reject hypothesis H_0". "Certain" here is meant in the statistical sense, that is to say, with some level of risk, generally 5%. Hypothesis tests are, therefore, to be used in contexts that are uncertain due to the measurement dispersion or because of the small amount of information available. The hypothesis test is a very useful addition to experimental test plans and so deserves to be expanded upon in this chapter.

4.4.2. 1st and 2nd order error: a test's power

As explained in the previous section, statistical certainty is a delicate notion. It is possible for the test to suggest rejection and for this result to be false, for example, because the sample contains statistical elements that are barely present. This error is called error α. Similarly, it is possible for the test to suggest acceptance when the hypothesis should be rejected. This alternative error is called error β. Table 4.13 and Figure 4.11 show different possible situations. Even if it is more difficult to manipulate, error β is of great practical importance. In fact, failing to reject a hypothesis that should be rejected means that the test carried out does not discriminate effectively. $(1–\beta)$ is called the *power* of the test as it quantifies the test's capacity to give the usable information sought (rejection).

A test is even more powerful when the dispersion is reduced. Increasing the power of the test therefore comes down to:

– working on the measuring tools, to reduce measuring error;

– altering testing conditions to limit dispersion, for example by eliminating inter-lot variability, or controlling environmental conditions (temperature, humidity) better;

– increasing the number of tests so that dispersion over the average is reduced and the statistical law is better controlled. It must however be noted that dispersion over the average only varies in $1/\sqrt{N}$, which involves a great deal of effort for a limited result.

Hypothesis H_0	Acceptance	Rejection
TRUE	Good decision	1st order error (α)
FALSE	2nd order error (β)	Good decision (1- β)

Table 4.13. *1st and 2nd order error in statistical tests*

Despite is practical importance, it is impossible by definition to know the real value of test T and it is strictly speaking impossible to describe β and $(1-\beta)$. An estimation is possible in spite of everything, if we assume there is a minimal desirable distance between two series of measurements. By giving the number of tests and a standard deviation for each case, it is entirely

possible to know the upper value T_{max} for the confidence interval attached to the hypothesis H_0, then the probability level attached to the true distribution, for value T_{max} (see Figure 4.11). Finally, as the essential parameter is the number of tests in each case, it is possible to establish the minimal number of tests necessary to distinguish between the two averages. This approach is a predictive one based on numerous hypotheses, but carries the advantage of examining a study's feasibility *a priori*. Traditionally, the test's power is adjusted to 80%.

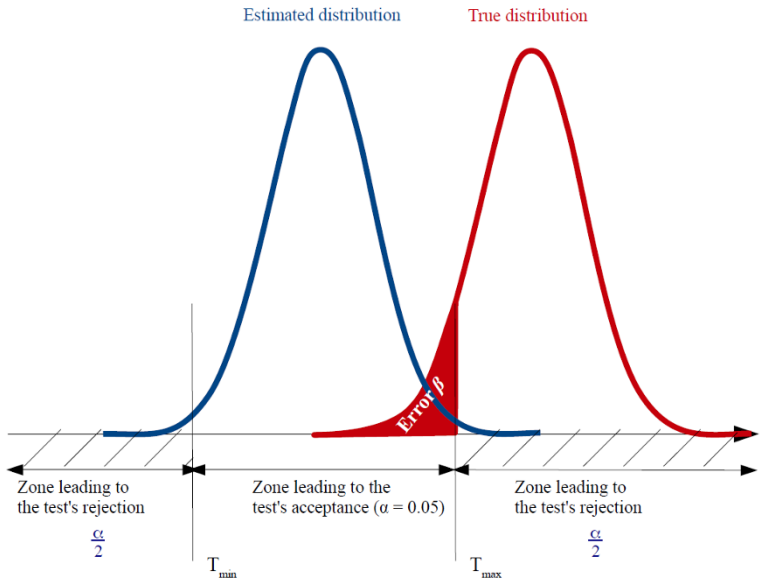

Figure 4.11. *Illustration of 1st and 2nd order risks*

NOTE.– Numerous considerations besides this technical aspect are involved in defining the number of tests. For example, for biomechanics, patient safety limits the number of tests. In fact, the higher the number of patients, the greater is the probability of there being an undesired secondary effect.

NOTE.– Increasing a test's power, to make its result statistically significant enables the smallest differences to be distinguished. We should not lose sight of the physical sense behind the experimental methodology. This difference could very well be so small that its practical importance is null.

4.4.3. *Choosing a statistical law*

The central limit theorem states that the statistical law following a sum of random events of any statistical law tends towards normal law. This very important result is evidently applicable to the average. If the number of random events is not high enough, the deviations from normal law can become significant, which is the case in most experiments.

At this stage, two cases can be identified: in the first case, the random events follow a normal law; for small numbers of points, it is enough to substitute normal law with Student law (see Table 4.2). But if there is no argument to justify a normal law, or if the law is manifestly different, non-parametric tests should be used. Many tests exist and the reader will eventually be able to refer to specialist works (see for example [PIE 04]). Here, only the Mann-Whitney-Wilcoxon test is introduced.

The Mann-Whitney-Wilcoxon test enables two averages that do not follow normal law to be compared, as the tests for each group are independent. The principle is the following: independently of the statistical law for the two groups, the probability that a term taken at random from the first group is greater to a term taken at random from the second is 0.5, if their averages are equal. It is therefore a question of examining all the possible comparisons between the elements of each of the groups and establishing two scores, by comparing the first group with the second (U_{xy}), then by comparing the second with the first group (U_{yx}). In the first case, each time an element from the 1st group is higher than an element of the 2nd, the U_{xy} score increases by 1. If an element from the 1st group has an identical value to an element in the 2nd, the U_{xy} score increases by 0.5. This is the same in the second case for U_{yx}. The sum of the two scores is equal to the number of possible combinations, that is to say the product of the number of tests for each group $n_1 \times n_2$. It is then enough to check that the value of the smaller of the two scores is less than a tabulated value (see for example Table 4.14).

If the number of tests n_1 and n_2 is greater than 10, the variable of U approximately follows the normal law, of variance:

$$\sigma_U^2 = n_1 \times n_2 \times (n_1 + n_2) / 12 \qquad [4.55]$$

It is therefore enough to center and reduce the statistical U to return to a parametric test following normal law.

α = 005	n_1								
	U_{crit}	3	4	5	6	7	8	9	10
	3		0	0	1	1	2	2	3
	4		0	1	2	3	4	4	5
	5	0	1	2	3	5	6	7	8
n_2	6	1	2	3	5	6	8	10	11
	7	1	3	5	6	8	10	12	14
	8	2	4	6	8	10	13	15	17
	9	2	4	7	10	12	15	17	20
	10	3	5	8	11	14	17	20	23

Table 4.14. *Critical value of the Mann-Whitney-Wilcoxon test (two-directional case)*

4.4.4. *Examples*

EXAMPLE 1.– *Manufacturing composites*

Two composite materials are manufactured according to two different methods (pre-preg and resin infusion). The stacking, choice of fibers and resin are the same. Two traction tests are carried out: in the first case, the modulus (in the x direction) is $m_1 = 72$ GPa ($s_1^2 = 25$, $n_1 = 9$). In the second case, the modulus is $m_2 = 69$ GPa ($s_2^2 = 20.25$, $n_2 = 11$).

The number of cases tested is not high enough for normal law to be established. However, the hypothesis for dispersion according to Gaussian law is reasonable. In this case, a Student test is appropriate.

In the hypothesis where the two series of tests are identical (hypothesis H_0), the best estimation of the variance is a weighted sum of variances estimated in each of the two cases.

$$s^2 = \frac{s_1^2 \times (n_1 - 1) + s_2^2 \times (n_2 - 1)}{n_1 + n_2 - 2} \qquad [4.56]$$

The Student test compares the difference of the averages at the square root of the variance. The variance over the difference of the averages is the sum of the variances over each of the averages. The test is written:

$$t = \frac{(m_1 - m_2)}{\sqrt{\frac{s^2}{n_1} + \frac{s^2}{n_2}}} \qquad [4.57]$$

Finally, the number of degrees of freedom of Student law from the difference is the total number of tests minus two, since two averages have been calculated ($n_1 + n_2 - 2 = 18$). In this example, $t = 2.43 > 2.1$: taking account of the information available, the hypothesis of equality between the two cases should be rejected. The elasticity modulus with the second process (resin infusion) is therefore significantly weaker than with the first (pre-preg).

EXAMPLE 2.– *Applying pressure using compression stockings*

Different methodologies for applying compression stockings are used in treating venous insufficiency. According to the first, written as methodology A, the average stretch for the band is $m_1 = 1.28$ ($s_1^2 = 2.5\ 10^{-3}$, $n_1 = 15$). According to the second, written methodology B, the stretch is $m_2 = 1.27$ ($s_2^2 = 2.5\ 10^{-3}$, $n_1 = 15$). However, in this case, the Jarque–Bera test invalidates the normality hypothesis. It is therefore necessary to use a non-parametric test. The values obtained are summarized in Table 4.15. In this case, $U_{BA} > 8$, which means that the hypothesis cannot be rejected with the information at our disposal, it is impossible to conclude that the hypothesis for the stretch equality is to be rejected.

4.4.5. *Test for model adjustment: a return to ANOVA analysis*

The quantities defined in section 4.3.6 can now be used in the context of the hypothesis test. The different usual tests are summarized in Table 4.16. The model's validity and its adjustment rely on tests that combine two random Student variables. In this situation – the relationship of two Student laws – the test follows a Fisher law. These two tests are essential to the continuous acquisition process: if they are positive, it is not necessary to refine the model. The significance of the sensitivity parameters β_i is used if the model is suitably adjusted. It enables the predictors' effects to be classed by intensity and only those that are statistically significant to be retained. Be

careful, however: a parameter can be statistically significant, without its sensitivity being great enough to influence the result. It is enough that its uncertainty is sufficiently low.

Methodology	Stretch	U_{AB}	U_{BA}
B	1.282	6	0
A	1.288	0	5
B	1.288	5	0
B	1.29	5	0
A	1.294	0	3
B	1.294	4	0
A	1.298	0	2
B	1.308	3	0
A	1.312	0	1
B	1.313	2	0
A	1.321	0	0
A	1.325	0	0
		$U_{AB} = 25$	$U_{BA} = 11$

Table 4.15. *Mann-Whitney-Wilcoxon test for venous compression. The table shows results after they have been classed in decreasing order*

Question	Statistical test	Statistical law
Model's validity	$t = \frac{MSR}{MSE}$	Fisher law
Significance of each parameter β_i	$t = \frac{\hat{\beta}}{\sqrt{Var\left(\hat{\beta}\right)}}$	Student law
Model Adjustment	$T = \frac{MSLOF}{MSPE}$	Fisher law

Table 4.16. *Statistical tests for a regression model's quality*

5

Exercises

5.1. Multiple-choice questions

1) A normalized mechanical test is used to:

a) validate a model;

b) quantify parameters;

c) develop understanding of a physical reality;

d) check properties defined in specifications.

2) To estimate the final traction/compression values for a slender structure, the following type of test is used:

a) a 3 point bending test;

b) a 4 point bending test.

3) An optimal 2^n plan is constructed by varying the input parameters:

a) successively;

b) simultaneously.

4) A piezoelectric sensor is optimal for the following types of test:

a) static;

b) dynamic.

5) An accelerometer's cut-off frequency increases with:

a) its mass;

b) its rigidity.

Experimental Mechanics of Solids and Structures, First Edition. Jérôme Molimard.

5.2. Problem: designing a torque meter

An industrial laboratory has developed a torque meter internally. The assembly produced, shown in Figure 5.1, should be studied. It is made up of two disks, one mounted on the machine frame, the other supporting the items to be tested. Four flexible steel blades provide the link between the two disks. They are made of rectangular sections, the largest side, of size b, being in the radial direction of the cylinders. These blades are equipped with strain gauges on the two opposite sides of each blade.

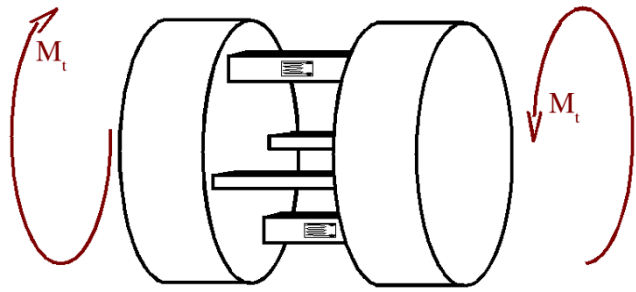

Figure 5.1. *Torque*

5.2.1. *Mechanical analysis*

QUESTION 5.1.–

What is the nature of the load applied on each blade?

QUESTION 5.2.–

Give the resultant force F depending on the moment of torsion M_t undergone by each of the blades when operated. It will be assumed that they all work in the same way.

A.N.:

Maximal moment $M_i^{\max} = 100\ Nm.$

Distance from the center of torsion to the axis of each blade r = 30 mm.

QUESTION 5.3.–

The gauges are placed at the site of maximal strain. The expressions for these maximal strains are: $\varepsilon_{11}^{\max} = \frac{Flh}{4EI}$ and $\varepsilon_{11}^{\min} = \frac{-Flh}{4EI}$.

Knowing that the bending inertia is given by $I = \frac{bh^3}{12}$, express the thickness h according to the other parameters so that the stress remains less than the maximal stress σmax. For simplicity, the value found will hereafter be rounded up to the millimeter above.

A.N.:

Maximal admissible constraint $\sigma_{max.}$ = 1250 N/mm².

Blade length l = 60 mm.

Blade width b = 14 mm.

Young's modulus E = 210 000 N/mm².

5.2.2. *Electrical installation*

QUESTION 5.4.–

Give the half-bridge assembly enabling bending strain to be measured.

QUESTION 5.5.–

Find an assembly using all the strain gauges as described in Figure 5.2. Then give the relationship between the tension read and the strain of each gauge.

QUESTION 5.6.–

Establish the relationship between the torque applied and the tension read at the output of the Wheatstone bridge.

A.N.:

Supply voltage U_0 = 5 V.

Gauge factor GF = 2.

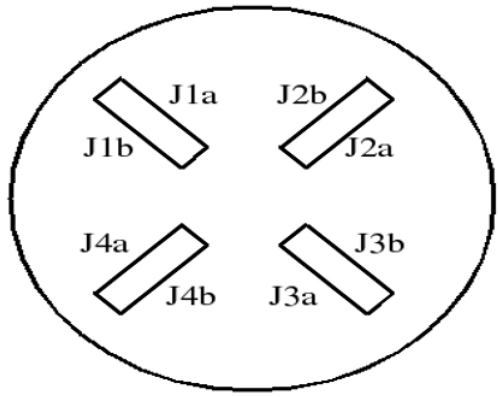

Figure 5.2. *Diagram for implanting gauges*

5.2.3. *Analyzing uncertainty*

QUESTION 5.7.–

The thickness of the blades h is measured using a caliper; the smallest scale on this instrument is 0.1 mm. Give an uncertainty for the measurement for thickness.

QUESTION 5.8.–

Evaluate the uncertainty caused by not knowing the thickness on the torque.

A.N.: Using this, make a numerical application for the maximal torque.

QUESTION 5.9.–

An operator decides to make 5 thickness measurements per blade. They then establish an average and use it to calculate the torque. What is the uncertainty on the average calculated in this way?

QUESTION 5.10.–

Quantify the impact of such a choice on the uncertainty on the torque linked to the thickness.

5.3. Problem: traction test on a composite

The subject of interest is a composite beam subject to a traction force. The beam is assumed to be isotropic with the properties E = 120 GPa, $\upsilon = 0.3$. Its dimensions are a section of 2×26 mm^2 and a length between bits of 220 mm.

5.3.1. *Sizing a traction test*

1) A strain gauge is used to track the strain caused by the traction.

2) What is the appropriate conditioning in this case? Give the corresponding basic equation.

3) It is necessary to measure the variation in tension with an acquisition card that samples on 1024 levels. The input tension at the card terminals should range from 0 to 10 volts. The conditioner's input tension is 5 volts. Determine the amplification level required to obtain a discrimination threshold of 3 µ.

4) What is the maximal recordable strain?

5) Work out the maximal force corresponding to the composite plate.

5.3.2. *Measuring*

In the previous test, the force cell is a 100 kN cell. The maker gives an overall uncertainty of 0.1% for the measuring range. The traction test is equipped with two strain gauges either side of the plate; this is built as a half-bridge assembly. Finally, the caliper for measuring the section has a minimal scale, from two centimeters to a millimeter.

1) The experimenter makes several strain measurements at no load at close intervals. What is this type of test called? What does it show?

2) Give the relationship linking the Young's modulus to the traction test's other parameters.

3) Using the relationship above, express the relationship giving the uncertainty on the Young's modulus and the different sources of uncertainty.

4) The specimen is thermally regulated to ±2°C. Knowing that the thermal dilatation coefficient of the material used is 2 µm/m/°C, what is the uncertainty linked to this variation? Knowing that the resolution on the strain measuring system is 3 µm/m (95%), find the uncertainty linked to the strain measurement.

5) Calculate the uncertainty on the Young's modulus for a force of 10 kN. Taking account of the value given in exercise 1, does this value seem correct to you?

5.3.3. *Photomechanics*

We wish to make a measurement using the grid method. The grid is attached to the center of the specimen, whose length is 220 mm between the jaws.

1) What is the maximal movement between jaws for the 10 kN force? Find the optimal choice of grid (from 100, 200, 300 or 400 µm). Explain your choice.

2) It is supposed *a priori* that the movement has a standard uncertainty within the range of $1/100^{e}$. Give an estimation for the uncertainty on the movement.

3) We wish to estimate strains with an uncertainty of less than 10^{-4} m/m (95%). What should the minimal distance between two measuring points be to make the derivation?

4) If a hole is made in the plate, what would be the maximal reasonable force required to remain in the elastic domain, taking account of a concentration factor of 3.

5.4. Problem: optic fiber Bragg gratings

An optic fiber Bragg grating is a silica optic fiber in which weak periodic variation of the refractive index has been photo-inscribed (the Bragg

grating). The diameter of the fiber's core it 50 µm, so that infra-red light (1450-1550 nm) can only pass through it in a single mode. This type of fiber, which is very thin (the core plus the coating is 100 µm in diameter), is used in particular to monitor the making of composite materials. If a light coming from a broadband source is injected into the fiber, all the wavelengths present are transmitted, except one wavelength, called the Bragg wavelength, which is expressed in the following way:

$$\lambda_B = 2n\Lambda \qquad [5.1]$$

where n is the medium's effective index and the photo-inscription period.

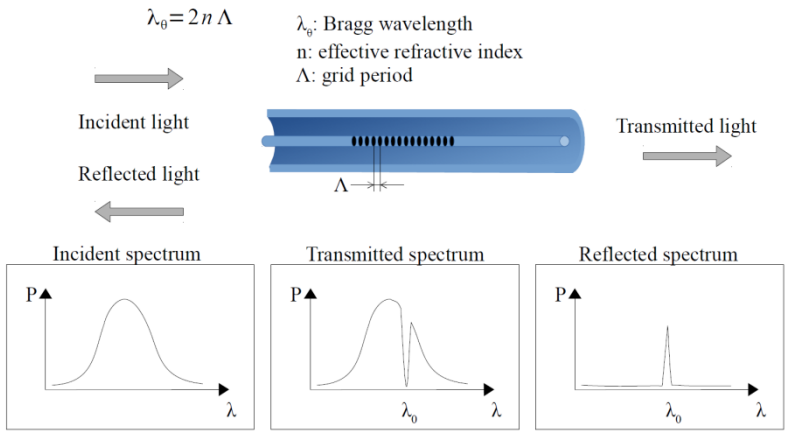

Figure 5.3. *Diagram showing the principle of optic fiber Bragg networks*

What happens when the temperature varies?

Give the expression for the wavelength varying according to the variation in temperature, for the environment's thermal dilatation coefficient, and the initial wavelength.

5.4.1. *What happens when there is traction on the fiber?*

Give the expression for the variation in wavelength depending on the strain.

5.4.2. *What will the effective index become depending on the temperature and strain parameters?*

Find the overall sensitivity relationship at these two loads; this is limited to a model with small linear disturbances; the index's sensitivity to strain is called the opto-elastic coefficient, and the temperature the opto-thermal coefficient.

5.4.3. *Separating temperature and mechanics*

Using a manufacturing trick, it is possible to regulate sensitivity to temperature and strain. If two Bragg gratings are inscribed with different wavelengths and sensitivities at the same geographical place, it becomes possible to separate axial and temperature strain. However, the sensitivities remain close. Express the strains of mechanical origin and the temperatures according to variations in wavelength depending on relationships [5.2] and [5.3]:

$$\frac{\delta\lambda_1}{\lambda_1} = 1.2 \in +12\delta T \qquad [5.2]$$

$$\frac{\delta\lambda_2}{\lambda_2} = 1.1 \in +13\delta T \qquad [5.3]$$

5.4.4. *Analyzing uncertainty*

The Bragg wavelengths for each of the sensors (λ_1 = 1532 nm, λ_2 = 1632 nm) and the uncertainty measurement for the variation in wavelength (10 pm) are given. Estimate the uncertainty on the strain, then on the temperature.

5.5. Problem: bending a MEMS micro-sensor

MEMS structures have largely unknown mechanical properties. In particular, it is difficult to determine their elastic properties. Here, we wish to study an ion sensor, a photo of which is given in Figure 5.4. Due to the presence of two different materials, each of the sensors' faces has a different sensitivity to different loads, and in particular the adsorption of

electromagnetic charges, which causes the ensemble to bend according to the bimetallic strip principle.

Figure 5.4. *Charge micro-sensor [GAR 06]*

5.5.1. *Suggesting a mechanical model for this problem*

5.5.1.1. *Choosing instrumentation*

If the maximal beam flexion is 1.5 µm, what physical principle (and what mounting) could be used to measure this deflexion?

5.5.1.2. *Metrology*

A metrological test is carried out to evaluate the measurement quality. The result is shown in Figure 5.5. What does this test quantify? Comment on the first part of the curve (in dotted lines). How can this behavior be explained? The second (horizontal) part is more unexpected. What does it show? What phenomena may give rise to it?

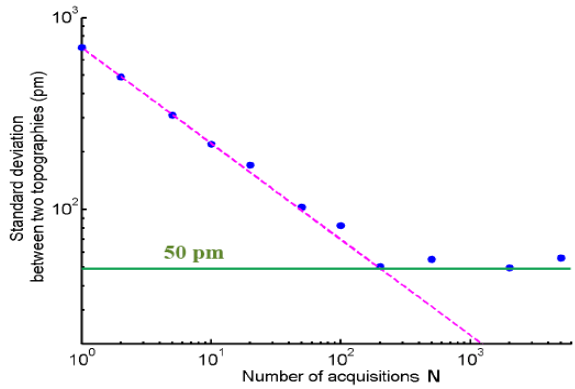

Figure 5.5. *First metrological tests [GAR 06]*

5.6. Problem: studying a 4-point bending system

It is suggested that we study the mechanical device shown in Figure 5.6. It is a 4-point beam bending device *in a single piece*. The bending beam is in the central part. The links are flexible and made of steel. We observe a beam (lower part) and a crosshead (upper, part). Between the two parts, a very small amount of play (W/9) allows vertical movements.

The whole of this apparatus is suggested as calibration tool for optical full field methods. It has already been used for inter-comparisons between laboratories.

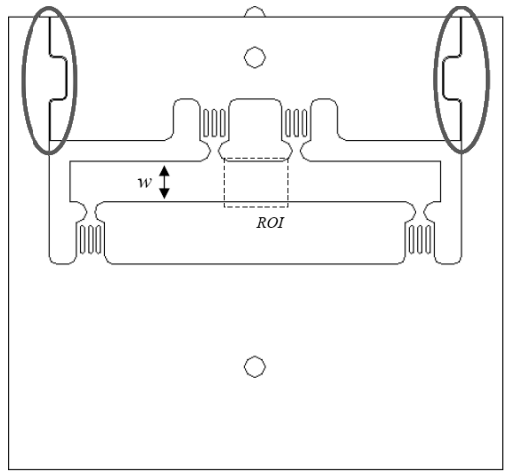

Figure 5.6. *Apparatus for testing reference suggested by the European project SPOTS*

5.6.1. *Analyzing the device*

1) How is it loaded? Why has a play of 2 gaps, as well as the half-moon, been anticipated above?

2) In your opinion, why are the links chosen flexible links?

3) The width of the specimen is written W; the distance between each of the exterior supports and the nearest interior support is 3 W. The distance between the two interior supports is 2 W. What can be said about the conditions in light of beam theory?

4) Why is the region of interest (ROI) between the two interior supports?

5) What might be the use of the two retaining walls circled?

5.6.2. *Mechanical analysis*

The whole thing is modeled as a 4-point bending beam. Its Young's modulus is written E, and its thickness h. The beam is subject to a vertical load F.

1) In classic beam hypotheses, give the bending moment for each point on the beam.

2) What, in this case, is the strain field for the beam?

3) Give the expression for the Young's modulus E depending on the local strains.

5.6.3. *Analyzing uncertainties*

1) We now suppose that $h = W = 10$ mm. The dimensional tolerances are given at 0.05 mm. Express the uncertainty on the Young's modulus E depending on the uncertainty on the sides of the specimens.

2) The force cell used is a 150 kN cell. The uncertainty on the force cell is 0.1% of the whole scale. What is the uncertainty induced on the module?

3) What other sources of uncertainty have not been taken into account? Combine them with the previous uncertainties and give the total uncertainty on determining E.

4) Taking account of the previous analysis, where do we place a strain gauge?

5) Numerical application: knowing that the gauge's uncertainty is 10 μm/m, that its nominal value is 860 μm/m, and that the charge is 100 kN, give the uncertainty value on E.

5.6.4. *Optical full field methods*

Consider an optical full field method enabling 300 × 600 strain measuring points to be obtained. These are also distributed in the region of interest, that is to say between the two upper supports. The resolution for

measuring strain is 50 μm/m (95%). Each measuring point enables E to be determined. The average is then calculated. Give the uncertainty on the average of all these values.

5.7. Digital pressure tester: statistical tests

The aim of this PT is to describe a program that can predict the number of tests necessary to distinguish a certain level of effect; the input values are assumed to follow a normal law to infinity. The PT can be carried out using Matlab or Scilab.

5.7.1. *Discovering the statistical functions library*

What statistical law should really be implemented in the code?

In the code's help section, see implementation of the following functions: probability density, cumulative function, inverse cumulative function and random number generator.

5.7.2. *Estimating a confidence interval*

Write a function enabling (for a given number of runs n_0) the confidence interval of a statistical variable centered on m_0 and standard deviation σ_0 for an arbitrary level α to be known. Beware; this focuses on distance from a mean: this distance is therefore symmetrical.

Draw a graphic showing the distribution of the statistical variable and its two limits. What happens if the number of points becomes very large?

5.7.3. *Calculating a test's power*

Establish the value of the probability density function of the Student law for a given point, the law being known by its average value, its standard deviation and a number of runs. Give the cumulative value. In this case, the law is taken unilaterally.

Write the function enabling the test's power to be calculated. The standard deviation of the distribution and the average value as well as the

minimal measurable distance are known. Suppose further that each of the two tests will be performed an equal number of times. Finally, make a loop enabling the power to be shown graphically according to the number of tests.

Conclusion

Designing and optimizing objects requires an approach that is both numerical and experimental. These two approaches co-exist more or less happily in the world of industry. In too many cases, the mechanical test is exclusively the responsibility of a technician, the design engineer only becoming involved as a client. Yet, as this book attempts to illustrate, a mechanical test involves hypotheses, implementation techniques and instrumentations that have their own limits and can be very elaborate. Interpreting the result and comparing it with the numerical model is only possible by remaining aware that this mechanical test is itself a model, an experimental model of which it is sensible to master the complexities.

One of the reasons for this lack of curiosity in experimental mechanics, especially structural mechanics, lies in its neglect in engineering schools. A rapid exploration of the French bibliography certainly reveals specialist works, such as for example [AVR 74] and [GRE 11], but no general work for the use of engineers in solid and structural mechanics, to our knowledge, since Charles Rabut's exploration [RAB 06] from 1906. Despite this, experimental techniques have not stopped developing and being renewed. In the field of experimental mechanics of course very high quality works on particular techniques will be retained, for example, photomechanics [SCH 09], but in experimental domains in other disciplines as well, particularly in medicine where biostatistics, which appeared in the 1930s, have revolutionized clinical approaches since the middle of the 1980s, and also in metrology where a statistical approach has replaced the determinist approach, which was still being taught only 15 years ago.

Experimental Mechanics of Solids and Structures, First Edition. Jérôme Molimard.

This book therefore presents both a coherent body of technical expertise enabling an experimental model to be put in place, instrumentalized with classic devices such as strain gauges or more modern ones such as optical full-field methods. It also aims to take a decisive step towards the most up-to-date experimental practices by introducing uncertainty analysis and the development of experimental designs and their interpretation on a clear basis of probability.

The contents of this work reflect the knowledge acquired and put into practice by the author in the course of his 20 years' practice in research and teaching experimental mechanics. It is not therefore exhaustive, could it be otherwise? In particular, signal processing methods are not tackled except in the framework of field methods. Readers interested in this domain will be able to consult one of the many works published on this subject, for example [BLA 14]. Similarly, the identification of properties is only mentioned in passing although the methodologies are fascinating [GRE 11, PIE 12]. A further edition will perhaps enable these subjects to be addressed.

Bibliography

[ALL 94] ALLAIS L., BORNERT M., BRETHEAU T. *et al.*, "Experimental characterization of the local strain field in a heterogeneous elastoplastic material", *Acta Metallurgicaet Materialia*, vol. 42, no. 11, pp. 3865–3880, 1994.

[AMI 13] AMIOT F., BORNERT M., DOUMALIN P. *et al.*, "Assessment of digital image correlation measurement accuracy in the ultimate error regime: main results of a collaborative benchmark", *Strain*, vol. 49, no. 6, pp. 483–496, 2013.

[AVR 74] AVRIL J., *Encyclopédie Vishay d'analyse des contraintes*, Vishay Micromesures, Paris, 1974.

[AVR 04] AVRIL S., FERRIER E., VAUTRIN A. *et al.*, "A full-field optical method for the experimental analysis of reinforced concrete beams repaired with composites", *Composites Part A: Applied Science and Manufacturing*, vol. 35, nos. 7–8, pp. 873–884, 2004.

[AVR 08] AVRIL S., FEISSEL P., PIERRON F. *et al.*, "Estimation of the strain field from full-field displacement noisy data", *European Journal of Computational Mechanics*, vol. 17, nos. 5–7, pp. 857–868, 2008.

[BAD 09] BADULESCU C., GRÉDIAC M., MATHIAS J.D. *et al.*, "A procedure for accurate one-dimensional strain measurement using the grid method", *Experimental Mechanics*, vol. 49, no. 6, pp. 841–854, 2009.

[BAD 13] BADULESCU C., BORNERT M., DUPRÉ J.C. *et al.*, "Demodulation of spatial carrier images: performance analysis of several algorithms using a single image", *Experimental Mechanics*, vol. 53, no. 8, pp. 1357–1370, 2013.

[BER 09] BERGE-GRAS R., MOLIMARD J., "Optimisation de la dérivation en fonction de la Résolution et de la Résolution Spatiale sur les déformations", *XIX*^{ème} *Congrès Français de Mécanique*, Marseille, France, 2009.

Experimental Mechanics of Solids and Structures, First Edition. Jérôme Molimard.

[BER 11] BERGE-GRAS R., Analyse expérimentale de la propagation de fissures dans des tôles minces en Al-Li par méthodes de champs, Thèse de doctorat, Mines Saint-Etienne, 2011.

[BES 06] BESNARD G., HILD F., ROUX S., "Finite-element' displacement fields analysis from digital images: application to Portevin-Le Châtelier bands", *Experimental Mechanics*, vol. 46, pp. 789–803, 2006.

[BIP 08a] BIPM, *Evaluation of measurement data – Guide to the expression of uncertainty in measurement, CGM 100:2008, (GUM 1995 with minor corrections)*, Sèvres, 2008.

[BIP 08b] BIPM, *Evaluation of measurement data – Supplement 1 to the "Guide to the expression of uncertainty in measurement" – Propagation of distributions using a Monte Carlo method, JCGM 101:2008*, Sèvres, 2008.

[BIP 12] BIPM, *Vocabulaire international de métrologie – Concepts fondamentaux et généraux et termes associés (VIM, 3e édition) JCGM 200:2012 (JCGM 200:2008 avec corrections mineures)*, Sèvres, 2012.

[BLA 14] BLANCHET G., CHARBIT M., *Digital Signal and Image Processing using Matlab® – 2nd edition, Volume 1 – Fundamentals*, ISTE, London, and John Wiley & Sons, New York, 2014.

[BOE 98] BOEHM M., Approche physico-chimique de l'action des additifs de lubrification lors du laminage à froid, doctoral thesis, École Centrale de Lyon, 1998.

[BON 15] BONNAIRE R., Caractérisation mécanique des orthèses: application aux ceintures de soutien lombaire dans le cadre de la lombalgie, doctoral thesis, Mines Saint-Étienne, 2015.

[BOR 09] BORNERT M., BRÉMAND F., DOUMALIN P. *et al.*, "Assessment of digital image correlation measurement errors: methodology and results", *Experimental Mechanics*, vol. 49, no. 3, pp. 353–370, 2009.

[BOY 10] BOYER G., Modélisation du comportement mécanique de la peau humaine in vivo: application au vieillissement et aux gestes du clinicien, doctoral thesis, Mines Saint-Etienne, 2010.

[BRÈ 04] BRÈQUE C., DUPRÉ J.C., BRÉMAND F., "Calibration of a system of projection moire for relief measuring: biomechanical applications", *Optics and Lasers in Engineering*, vol. 41, pp. 241–260, 2004.

[BRU 00] BRUNO L., PAGNOTTA L., POGGIALINI A., "Laser speckle decorrelation in NDT", *Optics and Lasers in Engineering*, vol. 34, pp. 55–65, 2000.

[COU 00] COURONNÉ-DARRAK I., Étude expérimentale du comportement de graisses lubrifiantes pour roulements à billes, doctoral thesis, INSA de Lyon, 2000.

[DEB 11] DEBELLA-GILO M., KÄÄB A., "Sub-pixel precision image matching for measuring surface displacements on mass movements using normalized cross-correlation", *Remote Sensing of Environment*, vol. 115, no. 1, pp. 130–142, 2011.

[FIG 00] FIGLIOLA R.S., BEASLEY D.E., *Theory and Design for Mechanical Measurements – Third edition*, John Wiley & Sons, New York, 2000.

[FOR 84] FORSTNER W., "Quality assessment of object location and point transfer using digital image correlation techniques", *International Archives of Photogrammetry, Proceedings of ISPRS Congress*, Rio de Janeiro, Brazil, vol. 23, no. 3, p. 23, 1984.

[GAR 06] GARRAUD N., AMIOT F., HILD F. *et al.*, "Full-field measurement of microcantilever displacement induced by molecule adsorption–identification of mechanical parameters", *Photomechanic 2006*, Clermont-Ferrand, France, 2006.

[GER 07] GERMANEAU A., DOUMALIN P., DUPRÉ J.-C., "3D strain field measurement by correlation of volume images using scattered light: recording of images and choice of marks", *Strain*, vol. 43, no. 3, pp. 207–218, 2007.

[GIG 09] GIGLIOTTI M., MOLIMARD J., JACQUEMIN F. *et al.*, "Maximum curvatures of 0/90 plates under thermal stress: modelling and experimental validation", *Composites Science and Technology*, vol. 69, pp. 93–96, 2009.

[GOË 92] LE GOËR J.L., AVRIL J., "Extensométrie", *Techniques de l'Ingénieur*, vol. R1 850, 1992.

[GOM 10] GOMES P., SESSELMANN M., FARIA C. *et al.*, "Measurement of scapular kinematics with the moiré fringe projection technique", *Journal of Biomechanics*, vol. 43, pp. 1215–1219, 2010.

[GOU 97] GOUPY J., "Plans d'expériences", *Techniques de l'Ingénieur, Traité Mesure et Analyse*, vol. P 230, pp. 1–24, 1997.

[GRÉ 94] GRÉDIAC M., PIERRON F., VAUTRIN A., "The Iosipescu in-plane shear test applied to composites: a new approach based on displacement field processing", *Composites Science and Technology*, vol. 51, no. 3, pp. 409–417, 1994.

[GRÉ 99] GRÉDIAC M., PIERRON F., SURREL Y., "Novel procedure for complete in-plane composite characterization using a single T-shaped specimen", *Experimental Mechanics*, vol. 39, no. 2, pp. 142–149, 1999.

[GRE 11] GRÉDIAC M., HILD F., *Full-Field Measurements and Identification in Solid Mechanics*, ISTE, London, 2011.

[GRE 12] GRÉDIAC M., TOUSSAINT E., "Studying the mechanical behaviour of asphalt mixture with the grid method", *Strain*, vol. 49, no. 1, pp. 1–15, 2012.

[KÜH 07] KÜHMSTEDT P., MUNCKELT C., HEINZE M. *et al.*, "3D shape measurement with phase correlation based fringe projection", *SPIE Proceedings*, vol. 6616, pp. 66160B-66160B-9, 2007.

[LAG 01] LAGARDE J.M., ROUVRAIS C., BLACK D. *et al.*, "Skin topography measurement by interference fringe projection: a technical validation", *Skin Research Technology*, vol. 7, no. 2, pp. 112–121, 2001.

[LEA 10] LEANDRY I., BREQUE C., LACOUTURE P. *et al.*, "3D shape reconstruction from relief calculation: application to human body", *EPJ Web of Conferences*, vol. 6, p. 12003, 2010.

[LEA 11] LEANDRY I., Adaptation de la méthode de projection de franges pour la mesure du relief de grands objets et pour la modélisation anthropométrique: application à l'étude de flotteurs sous pression et au suivi de pathologie de l'abdomen, doctoral thesis, University of Poitiers, 2011.

[LEE 04a] LEE J.R., MOLIMARD J., VAUTRIN A. *et al.*, "Digital phase-shifting grating shearography for experimental analysis of fabric composites under tension", *Composites: Part A*, vol. 35, pp. 849–859, 2004.

[LEE 04b] LEE J.R., MOLIMARD J., VAUTRIN A. *et al.*, "Application of grating shearography and speckle shearography to mechanical analysis of composite material", *Composites Part A: Applied Science and Manufacturing*, vol. 35, nos. 7–8, pp. 965–976, 2004.

[MOL 99] MOLIMARD J., Étude expérimentale du régime de lubrification en film mince – Application aux fluides de laminage, doctoral thesis, INSA de Lyon, 1999.

[MOL 05] MOLIMARD J., LE RICHE R., VAUTRIN A. *et al.*, "Identification of the four orthotropic plate stiffnesses using a single open-hole tensile test", *Experimental Mechanics*, vol. 45, no. 5, pp. 404–411, 2005.

[MOL 08] MOLIMARD J., CORDERO R., VAUTRIN A., "A signal-to-noise based local decorrelation compensation for speckle interferometry applications", *Applied Optics*, vol. 47, no. 19, pp. 3535–3542, 2008.

[MOL 09a] MOLIMARD J., DARRIEULAT M., "Quantitative analysis of heterogeneities of deformation with the grid method", *Archives of Metallurgy and Materials, Versita*,vol. 54, no. 1, pp. 7–17, 2009.

[MOL 09b] MOLIMARD J., DOLINKO A., KAUFMANN G., "Experimental study of thick composites stability under thermal loading using 3D ESPI set-up", in DIRCKX G.J., BUYTAERT J. (eds), *Optical Measurement Techniques for Systems & Structures, Shaker Publishing*, Maastricht, pp. 255–264, 2009.

[MOL 10] MOLIMARD J., BOYER G., ZAHOUANI H., "Frequency-based image analysis of random patterns: an alternative way to classical stereocorrelation", *Journal of the Korean Society of Non Destructive Testing*, vol. 30, pp. 181–193, 2010.

[MOL 11] MOLIMARD J., "Implementation of the direct evaluation of strains in a frequency-based image analysis code for random patterns", *Optics and Laser in Engineering*, vol. 49, nos. 9–10, pp. 1194–1200, 2011.

[MOL 13] MOLIMARD J., NAVARRO L., "Uncertainty on fringe projection technique: a Monte-Carlo-based approach optics and laser in engineering", *Optics and Laser in Engineering*, vol. 51, pp. 840–847, 2013.

[MON 94] MONTMITONNET P., Le laminage, aspects mécaniques, course, MatMaf, ENSMP/CEMEF, 1993–1994.

[MOR 92] MOREAU M.R., LE BECHEC J., "Force. Couple", *Techniques de l'Ingénieur, Traité Mesure et Analyse*, vol. R1 820, pp. 1–19, 1992.

[MOU 98] MOUZIN O., Contribution à la dynamique des structures précontraintes: application aux roues de vélos à rayons, doctoral thesis, INSA de Lyon, 1998.

[NIS 10] NISTEA I., Développement des techniques optiques et acoustiques de mesure de champs orientées vers la vibroacoustique, doctoral thesis, INSA de Rouen, 2010.

[PIE 15] PIERRAT B., MILLOT C., MOLIMARD J. *et al.*, "Characterisation of knee brace migration and associated skin deformation during flexion by full-field measurements", *Experimental Mechanics*, vol. 55, pp. 349–360, 2015.

[PIE 98] PIERRON F., ALLOBA E., SURREL Y. *et al.*, "Whole-field assessment of the effects of boundary conditions on the strain field in off-axis tensile testing on unidirectional composites", *Composite Science and Technology*, vol. 58, pp. 1939–1947, 1998.

[PIE 99] PRIEL M., "Incertitude de mesure et tolérances", *Techniques de l'Ingénieur, Traité Mesures et Analyses*, vol. R 285, pp. 1–14, 1999.

[PIE 04] POINSOT D., Statistique pour les statophobes, available at: http://perso.univ-rennes1.fr/denis.poinsot, Université Rennes 1, 2004.

[PIE 07] PIERRON F., GREEN B., WISNOM M.R., "Full-field assessment of the damage process of laminated composite open-hole tensile specimens. Part I: Methodology", *Composites*, *Part A: Applied Science and Manufacturing*, vol. 38, no. 11, pp. 2307–2320, 2007.

[PIE 12] PIERRON F., GRÉDIAC M., *The Virtual Fields Method, Extracting Constutive Mechanical Parameters from Full-Field Deformation Measurements*, Springer, New York, 2012.

[RAB 06] RABUT C., Cours de mécanique expérimentale des solides, http://patrimoine.enpc.fr/document/ENPC02_COU_4_25388_1906, Bibliothèque numérique patrimoniale des ponts et chaussées, 1906.

[REU 12a] REU P., "A Monte Carlo approach to assessing uncertainty in digital image correlation (DIC)", *Asian Conference on Experimental Mechanics*, Taipei, Taiwan, 2012.

[REU 12b] REU P., "Uncertainty quantification for 3D digital image correlation (DIC)", *Society for Experimental Mechanics Annual Conference*, Costa Mesa, USA, 2012.

[SCH 09] SCHREIER H., ORTEU J.-J., SUTTON M., *Image Correlation for Shape, Motion and Deformation Measurements Basic Concepts, Theory and Applications*, Springer-Verlag, Berlin, 2009.

[SIL 07] SILVA G., LE RICHE R., MOLIMARD J. *et al.*, "Identification of material properties using FEMU: application to the open hole tensile test", *Applied Mechanics and Materials*, vol. 7–8, pp. 73–78, 2007.

[SUR 06] SURREL Y., "Contrôle de défauts d'aspect et de qualité de surface, La solution par la déflectométrie", *Contrôles-Essais-Mesures*, pp. 11–14, April 2006.

[SUT 83] SUTTON M.A., WOLTERS W.J., PETERS W.H. *et al.*, "Determination of displacements using an improved digital image correlation method", *Image and Vision Computing*, vol. 1, no. 3, pp. 133–139, 1983.

[SVA 06] SVANBRO A., SJÖDAHL M., "Complex amplitude correlation for compensation of large in-plane motion in digital speckle pattern interferometry", *Applied Optics*, vol. 45, pp. 8641–8647, 2006.

[SUT 98] SUTTON M.A., MCNEILL S.R., HELM J.D. *et al.*, "Measurement of crack tip opening displacement and full-field deformations during fracture of aerospace materials using 2D and 3D image correlation methods", in LAGARDE A. (ed.), *IUTAM Symposium on Advanced Optical Methods and Applications in Solid Mechanics*, Kluwer Academic/Plenum Publishers, Dordrecht, pp. 571–580, 1998.

[TIN 10] TINSSON W., *Plans d'expérience: construction et analyses statistiques*, Springer-Verlag, Berlin, 2010.

[TRI 07] TRICONNET K., Identification des propriétés mécaniques à partir de mesures de champs dans un matériau multi-phase, doctoral thesis, École Nationale Supérieure des Arts et Métiers, 2007.

[VAU 09] VAUTRIN A., SILVA G., MOLIMARD J. *et al.*, "Localisation et identification de l'hétérogénéité de comportement mécanique de matériaux", *19ème Congrès Français de Mécanique*, Marseille, France, August 2009.

[VIO 06] VIOTTI M., KAUFMANN G., "Measurement of elastic moduli using spherical indentation and digital speckle pattern interferometry with automated data processing", *Optics and Lasers in Engineering*, vol. 44, pp. 495–508, 2006.

[WIS 97] WISNOM M.R., ATKINSON J.W., "Reduction in tensile and flexural strength of unidirectional glass fibre-epoxy with increasing specimen size", *Composite Structures*, vol. 38, nos. 1–4, pp. 405–411, 1997.

Index

Experimental Mechanics of Solids and Structures, First Edition. Jérôme Molimard.

Other titles from

in

Mechanical Engineering and Solid Mechanics

2016

BOYARD Nicolas
Heat Transfer in Polymer Composite Materials

DE SAXCÉ Géry
Galilean Mechanics and Thermodynamics of Continua

2015

KARLIČIĆ Danilo, MURMU Tony, ADHIKARI Sondipon, MCCARTHY Michael
Non-local Structural Mechanics

SAB Karam, LEBÉE Arthur
Homogenization of Heterogeneous Thin and Thick Plates

2014

ATANACKOVIC M. Teodor, PILIPOVIC Stevan, STANKOVIC Bogoljub, ZORICA Dusan
Fractional Calculus with Applications in Mechanics: Vibrations and Diffusion Processes

ATANACKOVIC M. Teodor, PILIPOVIC Stevan, STANKOVIC Bogoljub, ZORICA Dusan
Fractional Calculus with Applications in Mechanics: Wave Propagation, Impact and Variational Principles

CIBLAC Thierry, MOREL Jean-Claude
Sustainable Masonry: Stability and Behavior of Structures

ILANKO Sinniah, MONTERRUBIO Luis E., MOCHIDA Yusuke
The Rayleigh−Ritz Method for Structural Analysis

LALANNE Christian
Mechanical Vibration and Shock Analysis – 5-volume series – 3rd edition
Sinusoidal Vibration – volume 1
Mechanical Shock – volume 2
Random Vibration – volume 3
Fatigue Damage – volume 4
Specification Development – volume 5

LEMAIRE Maurice
Uncertainty and Mechanics

2013

ADHIKARI Sondipon
Structural Dynamic Analysis with Generalized Damping Models: Identification

ADHIKARI Sondipon
Structural Dynamic Analysis with Generalized Damping Models: Analysis

BAILLY Patrice
Materials and Structures under Shock and Impact

BASTIEN Jérôme, BERNARDIN Frédéric, LAMARQUE Claude-Henri
Non-smooth Deterministic or Stochastic Discrete Dynamical Systems: Applications to Models with Friction or Impact

EL HAMI Abdelkhalak, BOUCHAIB Radi
Uncertainty and Optimization in Structural Mechanics

KIRILLOV Oleg N., PELINOVSKY Dmitry E.
Nonlinear Physical Systems: Spectral Analysis, Stability and Bifurcations

LUONGO Angelo, ZULLI Daniele
Mathematical Models of Beams and Cables

SALENÇON Jean
Yield Design

2012

DAVIM J. Paulo
Mechanical Engineering Education

DUPEUX Michel, BRACCINI Muriel
Mechanics of Solid Interfaces

ELISHAKOFF Isaac *et al.*
Carbon Nanotubes and Nanosensors: Vibration, Buckling and Ballistic Impact

GRÉDIAC Michel, HILD François
Full-Field Measurements and Identification in Solid Mechanics

GROUS Ammar
Fracture Mechanics – 3-volume series
Analysis of Reliability and Quality Control – volume 1
Applied Reliability – volume 2
Applied Quality Control – volume 3

RECHO Naman
Fracture Mechanics and Crack Growth

2011

KRYSINSKI Tomasz, MALBURET François
Mechanical Instability

SOUSTELLE Michel
An Introduction to Chemical Kinetics

2010

BREITKOPF Piotr, FILOMENO COELHO Rajan
Multidisciplinary Design Optimization in Computational Mechanics

DAVIM J. Paulo
Biotribolgy

PAULTRE Patrick
Dynamics of Structures

SOUSTELLE Michel
Handbook of Heterogenous Kinetics

2009

BERLIOZ Alain, TROMPETTE Philippe
Solid Mechanics using the Finite Element Method

LEMAIRE Maurice
Structural Reliability

2007

GIRARD Alain, ROY Nicolas
Structural Dynamics in Industry

GUINEBRETIÈRE René
X-ray Diffraction by Polycrystalline Materials

KRYSINSKI Tomasz, MALBURET François
Mechanical Vibrations

KUNDU Tribikram
Advanced Ultrasonic Methods for Material and Structure Inspection

SIH George C. *et al.*
Particle and Continuum Aspects of Mesomechanics

WILEY END USER LICENSE AGREEMENT

Go to www.wiley.com/go/eula to access Wiley’s ebook EULA.